A study of cosmic ray protons at ground level

G. Brooke

Spare Copy

A Study of Cosmic Ray Protons at Ground Level

Ph.D. Thesis submitted by G. Brooke, 1964

ABSTRACT

The momentum spectra of cosmic ray protons and pions up to an energy of 150 GeV have been measured at Durham, 198 feet above sea-level. Assuming a particular model for the interaction of high energy nucleons, a new estimate has been made of the primary cosmic ray nucleon spectrum. This may be represented in the energy range 10^{10} to 3×10^{13} eV/nucleon by the expression:-

$$I(>E) = 0.87^{+0.52}_{-0.30}\ E^{-1.58}\ \text{cm}^{-2}\ \text{sec}^{-1}\ \text{sterad}^{-1},$$

where E is in units of GeV.

It has been shown that a model in which the mean value of the elasticity of nucleon-air nucleus collisions is not a function of the incident energy describes the experimental results accurately. The value found for the fraction of this energy retained by the incident nucleon is 53%.

The effect of large fluctuations in elasticity from collision to collision has been investigated and found to be negligible. The result of taking fluctuations into account is to give a mean value of elasticity ~3% lower than the value obtained assuming the elasticity not to fluctuate.

From the measured pion spectrum and a study of the propagation of pions in the atmosphere, values have been obtained for the elasticity of pion-air nucleus collisions. In contrast with nucleon collisions, it is found that pions retain 40% of their initial energy after collision at 5 GeV but that at 80 GeV their collisions are completely inelastic.

A Study of Cosmic Ray Protons at Ground Level

A Thesis submitted to the University of Durham for the Degree of Doctor of Philosophy

by

G. Brooke, B.Sc.

February, 1964

CONTENTS

ABSTRACT

The momentum spectra of cosmic ray protons and pions up to an energy of 150 GeV have been measured at Durham, 198 feet above sea-level. Assuming a particular model for the interaction of high energy nucleons, a new estimate has been made of the primary cosmic ray nucleon spectrum. This may be represented in the energy range 10^{10} to 3×10^{13} eV/ nucleon by the expression:-

$$I(>E) = 0.87^{+0.52}_{-0.30} E^{-1.58} \text{ cm}^{-2}\text{sec}^{-1}\text{sterad}^{-1}.$$

where E is in units of GeV.

It has been shown that a model in which the mean value of the elasticity of nucleon-air nucleus collisions is not a function of the incident energy describes the experimental results accurately. The value found for the fraction of its energy retained by the incident nucleon is 53%.

The effect of large fluctuations in elasticity from collision to collision has been investigated and found to be negligible. The result of taking fluctuations into account is to give a mean value of elasticity ~3% lower than the value obtained assuming the elasticity not to fluctuate.

From the measured pion spectrum and a study of the propagation of pions in the atmosphere, values have been obtained for the elasticity of pion-air nucleus collisions. In contrast with nucleon

collisions, it is found that pions retain 40% of their initial energy after collision at 5 GeV but that at 80 GeV their collisions are completely inelastic.

PREFACE

This thesis describes the measurement and interpretation of the momentum spectra of cosmic ray protons and pions at Durham.

The work was performed under the supervision of Dr. A.W. Wolfendale.

The operation of the spectrograph was carried out with the help of Professor M.A. Meyer, Dr. E.B. Hughes and Mr. A. Crispin. The analysis and interpretation of the data were the sole responsibility of the author. Dr. Y. Kamiya assisted with part of the numerical calculations concerned with the deduction of the primary cosmic ray spectrum.

The work on the sea-level proton and pion spectra was presented at the Kyoto Conference on Cosmic Rays and the Earth Storm (Brooke et al., 1962) and a further paper has been submitted to the Proceedings of the Physical Society.

The calculation of the primary cosmic ray spectrum has been published as a letter to Nature (Brooke et al., 1963) and a further, more detailed paper has been submitted to the Proceedings of the Physical Society.

A paper on the production of neutrons in lead by cosmic ray protons is to be published in the Proceedings of the Physical Society (Hughes et al., 1963).

CHAPTER 1

INTRODUCTION

The primary cosmic radiation incident on the earth's atmosphere consists mainly of protons, with 5.5% of α-particles and 0.5% of heavier nuclei (above 2.4 GeV/nucleon, Waddington (1960)). The percentage of nuclei heavier than helium in the primary radiation is notable in that it is many times higher than the cosmic abundance of such nuclei. The very large percentage of L-group (Li, Be, B) nuclei observed, $\sim 2 \times 10^5$ times the cosmic abundance, is probably due to fragmentation of heavier nuclei in their passage through space. The majority of the primary cosmic ray particles must originate therefore from some object which contains an excessive number of heavy nuclei. Such conditions are found in supernovae, dense old stars which, having used up all their light nuclei, obtain energy by forming heavier and heavier nuclei until at some point the star explodes. In the explosion the heaviest nuclei are formed by neutron capture processes. Six supernova explosions have been observed in our galaxy, in 185, 369, 1006 and 1054 A.D. (Crab nebula), seen by Chinese astronomers, 1572 A.D. (Tycho's star) and 1604 A.D. (Kepler's star), all of which are known to be sources of radio waves. The Crab nebula is the best studied of these, its optical and radio emissions being consistent with synchrotron radiation from electrons.

This shows that magnetic fields are almost certainly present in such a form as to be able to accelerate electrons and presumably protons and heavier nuclei up to high energies probably by a Fermi type process, Fermi (1949).

The low energy particle flux, that is particles with energy below about 10 GeV, is subject to time variations related to the activity of the sun. This and other stars must contribute an appreciable number of low energy cosmic ray protons and α-particles. For primary energies above a few times 10 GeV, the primary cosmic ray flux is remarkably free from time variations.

The galactic magnetic field is not strong enough to contain particles with energies greater than about 10^8 GeV within the galaxy and these might originate in colliding galaxies, Morrison, (1961).

On entering the earth's atmosphere, the primary particles interact with the air nuclei, producing pions and a small fraction of heavier mesons and hyperons. In a collision of a primary proton, about 50% of the incident energy is carried off by a single nucleon which continues to make further interactions. In the interactions of heavier nuclei, only one of the incident nucleons appears to take part, the remainder carrying on with their original energy. Thus the nucleon component at any level consists of primaries which have not interacted and nucleons which have emerged from interactions.

The charged pions produced in the interactions either decay with a mean lifetime of 2.6×10^{-8} sec or interact with air nuclei to produce more pions. The neutral pions have a mean lifetime of $\sim 10^{-16}$ sec and decay into two photons. If sufficiently energetic these photons materialize to produce electron pairs which in turn produce photons by the bremsstrahlung process. If the neutral pion has sufficient energy, these two processes are repeated many times resulting in an electron-photon cascade. At sea-level these electrons have momenta $\lesssim 500$ MeV/c.

The hyperons are removed either by interaction or decay into nucleons and light mesons before reaching ground level and similarly the heavy mesons are removed either by interaction or decay into light mesons.

At ground level, for momenta above 500 MeV/c, the radiation consists mainly of muons, with a small percentage of protons and neutrons and a very small flux of pions.

Information on the behaviour of high energy nuclear interactions can be deduced from a comparison of the pion production spectrum derived from the sea-level muon spectrum with that predicted from the primary spectrum. The sea-level muon spectrum has been measured by many workers, the most accurate being that due to Gardener et al. (1962) and Hayman and Wolfendale (1962), which together cover the momentum range 0.4 - 1000 GeV/c. By

assuming a theoretical variation of meson multiplicity with momentum in the primary interactions, Hayman (1962) has calculated the average inelasticities of these interactions. Similarly, the inelasticity of nucleon-air nucleus collisions can be found by comparing the sea-level proton spectrum with the primary spectrum or the proton spectrum at high altitude, if a model for the propagation of the nucleon component in the atmosphere is assumed.

Further reasons for measuring the proton spectrum are that in many experiments in which the behaviour or the form of the sea-level muon spectrum is studied, it is necessary to correct for the protons present in the sea-level intensity, and, in addition, it is necessary to know the sea-level proton intensity in designing experiments to study their interactions.

The work by Mylroi and Wilson (1951) is the only previous measurement of the vertical proton intensity at sea-level over a wide momentum interval, covering the range 0.6 - 12 GeV/c. Measurements by other workers have covered only comparatively narrow momentum intervals at momenta $\lesssim$2 GeV/c, with the exception of a measurement of low statistical accuracy by Pak and Greisen (1962) at a median energy of 22 GeV. The proton spectrum at an altitude of 3400 metres has been measured by Whittemore and Shutt (1952) up to 7 GeV/c and at 3200 metres by Kocharian et al. (1959) in a series of experiments, over the energy range 40 MeV - 66 GeV.

In the present work, descriptions of the Durham Cosmic Ray Spectrograph, as modified for the measurements of the proton intensity, the data recording system and the method of analysis are given in Chapter 2. Two methods have been used to measure the intensity of protons. In the first method, the proton component was identified by studying the difference in the absorption in lead of positive and negative particles. The two series of experiments performed using this method are described in Chapter 3. The proton component was found, by the second method, from the different numbers of neutrons produced in the interactions of positive and negative particles in an "International Geophysical Year" neutron monitor. The two experiments in which this method was used are described in Chapter 4. The method used and the momentum range over which the proton intensity could be calculated are summarized in Table 1.1, for each of the experiments performed.

Series	Method	Mean Magnet Current, A	Momentum Range GeV/c
P	Absorption in neutron monitor and 11 cm of Pb	11.3	0.65 - 47.7
AP	Absorption in 16.5 cm of Pb	15.81	0.60 - 4.00
S	Neutron production	11.42	0.70 - 50.0
H	Neutron production	59.6	0.70 - 150.0

Table 1.1

The derivation of the sea-level proton spectrum is given in Chapter 5, together with a detailed comparison with previous measurements. In Chapter 6, values of the elasticities of nuclear interactions are deduced from a comparison of the results from the present work with the primary spectrum given by Linsley et al. (1962), the so-called "M.I.T." spectrum. By considering the relation between the sea-level proton spectrum and the spectrum of pions at production, in Chapter 7 a newestimate is made of the primary cosmic ray intensities over a wide range of energy. The effect on these calculations of fluctuations in the total inelasticity and also in the fraction of the available energy going into the production of pions is considered in Chapter 8. In Chapter 9, a comparison is made with other measurements of primary intensities. In addition, the proton spectrum at 3,200 metres altitude is calculated from the present work and compared with direct measurements at that altitude. The sea-level pion spectrum is calculated in Chapter 10 from the rates of observation of nuclear interactions of negative particles in the neutron monitor. Values for the elasticity of pion interactions are deduced from a comparison with the pion production spectrum. Finally, a summary of the conclusions obtained from the present measurements is given in Chapter 11.

CHAPTER 2

THE DURHAM COSMIC RAY SPECTROGRAPH

2.1 The General Features

The Durham Cosmic Ray Spectrograph, shown in Fig. 2.1, consists of a Blackett-type electromagnet with trays of Geiger counters at the five levels A, B, G, C and D. The counters are used to select particles which pass through the spectrograph, those at level G ensure that particles pass through the magnetic field and eliminate particles which are scattered by the magnet pole-pieces. There is an array of flash-tubes at each of the levels A, B, C and D by means of which the positions of the particle trajectories can be found.

2.2 The Electromagnet

The electromagnet used in the spectrograph is one of the two originally used in the Manchester Spectrograph and has been described by Hyams et al. (1950). The maximum current through the magnet is 70 A at 440 volts giving a maximum field strength in the pole gap of 12,000 gauss and a value of 6.60×10^5 gauss-cm for $\int H d\ell$, the integral of the magnetic field along the trajectories of near vertical particles.

2.3 The Geiger Counter System

The Geiger counter trays at levels A and D each consist of twenty-five 60 cm long counters and the trays at B and C of eleven 26 cm long

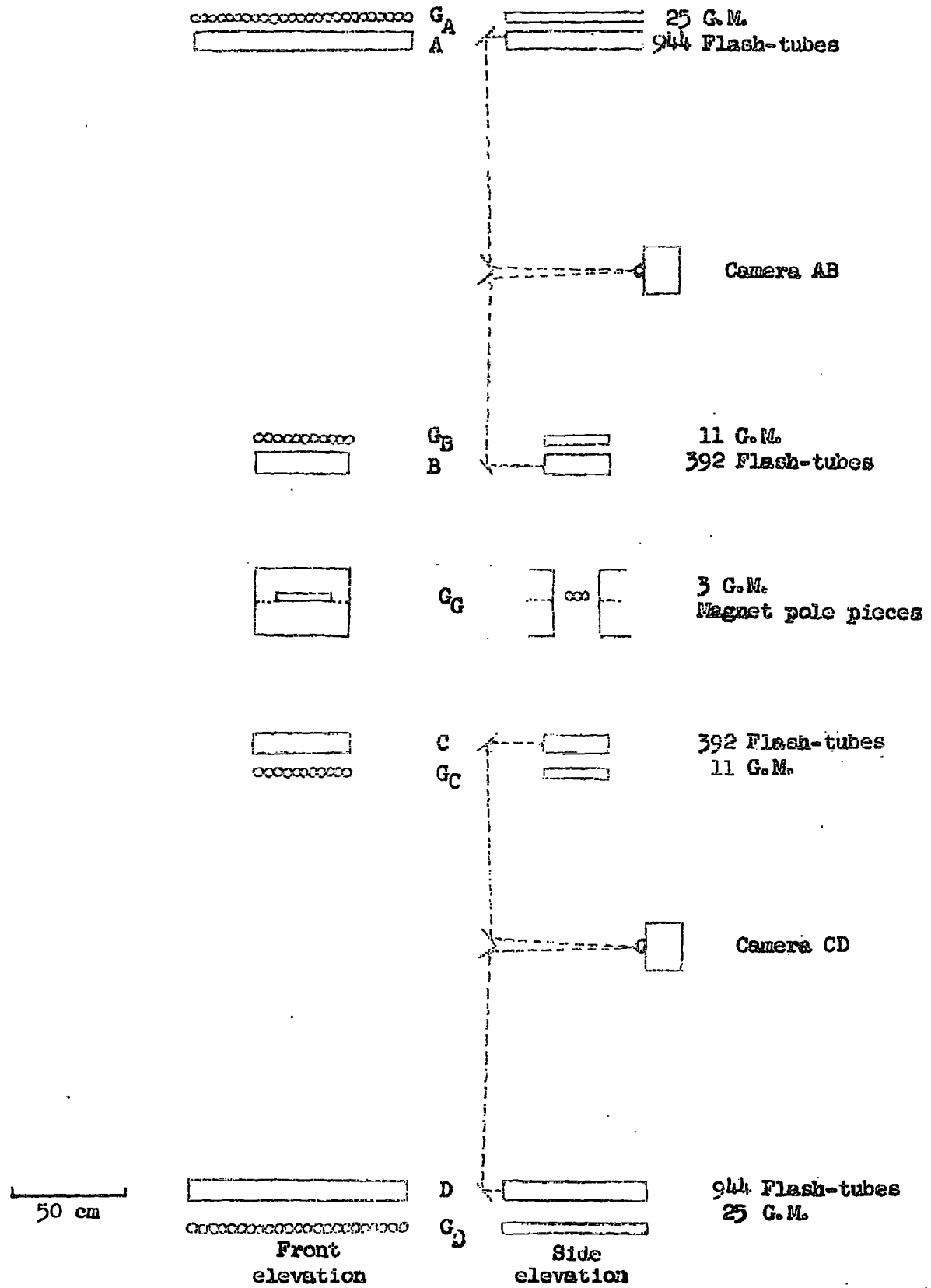

Fig. 2.1 The Spectrograph.

counters. All the counters in the trays at A, B, C and D are positioned with their axes parallel to the magnetic field. The tray at level G consists of three 26 cm long counters with their axes at 90° to the magnetic field. The counters are of the self-quenching type (20th Century G26, G60) but in order to reduce their dead-time, the discharge is also quenched electronically. The electronic circuits used with the Geiger counters are described fully by Jones et al., (1962).

An additional tray of Geiger counters, S, was also operated during the experiments to measure the proton spectrum (see Chapters 3 and 4). Coincidence between pulses from any desired group of Geiger counter trays was registered by a Rossi coincidence circuit.

2.4 The Neon Flash Tube

The neon flash-tube, first developed by Conversi et al., (1955) and later by Gardener et al. (1957), consists of a glass tube filled with neon gas. If a high voltage pulse is applied across the tube soon after the passage of an ionizing particle through it, there is a high probability of a discharge taking place in the tube. The flash of light is bright enough to be photographed through the end of the tube. The tubes can be operated in arrays, with many flash-tubes between each pair of electrodes. Photoionization of neighbouring tubes is prevented by painting the sides of the tubes black. The tubes used in the Durham Spectrograph have internal diameter 0.59 cm

and external diameter 0.72 cm. The tubes are filled with neon to a pressure of 2.3 atmos. and have a sensitive time of 39 μsec after the passage of an ionizing particle through them.

2.5 The Flash-Tube Arrays

Each array consists of eight layers of flash-tubes, the vertical separation of the layers being 1.15 cm. There are 944 tubes in each of the arrays A and D and 392 tubes in B and C. The axes of all the flash-tubes are parallel, being parallel to the magnetic field. The horizontal separation of the centres of the tubes in a layer is 0.80 cm. The design of the flash-tube arrays has been described by Hayman, (1962).

The original electrode system was as shown in Fig. 2.2, with two layers of flash-tubes between each pair of electrodes, which were of thin aluminium sheet. This arrangement gave a considerable variation in the brightness of flashes from the tubes which were adjacent to earthed electrodes and those which were adjacent to high voltage electrodes. A U.H.T. of 20 KV was required to operate the tubes.

New electrodes were used for the present experiments. These consist of 2 mm thick polyurathane foam sandwiched between sheets of thin card covered with aluminium foil, the resultant weight being very low. The total thickness of the electrodes was such as to fill the gap between the layers of flash-tubes, electrodes being placed

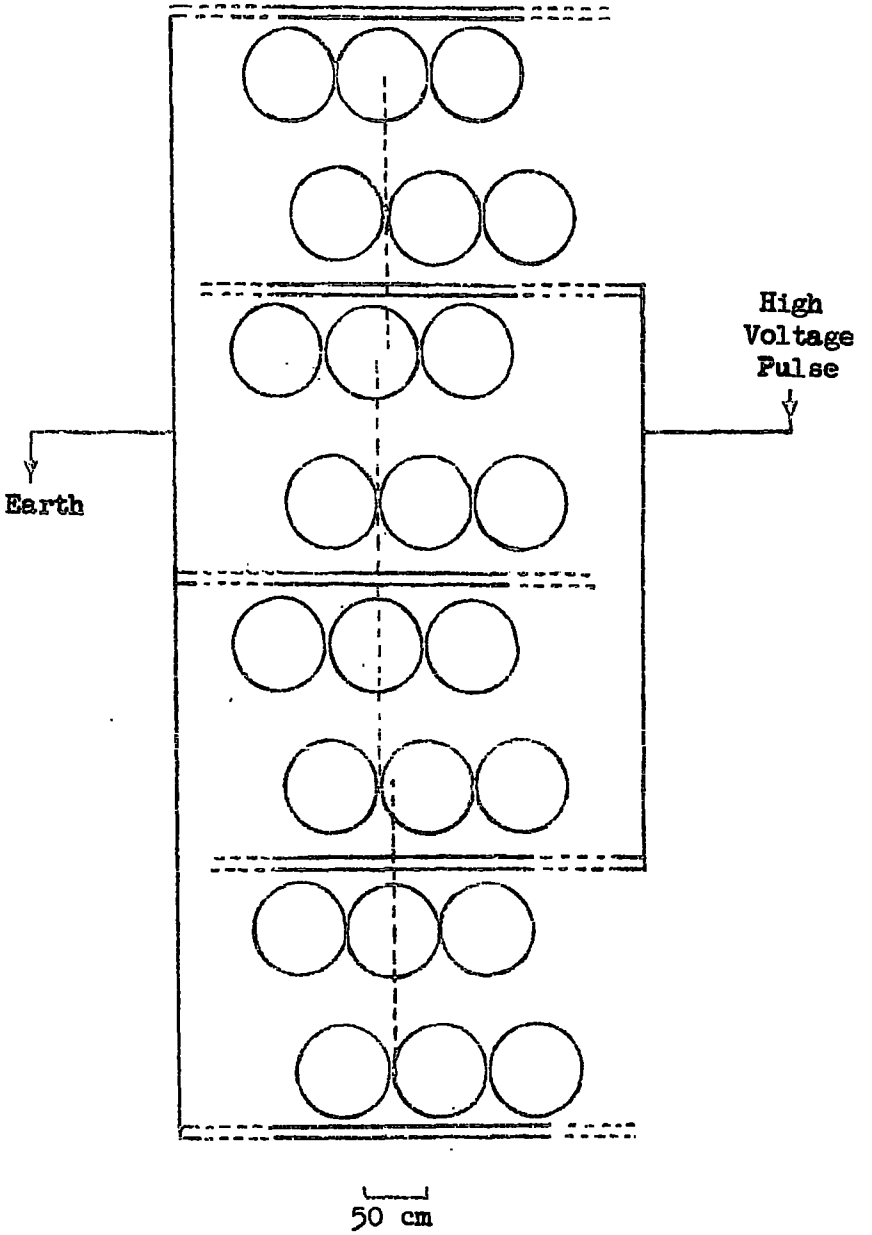

The Original Electrode System

Fig. 2.2

on both sides of each layer of tubes, making it possible to obtain the same electric field across the tubes as previously, using a U.H.T. of 5 KV (and at the same time eliminating the layer to layer variation in brightness). The new electrode system is shown in Fig. 2.3.

2.6 The Flash-Tube Pulsing System

The original method for applying the high voltage pulse to the flash-tubes was as follows. When the required Geiger counter configuration had been recorded, a low voltage trigger tube (CV 4018) was operated. The output pulse from this was then fed through a Ferroxcube pulse transformer to the grid of a high voltage hydrogen thyratron (XH8-100), the output of which triggered six 'trigatrons' (CV 85) in parallel. Each of these discharged a bank of condensers, charged to 8 KV, through a step-up voltage pulse transformer, the output being applied to the flash-tube electrodes (Fig. 2.4). Two pulses were applied to each of arrays A and D, one to the upper half and one to the lower half of each.

In the experiments to measure the proton intensity by absorption in lead placed above array D, the intermittent failure of one of the valves used to pulse array D would have resulted in a low overall efficiency for D in those cases. Some particles would appear to have been stopped by the absorber although they had not. This condition would have been difficult to recognize as a large number of events with no track in array D was expected.

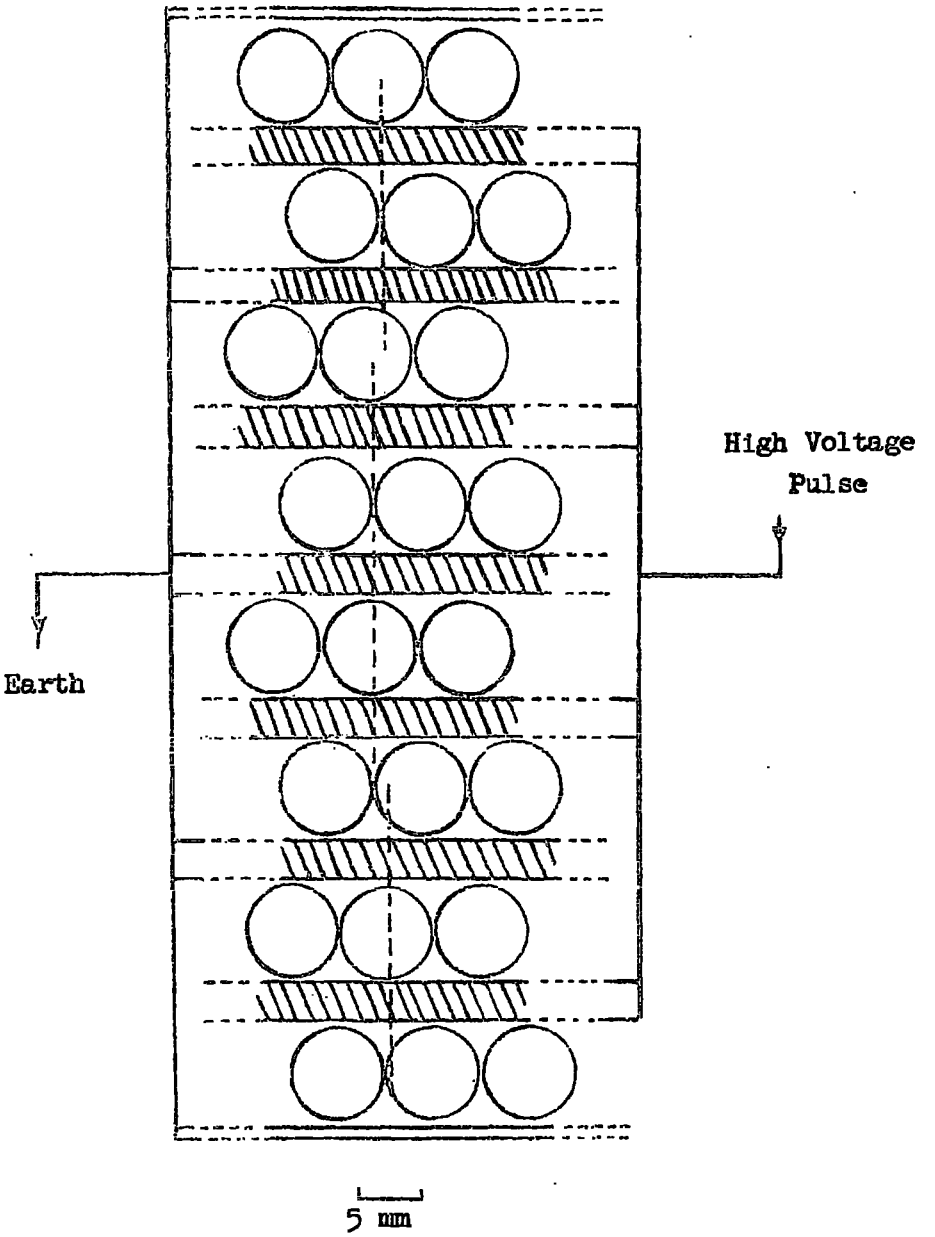

The New Electrode System

Fig. 2.3

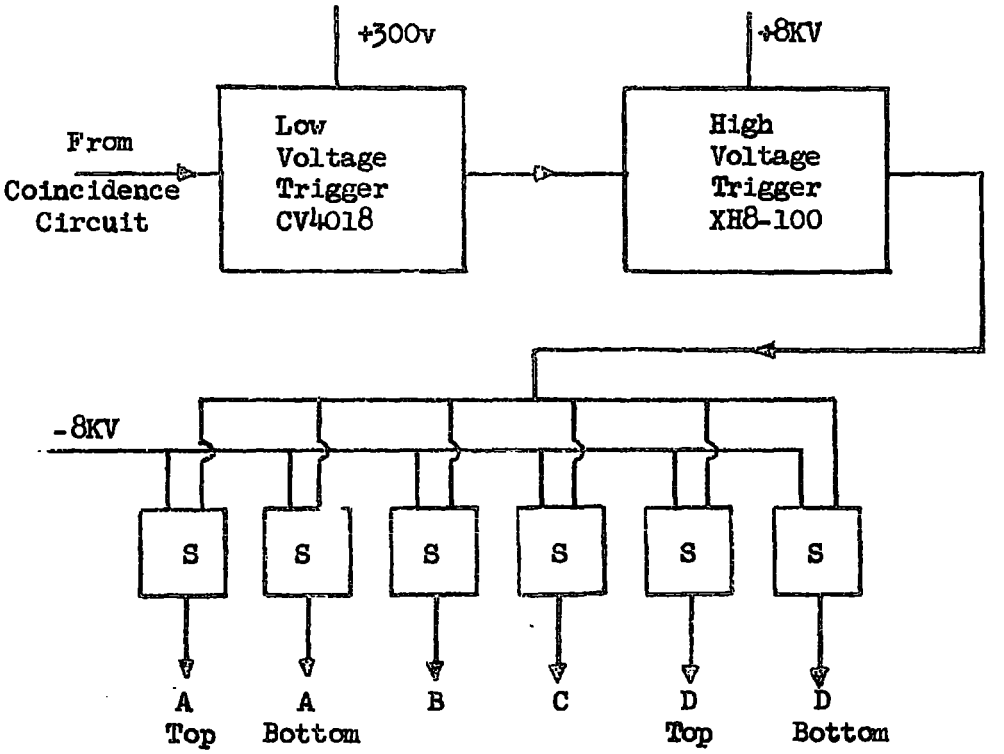

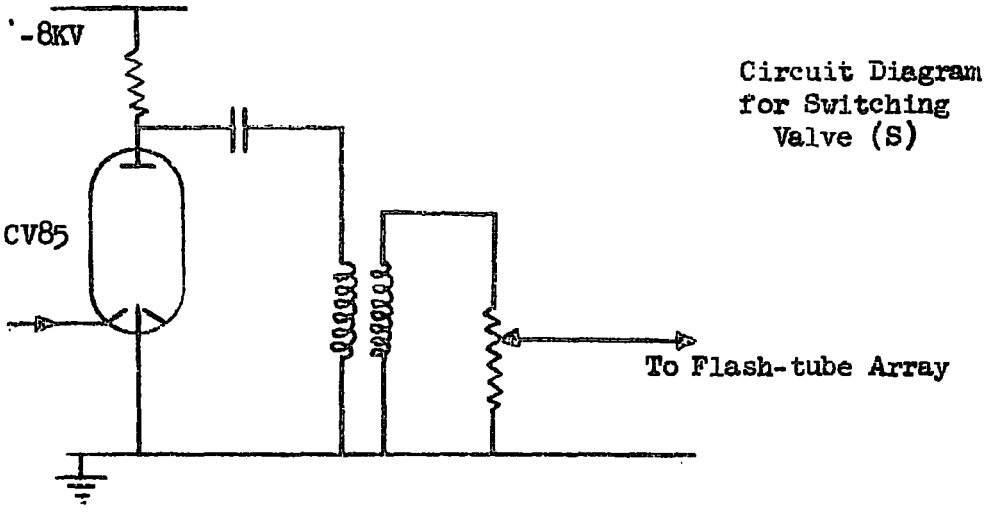

Circuit Diagram
for Switching
Valve (S)

The Original High Voltage Pulse Generator

Fig. 2.4

Consequently, the pulsing arrangement was changed to that shown in Fig. 2.5. The output from the low voltage trigger is now used to operate a mercury thyratron (CV 13), pulses being taken directly from the thyratron load to the electrodes. In this case, a spurious record of a particle stopping in the absorbing layer cannot be obtained due to failure of the pulsing system since, in the event of failure, no flashes would be observed in any of the arrays.

2.7 The Recording System

The flashes in the four arrays of flash-tubes A, B, C and D are recorded photographically (on 35 mm HPS film), using two cameras (with shutters fixed in front of them). By means of two mirror systems, Fig. 2.1, one camera records flashes in A and B and the other, flashes in C and D. Front aluminized mirrors are used except for the large mirrors immediately in front of arrays A and D which are back-silvered thin glass, bent so that the cameras look along the axes of the flash-tubes in these arrays. This is necessary as the discharges in the flash-tubes do not extend nearer to the front than the electrodes, i.e. the discharge stops $\sim 1\frac{1}{2}$" from the front of the tube. Without the use of curved mirrors only a small part of the discharge is seen by the camera for tubes near the ends of the large arrays and the resulting photographic image is very weak, Coxell et al. (1961).

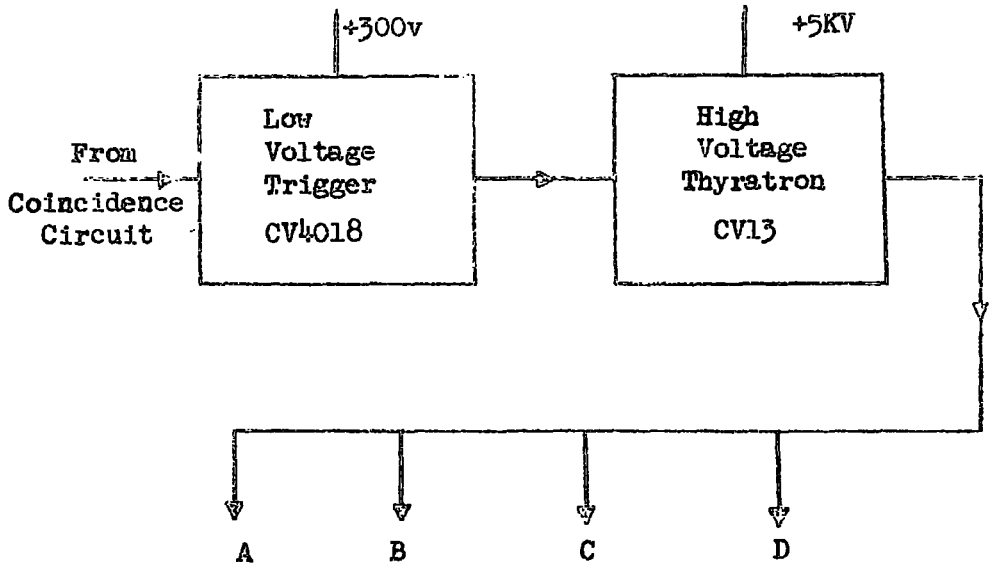

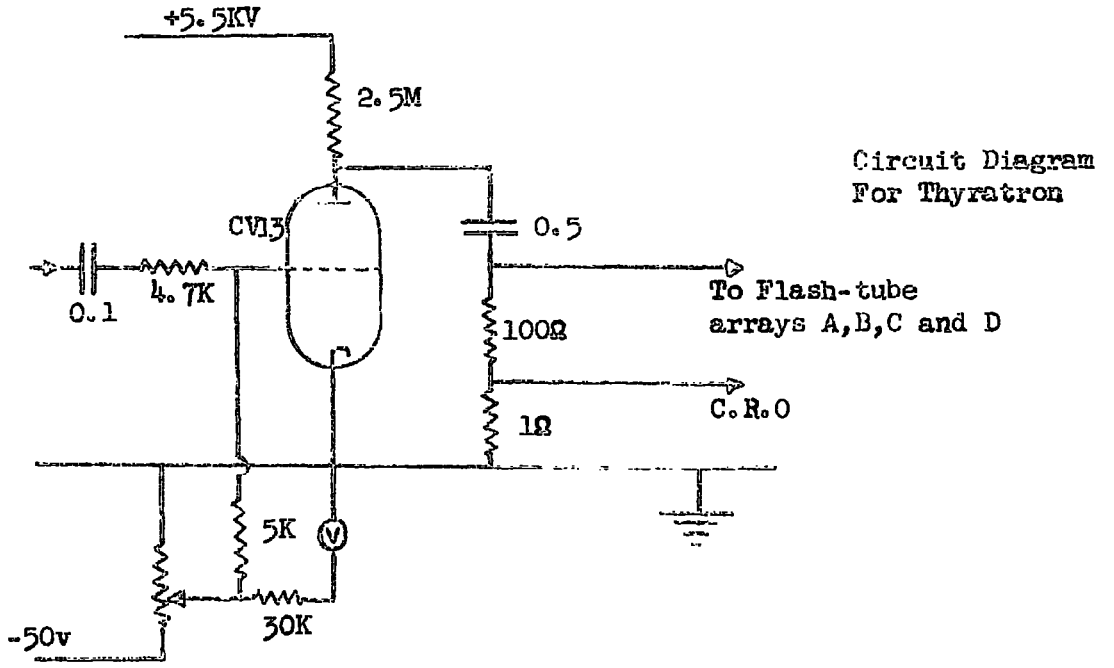

Circuit Diagram
For Thyratron

The New High Voltage Pulse Generator

Fig. 2.5

The sequence of operations when a particle has passed through the spectrograph and satisfied all the conditions required for the Geiger counters is:-

a) The Rossi coincidence circuit is paralysed.

b) i) If the Geiger counter pulses are the only basis for selection, then the high voltage pulse is applied to the flash-tubes and the flashes photographed, the camera shutters being permanently open in this case.

ii) If neutrons are required to be detected in coincidence with a Rossi pulse, a series of high voltage pulses is applied to the flash-tubes, the camera shutters being opened only if neutrons are detected. If no neutrons are detected, operations c) and d) are omitted.

c) Reference bulbs are illuminated to allow the identification of the tubes which have flashed when the photographs are examined. Also, two clocks are illuminated to enable corresponding AB and CD photographs to be easily found.

d) The cameras are wound on.

e) The paralysis is removed from the Rossi circuit.

2.8 The Maximum Detectable Momentum

The maximum detectable momentum, defined as the momentum corresponding to the angular deflection which is equal to the probable error in the measurements of the deflections, depends on the accuracy with which particle trajectories can be located at the measuring levels and also on the separation of these levels.

In previous experiments to measure the momentum spectrum of cosmic ray muons, all four measuring levels, A, B, C and D, were used to locate the particle trajectories, giving a maximum detectable momentum of ~700 GeV/c at a magnet current of 60 A. However, in the present experiments it waspossible to measure only three points on any particle trajectory, leading to a maximum detectable momentum lower, by a factor of approximately three, than that for the four tray instrument operated at the same magnet current. In fact, as is shown later, the intensity of protons falls so rapidly with momentum that the highest momentum point on the proton spectrum which it was possible to measure was set by the running time of the experiment.

2.9 The Acceptance Function

The five trays of Geiger counters at the levels A, B, C, G and S, which were used in coincidence for all the experiments, limit the possible angles of incidence of particles which can be accepted and also the area through which they must pass. Since

the particles are deflected in passing through the spectrograph, the acceptance is a function of the magnetic deflection and hence of momentum, falling to zero at the "least detectable momentum". The dimensions of the spectrographs are such that only particles with angles of incidence near to the vertical and angular deflections, ϕ, less than ~0.45 radians can be accepted, so that it is possible to put:-

$$A(\phi) = A_1(\phi).A_2$$

where $A(\phi)$ is the acceptance function measured in units of sterad. cm^2, $A_1(\phi)$ is the acceptance in the "deflection" plane, (rad. cm.) and A_2 is the acceptance in the "back plane" (rad. cm.) $A_1(\phi)$ is best evaluated graphically, as the theoretical treatment becomes complicated when the spectrograph is not symmetrical about the magnetic field. As there is no magnetic deflection of the particles in the back plane, A_2 is not a function of momentum but a constant for any given Geiger counter arrangement. In addition to the limits to the acceptance set by the Geiger counter trays, particles were required to have trajectories which would not have passed through the edges of D in either plane, the permissible area of array D being a function of the particle momentum and of the geometry of the absorber. This further limitation is easily introduced into the graphical evaluation of the acceptance function by

reducing the dimensions of array D in both planes by the appropriate amount for the momentum being considered. Details of the calculations of the acceptance functions and the values for the various experiments are given in Appendix 1.

2.10 The Measurement of the Positions of Particle Trajectories

2.10.1 The Projection Method

The photographs of the flashes were projected through a mirror system onto moveable boards on a table. On the boards circles had been drawn corresponding to the positions of the flash-tubes in each array. These positions were obtained by projecting onto the boards photographs in which all of the flash-tubes had flashed. The photographs were taken using a γ-source to make the tubes flash and applying a succession of high voltage pulses. The reference bulbs in each array were also illuminated.

The projected images of the flashes were positioned on the boards by means of the reference bulbs. There was a reference bulb at each end of all four arrays and these allowed the magnification and position of the images to be adjusted accurately. The measuring levels were taken to be immediately below the fourth row of flash-tubes from the top of each array, scales having been drawn on the boards at those positions. Measurements were made of the best estimates of the points of intersection of the particle trajec-

tories with the measuring levels. Distances measured were from fixed reference points in each array, the positions of these points with respect to the plumb line having been previously measured (Fig. 2.6). The best estimate of a particle track through a flash-tube array was made by eye using a cursor. The cursor was made to pass through all the tubes which had flashed and either miss, or pass as near to the edge as possible, tubes which had not flashed. Events were rejected for the following reasons:-

a) If in any array there were two adjacent flashes in two or more layers of flash-tubes, due to knock-on electrons.

b) If there were two particle tracks in any array of flash-tubes and it was not possible to tell, from their angles and the angles of the tracks in the other arrays, which was the track produced by the particle that had passed through the other arrays.

c) If two or more tracks were observed in each of two or more arrays of flash-tubes.

The accuracy of track location using the projection method is 1 mm r.m.s. at each measuring level.

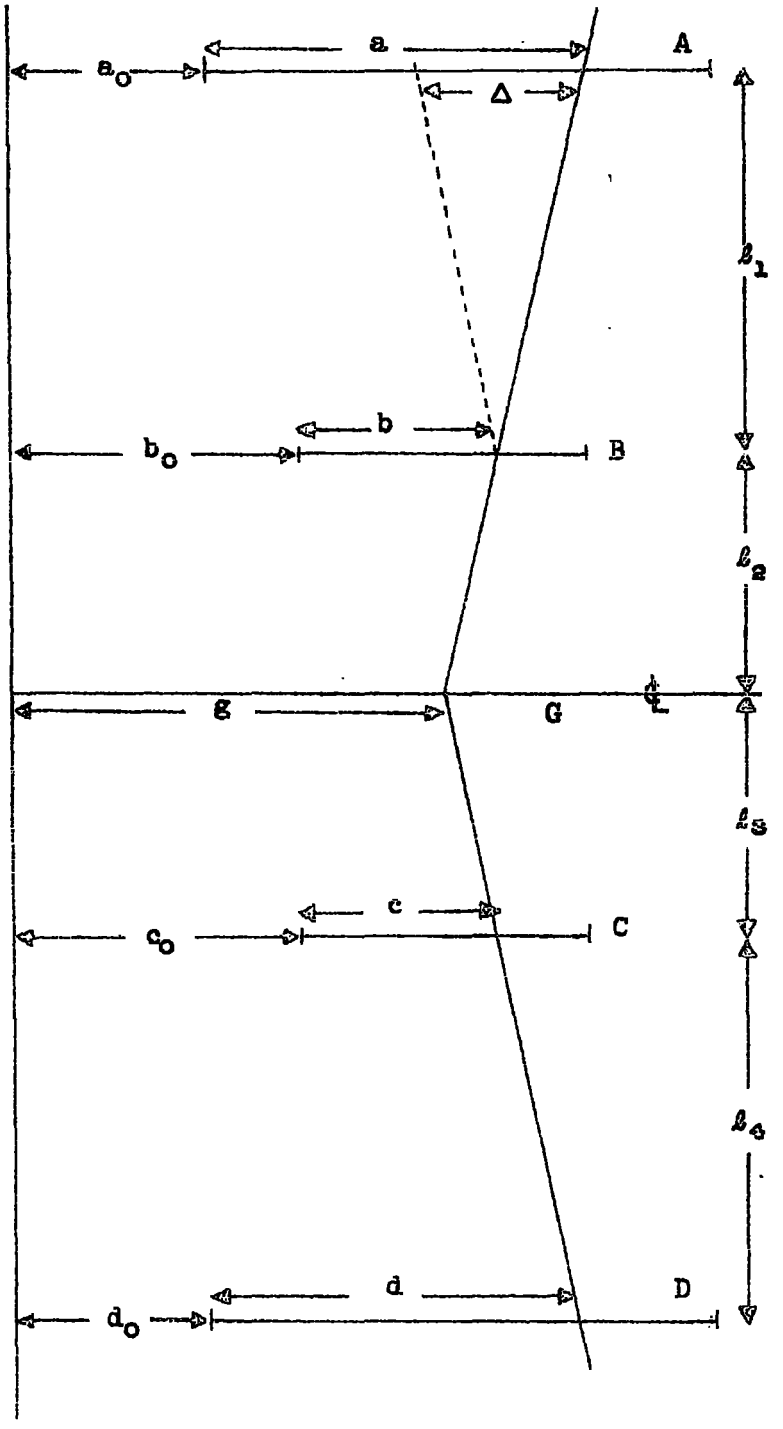

ℓ_1 = 184.3 cm
ℓ_2 = 61.4 cm
ℓ_3 = 60.0 cm
ℓ_4 = 189.5 cm
a_o = 9.38 cm
b_o = 36.54 cm
c_o = 36.52 cm
d_o = 10.97 cm

Vertical dimensions refer to the measuring levels in the flash-tube arrays and horizontal to the reference zero points in the arrays

The Spectrograph Dimensions

Fig. 2.6

2.10.2 The Track Simulator Method

The Track Simulator, described in detail by Hayman (1962), consists of a large scale model of a section of a flash-tube array. The scale is ten times in the horizontal direction and three times in the vertical direction. For a particle which was found by the projection method to have a high momentum, the configuration of flashes observed in each array was noted. Slots corresponding to the tubes which had flashed in a particular array were illuminated on the Track Simulator and a cursor was set to the angle given by the projection method for that particle trajectory. The possible limits to the position of the particle trajectory in the array, such that the cursor passed through only tubes which had flashed and avoided the others were found. The mean value of the limits to the position was taken to be the best estimate of the particle position at that level.

Some correction was made for the variation of the flash-tube efficiency as a function of their radius, Ashton et al. (1958), by decreasing slightly the width of the slots representing the flash-tubes.

The error in track location using the Track Simulator is 0.55 mm r.m.s.

2.11 The Calculation of Particle Momenta

The radius of curvature, ρ, of the trajectory of a particle mass m, velocity v, and charge e, on passing through a magnetic field of strength H is given by

$$Hev = \frac{mv^2}{\rho}$$

$$\text{or} \qquad \rho = \frac{mv}{He} \qquad 2.1$$

If $d\phi$ is the angular deflection of the particle in moving a distance $d\ell$, then:-

$$\rho . d\phi = d\ell \qquad 2.2$$

so that equation 2.1 may be written:-

$$\frac{d\ell}{d\phi} = \frac{mv}{He}$$

$$\text{or} \quad e.Hd\ell = mv.d\phi = pd\phi \qquad 2.3$$

(where p = particle momentum).

Integration gives

$$p.\phi = e.\int Hd\ell$$

$$\text{or} \qquad p = \frac{300 \int Hd\ell}{\phi} \qquad 2.4$$

with p in units of eV/c, $\int Hd\ell$ in gauss-cm and ϕ in radians.

For a given value of magnet current, $\int Hd\ell$ is constant and so equation 2.4 becomes:-

$$p = \frac{\text{constant}}{\phi}$$

Since the angles to the vertical of all particles which are accepted by the spectrograph are small, ϕ can be evaluated by finding the displacement, Δ, of the trajectory over a given arm (Fig. 2.6), taken by convention to be the distance, ℓ, between the measuring levels in arrays A and B.

If a, b, c and d are the positions of a trajectory measured with respect to fixed points in arrays A, B, C and D respectively and a_o, b_o, c_o and d_o are the distances of these points from a vertical reference line, then for the four tray instrument the displacement, Δ, is given by:-

$$\Delta = (a + a_o) - (b + b_o) - \frac{\ell_1}{\ell_4}(c + c_o) + \frac{\ell_1}{\ell_4}(d + d_o)$$

or

$$\Delta = (a - b) - .972\,(c - d) + \Delta_o \quad \text{(see Fig. 2.6)} \qquad 2.5$$

It is possible to calculate Δ from the measured positions in A, B, and C only.

The point of intersection of the trajectory at the level of G is at a distance from the reference line of:-

$$g = (a + a_o) + [(b + b_o) - (a + a_o)] \frac{(\ell_1 + \ell_2)}{\ell_1}$$

Then the angle to the vertical of the trajectory in the lower half of the spectrograph is:-

$$\frac{(c + c_o) - g}{\ell_3}$$

and hence

$$\Delta = (a + a_o) - (b + b_o) + \frac{\ell_1}{\ell_3} [-g + (c + c_o)]$$

$$= (a + a_o) - (b + b_o)$$

$$+ \frac{\ell_1}{\ell_3} \left\{ -(a + a_o) - [(b + b_o) - (a + a_o)] \frac{\ell_1 + \ell_2}{\ell_1} + (c + c_o) \right\}$$

$$= (a + a_o) \left(\frac{\ell_2 + \ell_3}{\ell_3} \right) - (b + b_o) \left(\frac{\ell_1 + \ell_2 + \ell_3}{\ell_3} \right) + (c + c_o) \frac{\ell_1}{\ell_3}$$

2.6

If a, b and c are measured in units of 8 mm (equal to the flash-tube spacing), then Δ, also measured in these units is given by:-

$$\Delta = 2.023a - 5.095b + 3.072c - 68.77 \qquad 2.7$$

Alternatively, the angular deflection, in radians, is given by:-

$$\phi = \frac{\Delta}{\ell_1} = .008792a - .02212b + .01333c - .2983 \qquad 2.8$$

a, b and c again being measured in units of 8 mm.

CHAPTER 3

THE ABSORPTION TECHNIQUE

3.1 Introduction

The rate of energy loss by a singly charged particle due to collision with the atomic electrons of the medium through which it is passing (the "collision" or "ionization" loss) is a function only of the velocity of the particle, in any given medium. Protons and muonswith equal momenta have different absorption ranges as their velocities will not be equal. For low velocities, the ionization loss is proportional to velocity^{-2}, so that for momenta less than a few GeV/c the difference in the ionization ranges of muons and protons is sufficient to allow these particles to be identified by an absorption method. In addition, protons lose energy by nuclear interaction which gives a probability, decreasing with increasing energy, of protons and their secondary particles being stopped by an absorber, for incident momenta greater than the total ionization loss in the absorber. Momentum loss by muons and protons due to direct pair production and bremsstrahlung is negligible in the momentum range considered.

The percentage of protons present in the sea level cosmic radiation can be found from the excess numbers of positive particles which appear to be stopped by an absorber. The lower momentum limit to the measurements of the proton intensity is set by the

momentum above which there is a high probability of a secondary particle emerging from the absorber from a nuclear interaction of a proton and being unrecognized as such.

3.2 Accepted Particles

Particles which satisfied the condition of five-fold coincidence between the Geiger counter trays at levels A, B, G, C and S and anti-coincidence in the Geiger counter tray at level D, below the absorber, were recorded. The recorded events were those in which particles had:-

1) been stopped by the absorber
2) been scattered by the absorber and which consequently did not pass through either the Geiger counter tray or the flash tube array below the absorber
3) passed between the Geiger counters below the absorber.

The particles in the first group were protons, low momentum muons, and a small percentage of pions. The muons were eliminated by rejecting all particles which had momentum less than that below which all muons would have been stopped by the absorber.

The particles in the second group were mainly muons. The number of particles in this group was reduced by rejecting particles which passed nearer to the edge of the flash-tube array

at D than a previously decided number times the r.m.s. displacement in the position of the trajectory at level D due to scattering in the absorber. Protons lost by this rejection were taken into account by suitably modifying the acceptance function.

Finally, the particles which had passed between the Geiger counters at D gave tracks in the flash-tube array below the absorber and were rejected by visual inspection.

The remaining particles were then protons, muons which had been scattered through several times the standard deviation for scattering in the absorber, and pions.

In any given momentum interval the number of protons was then taken to be the number of positive particles which had satisfied the acceptance criteria minus the corresponding number of negative particles multiplied by the positive-negative ratio for muons at that momentum, assuming this to have the same value for pions as for muons.

3.3 The Anticoincidence Unit

The circuit of the anticoincidence unit is shown in Fig. 3.1. The output from the Rossi coincidence circuit is used to operate a delay flip-flop (CV 858). This delay was introduced to take account of possibly late pulses from tray D Geigers and was set at 2 microseconds for all of the experiments. The output pulse

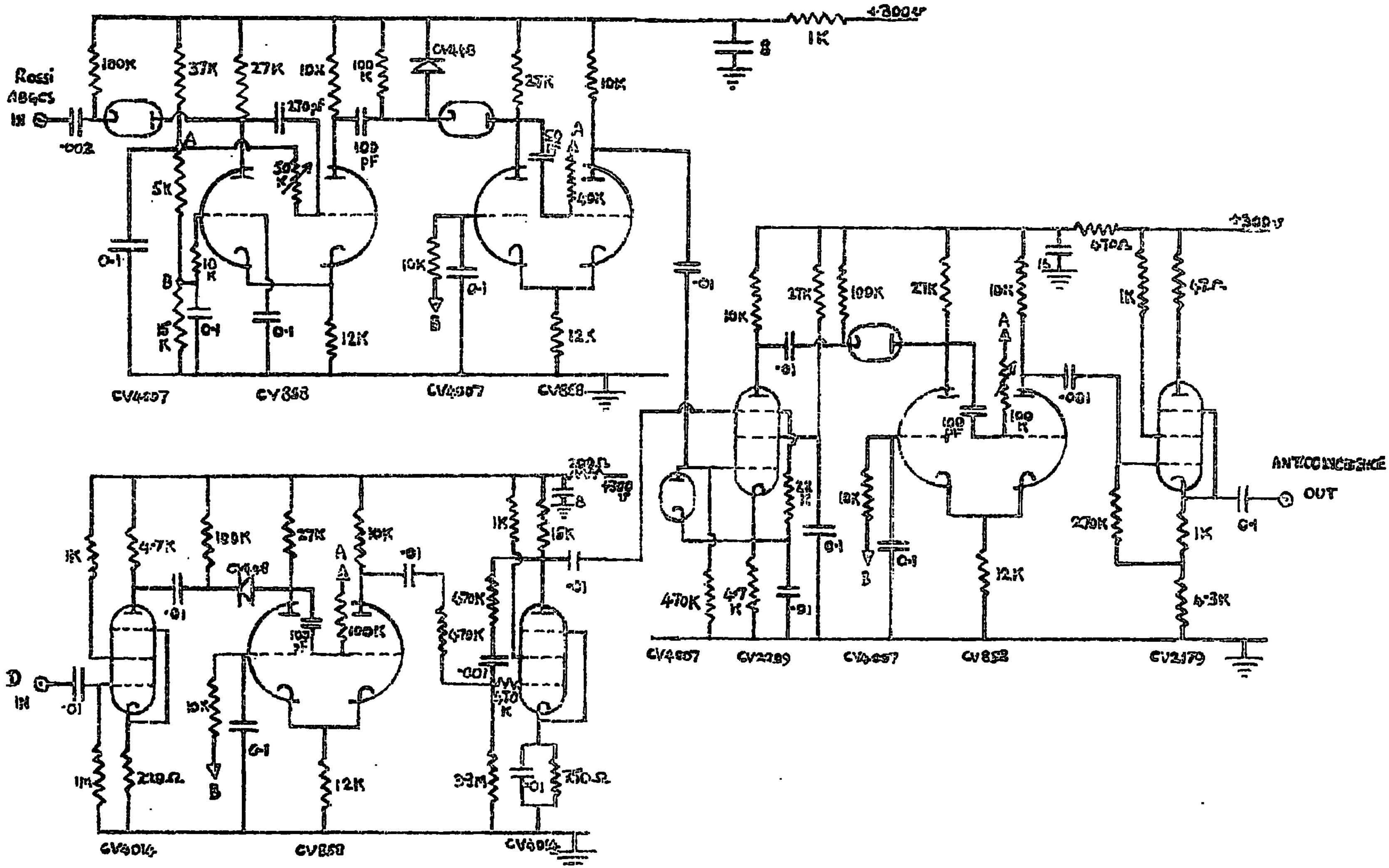

The Anticoincidence Unit

Fig. 3.1

from this stage is then taken to a second flip-flop (CV 858), a fast pulse generator. From there the positive output pulse is taken to the control grid of the gating valve (CV 2209).

Pulses from Geiger counter tray D are amplified and then lengthened by means of a flip-flop (CV 858), to 18 microseconds. The positive output from this is then taken through an inverter stage (CV 4014) to the suppressor grid of the gating valve.

The gating valve is normally almost cut off due to the high value of grid bias resistor used (4.7 KΩ). If a pulse from tray D arrives at the gating valve in coincidence with the pulse from the Rossi circuit, it remains non-conducting due to the ~60 volt negative pulse applied to the suppressor grid. If, however, there is no pulse from tray D, the gating valve conducts when the Rossi coincidence pulse is applied to it. The output pulse is taken through a flip-flop pulse shaper (CV 858) to a cathode follower output stage (CV 2179). The output pulse is 15 microseconds long and 100 volts positive, being used to trigger the flash-tube pulsing circuits and camera cycling system.

3.4 The Experimental Arrangement (P series)

A diagram of the apparatus is shown in Fig. 3.2. The absorbing material used in this experiment was the lead in the neutron monitor, with the addition of an 11 cm layer of lead below the neutron monitor.

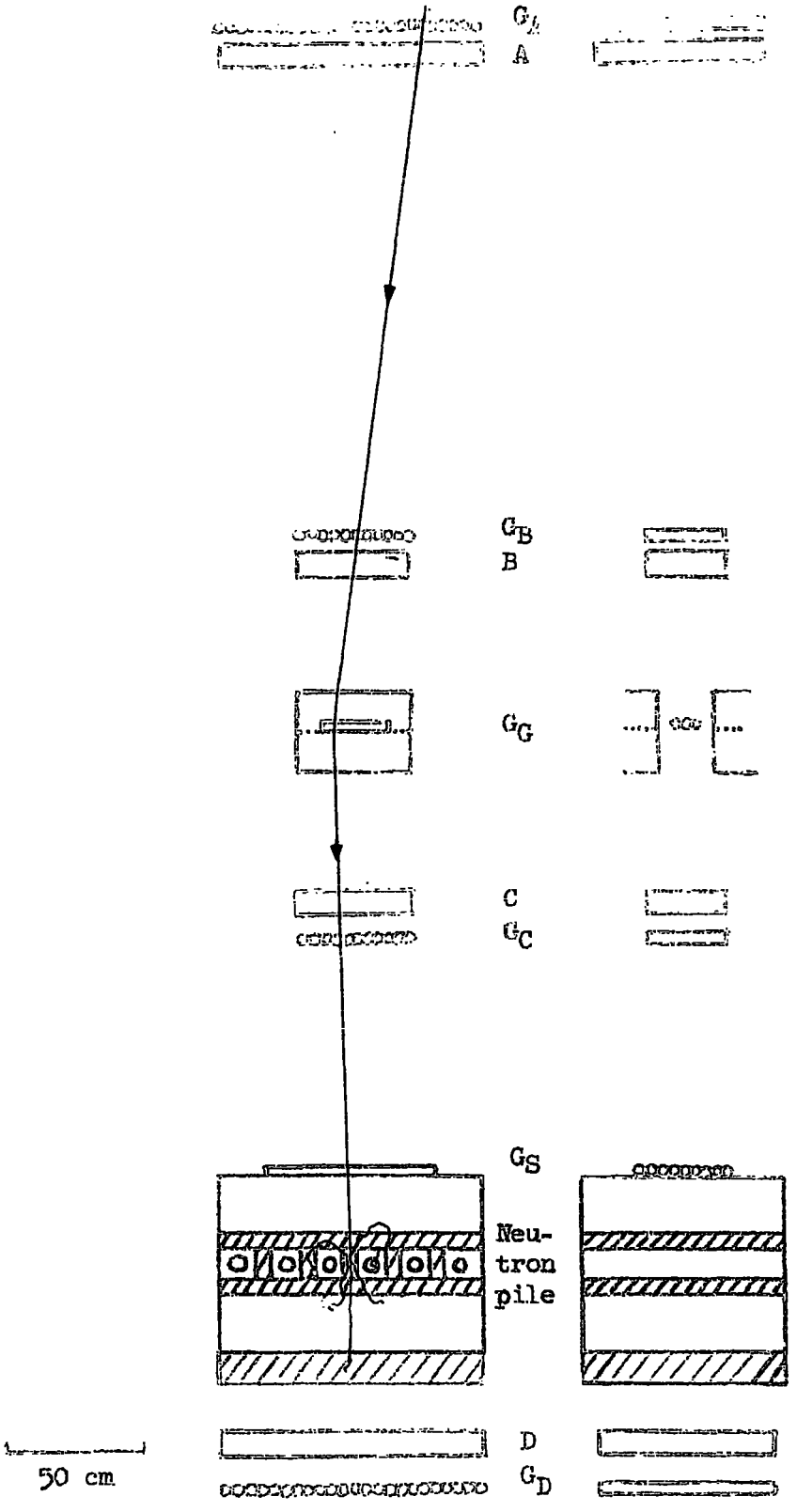

The Spectrograph and Neutron Pile (H, S and P Series)

Fig. 3.2

The lead in the neutron monitor consisted of two layers, one above and one below the neutron counters, each layer being 5 cm thick, and 12 cm thick blocks of lead between the neutron counters. The average thickness of lead in the neutron pile was 13.2 cm and the total average thickness of lead absorber was 24.2 cm. This thickness of absorber was such that muons with momenta less than 420 MeV/c and protons with momenta less than 1.2 GeV/c were stopped by ionization loss.

There are several measurements of the interaction length of high energy protons in lead. Ashmore et al. (1960) working at CERN with 24 GeV/c protons in lead found the absorption cross-section to be 1760 mb, which is geometrical with R_o = 1.26 fermis. Kocharian et al. (1959) working at 3200 metres above sea-level with a magnetic spectrograph obtained a cross-section of 1850 $\pm$ 260 mb for protons with momenta 4 - 8 GeV/c and 1770 $\pm$ 360 for momenta >8 GeV/c in lead. The value calculated for the interaction length for protons in lead from the optical model (Appendix 4) with a nucleon-nucleon cross-section of 40 mb is 16 cm which is not inconsistent with the measured cross-sections above. Therefore, taking this value of 16 cm of lead as the best estimate, the absorbing layer was 1.51 interaction lengths in thickness, giving a probability for interaction of 0.78.

The magnet was operated at a mean current of 11.3A giving $\int H d\ell = 1.59.10^5 \Gamma.cm$ and a maximum detectable momentum of ~45 GeV/c, using the "track simulator" for the measurements of track locations. The total running time of the experiment was 289.3 hours.

The tray of Geiger counters, S, immediately above the neutron pile consisted of nine 60 cm long counters (20th Century, G60) with their axes at 90°. to the magnetic field and in contact with each other. The counters were hodoscoped, in four groups. The first group consisted of the three counters at the centre of the tray and the other groups comprised pairs of counters which were equidistant from the centre of the tray. The tray was positioned symmetrically, in both planes, with respect to the flash-tube array at level D.

The Geiger counter tray at level D was operated in anticoincidence with the trays at levels A, B, C, G and S.

On receiving a pulse from the anticoincidence unit, the hodoscope unit illuminated a neon bulb corresponding to the group of counters in tray S through which the particle had passed. The illuminated neon bulbs were photographed by the camera used for arrays A and B. The hodoscope arrangement allowed particles to be rejected which would have passed too near to the edge of flash-tube array D in the back plane.

3.4.1 Scattering in the Absorber

The maximum thickness of lead in the neutron pile was 22 cm and the minimum 10 cm. Although non-vertical particles could pass through intermediate amounts of lead, it has been shown that in the particular case of absorber geometry used in this experiment, the average value for scattering in the pile is given accurately by taking a weighted mean of the scattering in the maximum and in the minimum thickness. The weighting factors are given by the areas presented to particles passing through the spectrograph by the different thickness of absorber.

The displacements in the particle trajectory at the measuring level in flash-tube array D due to scattering in the neutron pile and in the layer of lead below the pile were calculated as a function of momentum, from values given by Lloyd and Wolfendale (1957) and these were added in quadrature. The loss of energy by the particles in the absorber was taken into account using the range-momentum values given by Sternheimer (1960). For the momentum range covered by the present experiment, the r.m.s. projected displacement, s, in particle trajectories at the measuring level in array D is given to a good approximation by:-

$$\log_e s = 9.88 - 1.129 \log_e p \qquad 3.1a$$

where p is the particle momentum in units of MeV/c and s is in

units of 0.8 cm

or alternatively:-

$$\log_e s = 1.129 \log_e \phi + 5.51 \qquad 3.1b$$

where ϕ is the angular deflection of the particle in radians with $\int H d\ell = 1.59.10^5 \Gamma.cm$ and s is in units of 0.8 cm.

3.4.2 Acceptance Criteria

a) Deflection Plane

From the measurements of the positions of each particle trajectory at levels A, B and C, the position at level D through which the trajectory would have passed in the absence of absorbing material was calculated. Particles which had passed nearer to the edge of the flash-tube array than one and a half times the r.m.s. displacement at that level due to scattering were rejected.

b) Back Plane

For each hodoscope group of counters in tray S the momentum was calculated below which particles could pass nearer to the edge of flash-tube array D in the back plane than one and a half times the r.m.s. scattering displacement. These momentum values are given in Table 3.1. The hodoscope groups were numbered from the centre of the tray outwards.

Hodoscope Group Number, h	Minimum Momentum GeV/c	Maximum Angular Deflection for $\int Hd\ell =$ $1.59.10^5$ Γ. cm, radians
1	0.474	0.100
2	0.64	0.074
3	0.93	0.051
4	1.90	0.025

Table 3.1

Particles with momentum less than the value given in Table 3.1 for the hodoscope group through which they had passed, were rejected.

3.4.3 Analysis of the Data

The trajectory positions of a, b and c at the measuring levels in flash-tube arrays A, B and C were measured by the projection method for all events in which no track was observed in flash-tube array D. The hodoscope group number, h, of the tray S neon bulb which was illuminated was also noted. The data a, b, c and h were then transferred to computer tape.

The Ferranti Pegasus Computer of the Durham University Computing Laboratory was then used to calculate the angular deflections of the particle trajectories and to select those which would have passed through the permitted area of array D.

For each set of data the sequence of operations was as follows:-

a) The position of the trajectory at level D in the deflection plane, d_p, was calculated from a, b, and c.

b) The particle was rejected if d_p lay outside the limits of flash-tube array D.

c) The angular deflection, ϕ, was calculated.

d) The particle was rejected if ϕ was greater than the maximum acceptable angle for the observed value of h. (See Table 3.1).

e) The distance of d_p from the edge of array D was calculated.

f) The r.m.s. displacement of the particle trajectory at measuring level D was calculated using equation 3.1b.

g) The distance of d_p from the edge of array D was divided by the r.m.s. scattering displacement and if the result was less than 1.5, the particle was rejected.

h) For particles not rejected, ϕ, d_p, a and h were printed out.

a and h were used to identify the selected particles on the original data sheets. The positions of the trajectories of particles with $\phi < 0.01$ radians were remeasured using the "track simulator" method, d_p being used to set the angle of the cursor for the track in the lower half of the spectrograph.

Positively and negatively charged particles were divided separately into histograms, each distribution covering the deflection range of 0.001 - 0.074 radians. The number of negative particles in each histogram cell was multiplied by the positive-negative ratio for muons for the momentum interval covered by the cell and the result subtracted from the number of positive particles in the cell, giving the deflection distribution of protons which had been stopped by the absorber. This was then converted to a momentum distribution.

3.5 The Experimental Arrangement (AP series)

In this experiment, the absorption of particles in a 16.5 cm thick layer of lead, placed immediately above flash-tube array D, was studied. A tray S' of eight 60 cm long Geiger counters with their axes at 90° to the magnetic field and in contact with each other was operated above the absorber. This tray was positioned symmetrically above flash-tube array D and was operated in coincidence with the Geiger counter trays at levels A, B, G and C.

The magnet was operated at a mean current of 15.8 A, giving mean $\int Hd\ell = 2.21.10^5$ Γ.cm and the total running time was 180.7 hours.

In order to reduce the number of particles passing through the Geiger counter tray at level D and failing to discharge one of the counters in it, an additional layer of twenty four 60 cm long Geiger counters, D', was operated above the existing counters at that level. The new counters were staggered with respect to the original counters by half the spacing of the counters.

The double layer of Geiger counters DD' was operated in anticoincidence with trays A, B, G, C and S'.

A diagram of the apparatus is shown in Fig. 3.3.

3.5.1 The Absorbing Layer

The 16.5 cm thick layer of lead was sufficient to stop muons with momenta less than 320 MeV/c and protons with momenta less than 1 GeV/c by ionisation loss. The size of Geiger counter tray S' was chosen so that muons with momenta greater than 500 MeV/c which had passed through Geiger counter trays A, B, G, C and S' could not pass nearer the edge of flash-tube array D in either plane, than twice the r.m.s. displacement at that level due to scattering in the absorber.

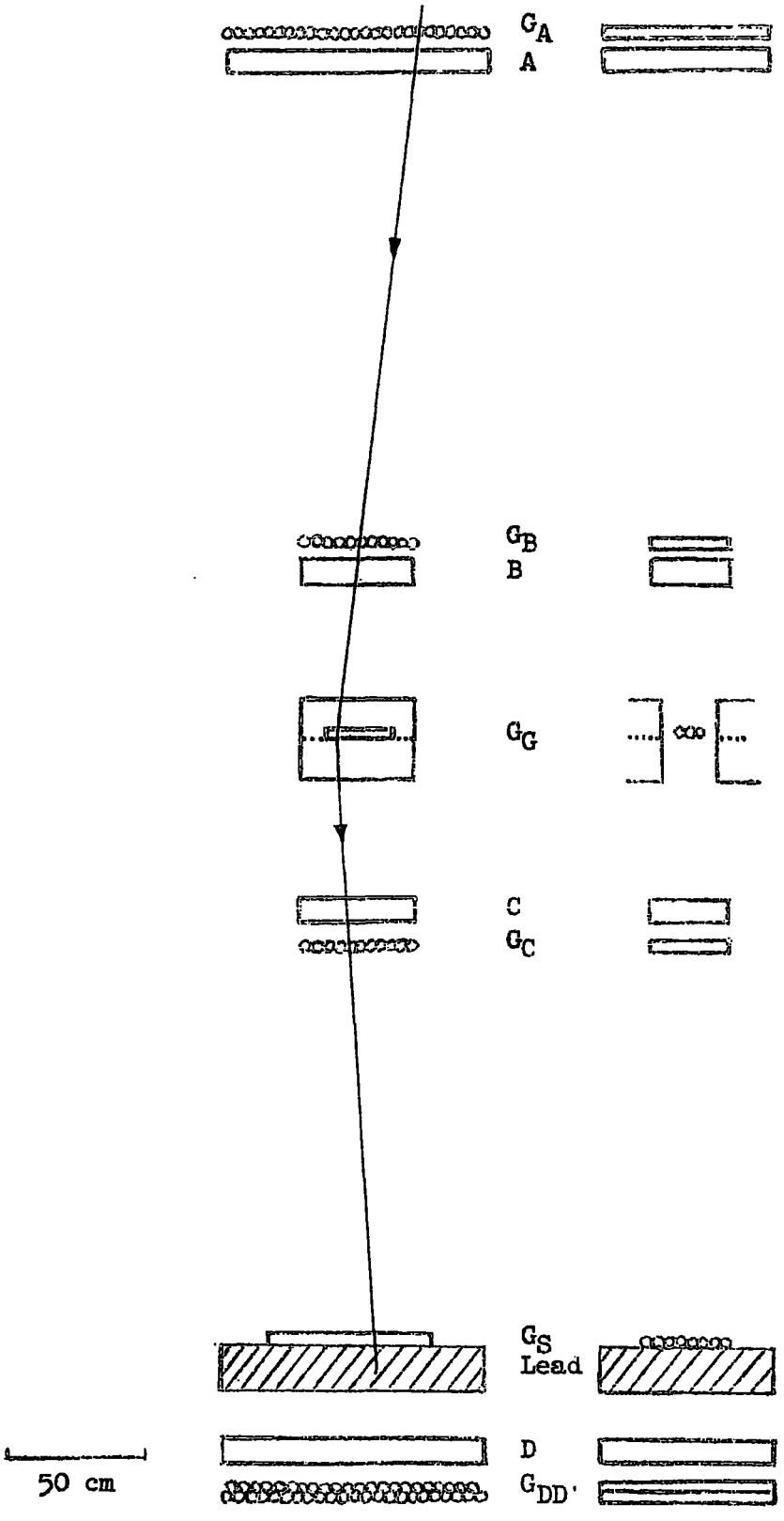

The Spectrograph and Lead Absorber (AP Series)

Fig. 3.3

With an interaction length of 16 cm for protons in lead, see Section 4, the thickness of the absorber was 1.03 interaction lengths, giving a probability of 0.641 for interaction in the absorber.

3.5.2 Acceptance Criteria

In the present experiment, the scattering displacements in particle trajectories at measuring level D were much smaller than in the P series as the absorbing layer was much nearer to level D. For 500 MeV/c muons, the r.m.s. displacement was 5.5 cm. All particles were restricted by tray S' to pass through flash-tube array D at least 11 cm from the edge. No further restriction to the acceptance was required and so the Geiger counters in tray S' were not hodoscoped.

All particles were accepted which had given single tracks in flash-tube arrays A, B and C and no track in D.

3.5.3 Analysis of the Data

The locations of particle trajectories at measuring levels A, B and C were found by the "projection method" for those events in which there was no track in array D. The displacements, Δ, of each trajectory was calculated and the results were divided into histogram cells, positive and negative particles being treated separately. The numbers of negative particles were multiplied by

the appropriate values of the positive-negative ratio for muons and the results subtracted from the number of positive particles in the corresponding displacement interval. Finally, the distribution of the positive excess of stopping particles (protons) as a function of displacement was converted to a distribution as a function of momentum.

3.6 Scattering in the Spectrograph

In passing through the spectrograph, particles are scattered by the Geiger counter trays and flash-tube arrays. Particles of a unique momentum will thus have a Gaussian distribution of deflections centred on the "theoretical" magnetic deflection. The effect on the deflection distribution is to smooth out any variation of particle intensity with respect to momentum which may be present.

For the spectrograph using flash-tube arrays A, B and C for measurements of particle deflections, the magnetic displacement of a particle trajectory, Δ, over an arm of 184.3 cm is given by:-

$$\Delta = \left(1 + \frac{\ell_2}{\ell_3}\right)(a + a_o) - \left(1 + \frac{\ell_1 + \ell_2}{\ell_3}\right)(b + b_o) + \frac{\ell_1}{\ell_3}(c + c_o) \qquad 3.2a$$

$$= 2.023a - 5.095b + 3.072c - 68.77 \qquad 3.2b$$

where Δ is in units of 0.8 cm and a, b and c are the positions of the trajectory in flash-tube arrays, A, B and C respectively, and

a_o, b_o, c_o are the distances of the zeros in arrays A, B and C, from some arbitrary vertical reference line, Fig. 2.6.

The effect on the calculated value of Δ due to scattering at any level can be found by calculating the effect on the measurements of a, b and c and substituting these in equation 3.2b.

If a particle is scattered through an angle ϕ_A in Geiger counter tray and flash-tube array A this will give a displacement in the location of the trajectory at level B of $\ell_1 \cdot \phi_A = \delta B_A$ and at level C of $(\ell_1 + \ell_2 + \ell_3)\phi_A = \delta C_A$. Then the error in Δ, $\delta\Delta_A$, due to scattering at level A is given by:-

$$\delta\Delta_A = -\left(1 + \frac{\ell_1 + \ell_2}{\ell_3}\right)\delta B_A + \frac{\ell_1}{\ell_3}\,\delta C_A$$

$$= -\left(1 + \frac{\ell_1 + \ell_2}{\ell_3}\right)\ell_1\,\phi_A + \frac{\ell_1}{\ell_3}\,(\ell_1 + \ell_2 + \ell_3)\phi_A = 0$$

i.e. any scattering at level A does not affect the measured value of Δ but merely changes the apparent angle of incidence of the particle.

If $\langle\phi_{B.f.}\rangle$, $\langle\phi_{B.G.}\rangle$ and $\langle\phi_G\rangle$ are the r.m.s. projected angles of scattering in flash-tube array B, Geiger counter trays B and Geiger counter tray G respectively then the r.m.s. errors in the measured values of Δ are given by:-

$$\langle \delta\Delta_{B.f.} \rangle = \frac{\ell_1}{\ell_3} \langle \phi_{B.f.} \rangle (\ell_2 + \ell_3) \qquad 3.3a$$

$$\langle \delta\Delta_{B.G.} \rangle = \frac{\ell_1}{\ell_3} \langle \phi_{B.G.} \rangle (\ell_2' + \ell_3) \qquad 3.3b$$

$$\langle \delta\Delta_{G} \rangle = \frac{\ell_1}{\ell_3} \langle \phi_{G} \rangle . \ell_3 \qquad 3.3c$$

The total r.m.s. error in the measured values of Δ due to scattering in the spectrograph $\langle \delta\Delta \rangle$ is then given by:-

$$\langle \delta\Delta \rangle^2 = \langle \delta\Delta_{B.G.} \rangle^2 + \langle \delta\Delta_{B.f.} \rangle^2 + \langle \delta\Delta_{G} \rangle^2 \qquad 3.4$$

Rossi (1952) gives for the r.m.s. projected angle of scattering $\langle \phi_s \rangle$ in a material of thickness t measured in radiation lengths, ignoring energy loss in the scattering medium,

$$\langle \phi_s \rangle = \frac{1}{\sqrt{2}} \frac{K . t^{1/2}}{p\beta} \quad \text{radians} \qquad 3.5$$

where K is a constant equal to 21 MeV/c, p is the momentum of the particle measured in MeV/c and βc its velocity. Hence $\langle \phi_s \rangle = \frac{0.01482}{p\beta} . t^{1/2}$ with p in units of GeV/c.

The Geiger counter trays have a mean thickness of 1.008 g.cm^{-2} of pyrex glass with radiation length 32.34 g.cm^{-2} giving $t^{1/2} = 0.176$ and hence

$$\langle\phi_{B.G.}\rangle = \langle\phi_G\rangle = \frac{2.608}{p\beta} \cdot 10^{-3} \text{ radians} \qquad 3.6$$

For the flash-tube arrays, the amount of material in the electrodes is negligible compared with the mean thickness of glass, 4.50 g.cm^{-2}. The radiation length for the glass used for the flash-tubes is 28.86 g.cm^{-2} giving $t^{1/2} = 0.395$.

Hence

$$\langle\phi_{B.f.}\rangle = \frac{5.85}{p\beta} \cdot 10^{-3} \text{ radians} \qquad 3.7$$

Substituting these values in expressions 3.3a, b and c and adding the results in quadrature gives

$$\langle\delta\Delta\rangle = \frac{3.02}{p\beta} \text{ in units of } 0.8 \text{ cm.} \qquad 3.8$$

For the AP-series, the magnetic displacement, Δ, in units of 0.8 cm is related to the momentum of a particle measured in GeV/c by:-

$$\Delta = \frac{15.27}{p,} \qquad 3.9$$

so that the ratio of r.m.s. scattering displacement to magnetic displacement for this series was:-

$$\frac{\langle\delta\Delta\rangle}{\Delta} = \frac{0.198}{\beta} \qquad 3.10$$

The measured displacement distribution was corrected for scattering as follows.

a) The effect of scattering on the observed distribution was calculated.

b) The ratio of the original height of the displacement distribution to the scattered height was found as a function of displacement.

c) The observed distribution was multiplied by the factors found in b).

d) The effect of scattering on the distribution given by c) was calculated and the ratio of the heights before and after scattering found as a function of displacement.

e) The observed displacement distribution was multiplied by the factors found in d).

Operations d) and e) were then repeated until the ratios of unscattered to scattered heights reached limiting values. It was necessary to perform operations d) and e) five times. The measured numbers of protons in each displacement interval in the AP-series were then multiplied by the appropriate mean values of the unscattered to scattered height ratios obtained by the above method.

The effect of scattering on a given distribution was calculated in the following manner. The distribution was divided into twenty-four cells and the contribution from each of these which, due to scattering, would appear in one chosen cell, was calculated. The total was found, giving the scattered height at that point. The effect of scattering was calculated for six points on the distribution. Particles from each cell were assumed to have a Gaussian distribution about the centre of the cell with standard deviation given by equation 3.10.

From the P-series, $\Delta = \frac{11.3}{p}$, where Δ is the magnetic displacement measured in units of 0.8 cm and p is the particle momentum in GeV/c, so that from equation 3.8:-

$$\frac{\langle \delta\Delta \rangle}{\Delta} = \frac{0.267}{\beta} \qquad 3.11$$

The effect of scattering on the AP-series displacement distribution corrected for scattering was calculated. The ratios of unscattered to scattered heights found by this method gave the correction factors to be applied to the P-series results.

CHAPTER 4

THE NEUTRON MONITOR TECHNIQUE

4.1 Introduction

When a nuclear interaction takes place, the nucleus is left in an excited state and subsequently emits low energy evaporation protons and neutrons. The evaporation neutrons can be detected by a neutron monitor - an array of BF_3 filled proportional counters in a paraffin moderator to reduce the neutrons to thermal or epithermal velocities.

In any given momentum interval, the mean number of neutrons produced by cosmic ray proton interactions can be found from the difference in the observed multiplicity distributions of neutrons from positive and negative cosmic ray particles in that momentum range. From the differences in the numbers of neutrons observed from positive and negative particle interactions and knowing the mean number of neutrons produced by a proton interaction as a function of momentum, the momentum spectrum of protons can be calculated.

4.2 The Experimental Arrangement

A standard I.G.Y. neutron monitor was operated above flash-tube array D. An additional tray of Geiger counters, S, was operated above the monitor. This consisted of a single layer of

nine 60 cm long counters (20th Century, G60) in contact with each other and with their axes at 90^{o} to the magnetic field. Events were photographed in which there was coincidence between the Geiger counter trays at levels A, B, G, C and S and one or more neutrons detected within a predetermined time interval after the Geiger counter coincidence had been recorded.

Two experiments were performed with the apparatus as described. The first, denoted as the S-series, had a total running time of 1023 hours. The magnet was operated at a mean current of 11.4 A giving $\int Hd\ell = 1.60 \times 10^{5}$ Γ.cm. In this experiment neutrons were required to be detected between 20 and 700 microseconds after the Rossi coincidence pulse. The second experiment, H-series, had a running time of 926 hours. The mean magnet current was 59.6 A, giving $\int Hd\ell = 6.11.10^{5}$ Γ.cm and neutrons were required to be detected between 20 and 250 microseconds after the Rossi coincidence pulse to avoid spurious records arising from pick-up by the neutron counters from the high voltage pulse applied to the flash-tube electrodes. The total counting rate of the six neutron counters in the pile was ~5000/min and in order to reduce the rate of chance coincidences between the 5-fold Geiger counter coincidence and a detected neutron the 700 or 250 microseconds maximum times for detecting neutrons after the Rossi coincidence pulse were imposed.

The number of neutrons detected was displayed by means of a trochotron register tube which showed countsup to nine and a neon bulb which was illuminated when ten or more neutrons had been detected. The total number of neutrons detected was the sum of these two, the maximum count which could be recorded being nineteen. The neon bulb and trochotron register tube were photographed by means of the camera used to photograph flash-tube arrays C and D.

Shutters were fixed in front of both of the spectrograph cameras. The sequence of operations when a 5-fold coincidence was recorded between Geiger counters at levels A, B, G, C and S was as follows.

1) Paralysis was applied to the Rossi coincidence circuit.
2) A high voltage pulse was applied to the flash-tube electrodes.
3) After 20 microseconds, a gate was opened and the number of neutrons detected in the pile during the following 680 microseconds (S-series) or 230 microseconds (H-series) was recorded and displayed for $\sim\frac{1}{2}$ second.
4) If no neutrons were recorded operations 5 and 6 were omitted. Nothing was recorded photographically.

5) If one or more neutrons were detected, five more pulses were applied to the flash-tube electrodes starting 6 milliseconds after the first pulse and at 6 millisecond intervals. The camera shutters were opening in about 12 milliseconds and the event photographed.

6) The reference bulbswere illuminated, the shutters closed and the cameras wound on.

7) The paralysis was removed from the Rossi coincidence circuit.

This is shown diagramatically in Fig. 4.1 and the time sequence for events in which neutrons were recorded is shown in Fig. 4.2.

This technique uses the fact that the flash-tubes have the property of being able to store information; a tube which has flashed has a very high probability of flashing again if a second pulse is applied across it after a short time. With the period between pulses used in the present experiments, 6 milliseconds, the probability of after-flashing is 95%, Coxell and Wolfendale (1960).

The efficiency of the neutron pile was measured using a calibrated radium-beryllium neutron source. This was placed at different locations within the pile and the counting rates noted. The weighted mean efficiency with infinite gate was

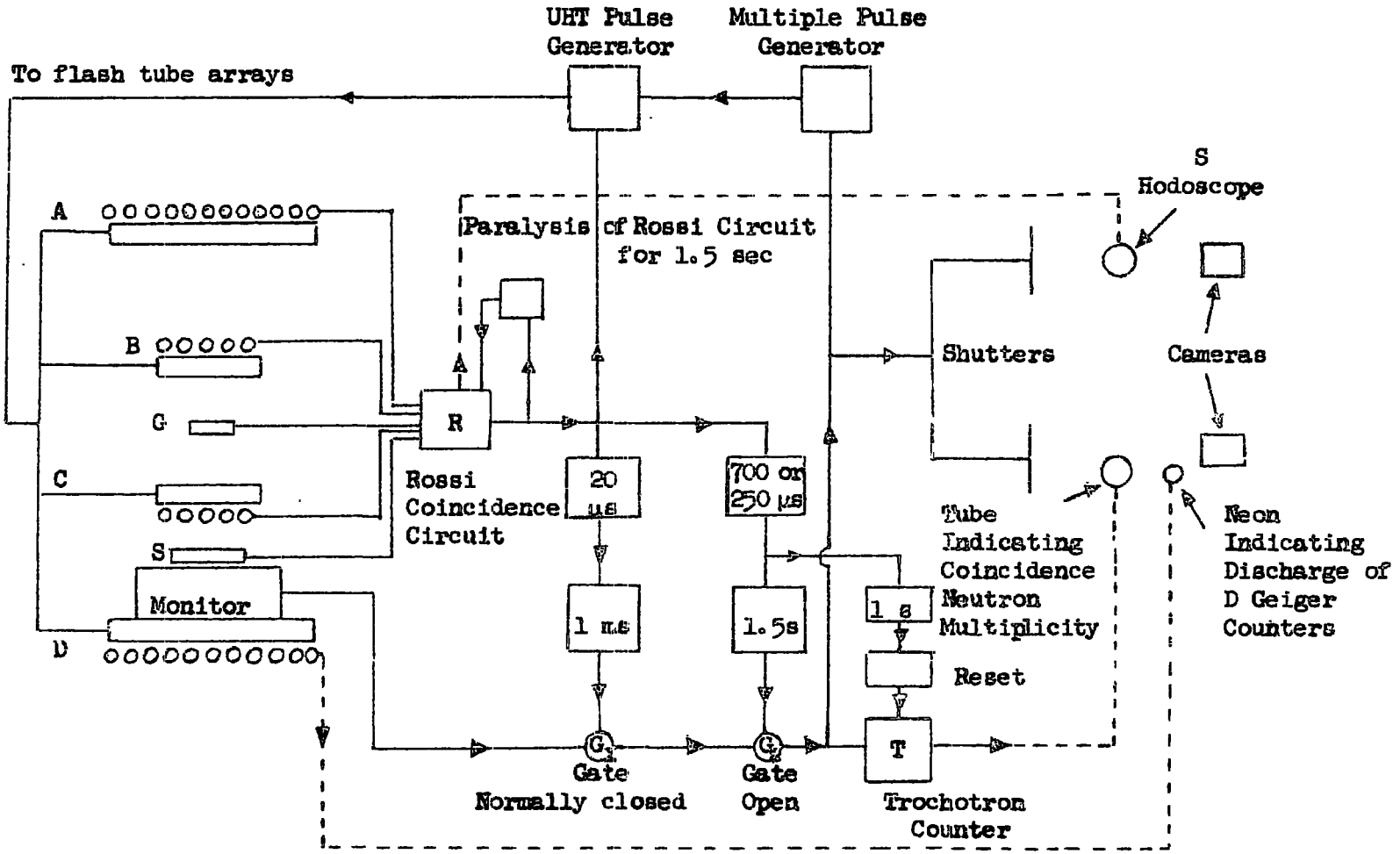

Block Diagram of the Experimental Arrangement (H and S series)

Fig. 4.1

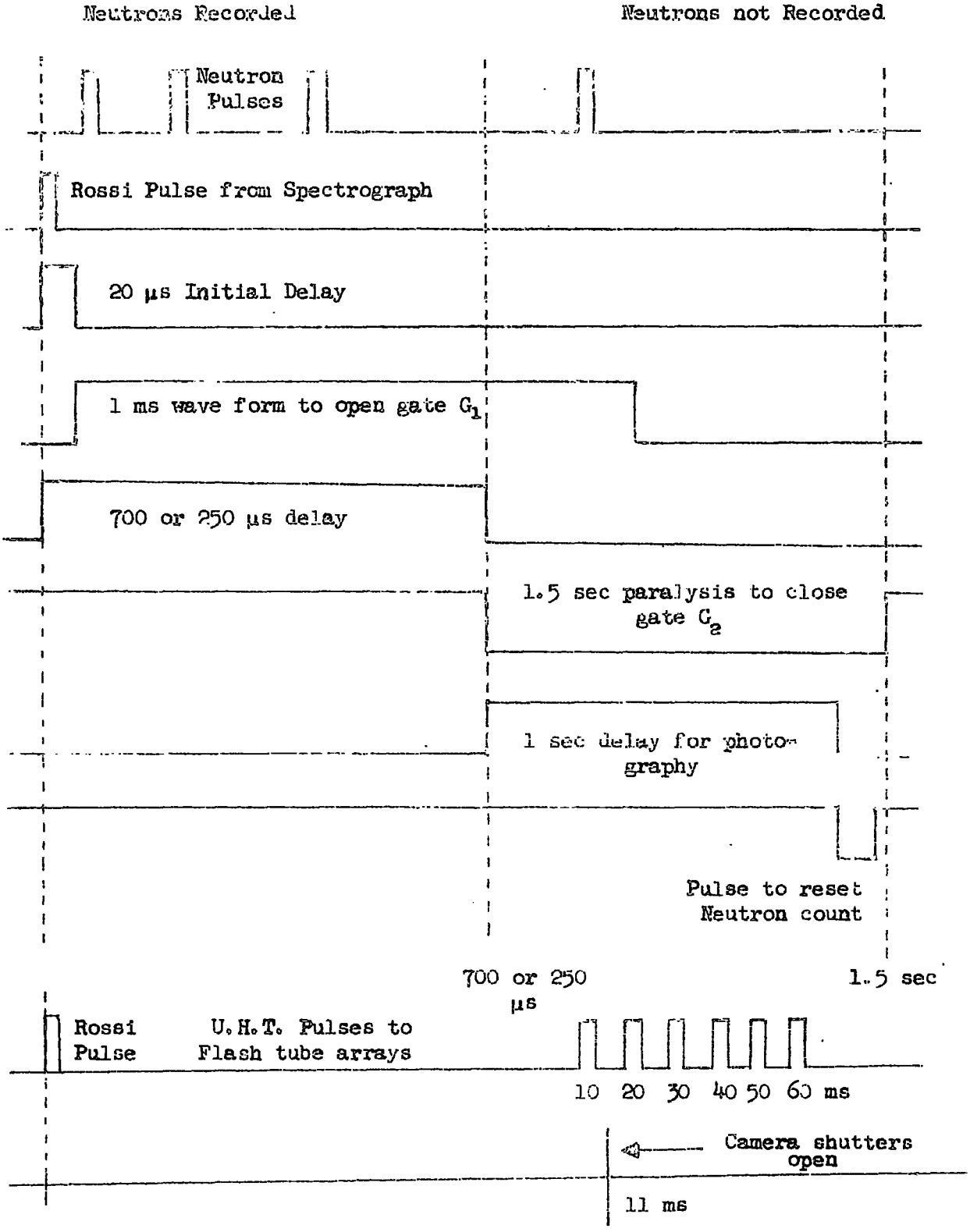

Time Sequence of the Experimental Arrangement
(H and S Series)
Fig. 4.2

found to be 3.03%. With the gate interval of 680 microseconds used for the S-series, the efficiency was 2.87% and with the gate interval of 230 microseconds used in the H-series the efficiency was 2.13%. These figures were calculated assuming that the rate of detection of neutrons after an interaction falls exponentially with a mean life of 250 microseconds (Geiger, 1956), after an initial increase during approximately the first 5 μs after an interaction. The momentum range covered by the S-series was 0.7 - 50 GeV/c and by the H-series was 0.7 - 150 GeV/c.

4.3 The Neutron Monitor

The neutron monitor is shown in Fig. 4.3. Six 54 cm long, 5.0 cm diameter neutron counters (20th Century, 40EB70/50G) were used. These were enclosed individually in paraffin wax moderator. The producer lead was positioned around the moderator and the whole was shielded from external neutrons by 20 cm thick blocks of paraffin wax. The monitor was positioned symmetrically above flash-tube array D with the axes of the neutron counters parallel to the direction of the magnetic field.

The neutron counters consist of proportional counters filled with boron trifluoride (BF_3) enriched in B_{10}.

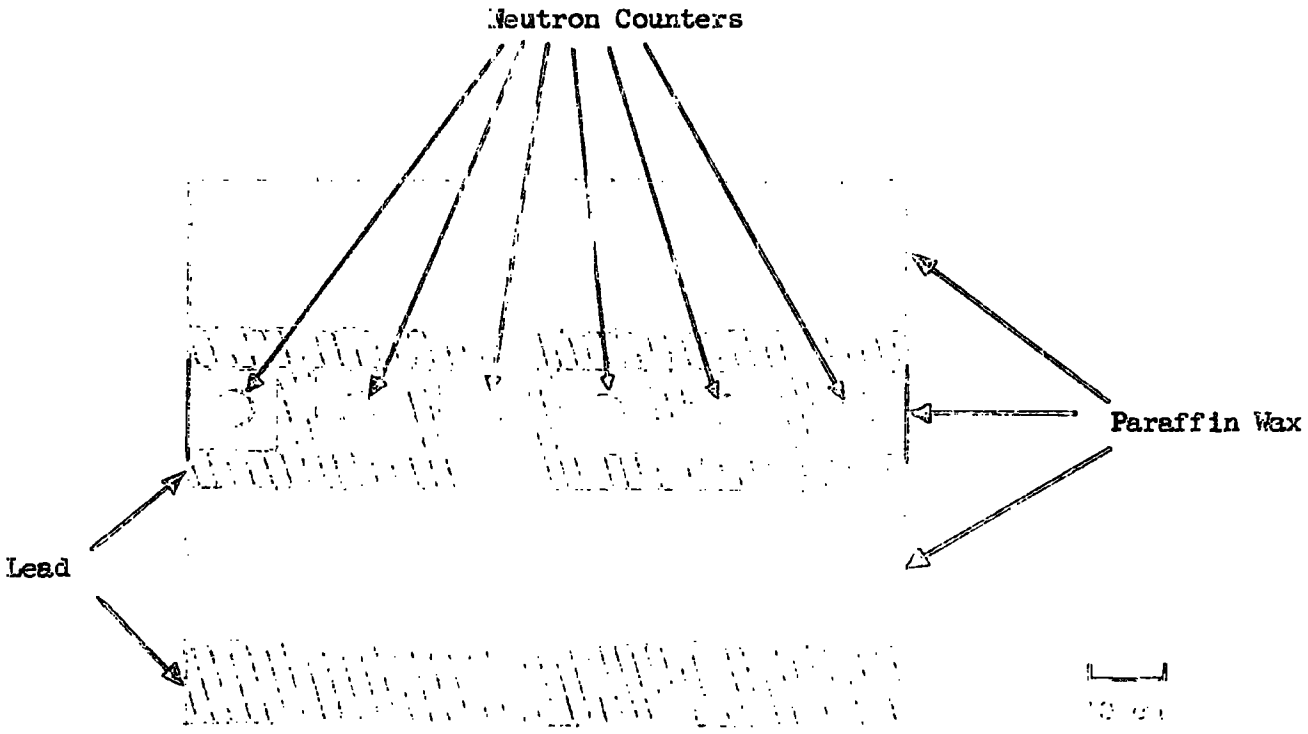

The Neutron Monitor and Lead Absorbing Layer

Neutrons are detected by the reaction:-

$$n + B_5^{10} \rightarrow Li_3^7 + He_2^4$$

which has a high cross-section for thermal and epithermal neutrons. A large amount of ionization is produced by the α-particle and Lithium nucleus, the total energy dissipated being ~2.4 MeV. It is therefore possible to differentiate between pulses from neutron interactions and pulses from singly ionizing particles passing through the counters.

The counters were operated with an E.H.T. of -3.0 KV stable to better than 1%. The electronic circuits used to count and record the numbers of neutrons recorded by the monitor within the required gating interval have been described by Hughes (1961). A block diagram of this apparatus is shown in Fig. 4.4.

4.4 The Multiple Pulser

The circuit diagram of the multiple pulsing unit is shown in Fig. 4.5. This unit was required to send a pulse to the high voltage flash-tube pulsing unit each time a Geiger counter coincidence occurred, followed by give more pulses if a neutron was detected during the gate interval and also in this case to apply a pulse to the camera shutter relays.

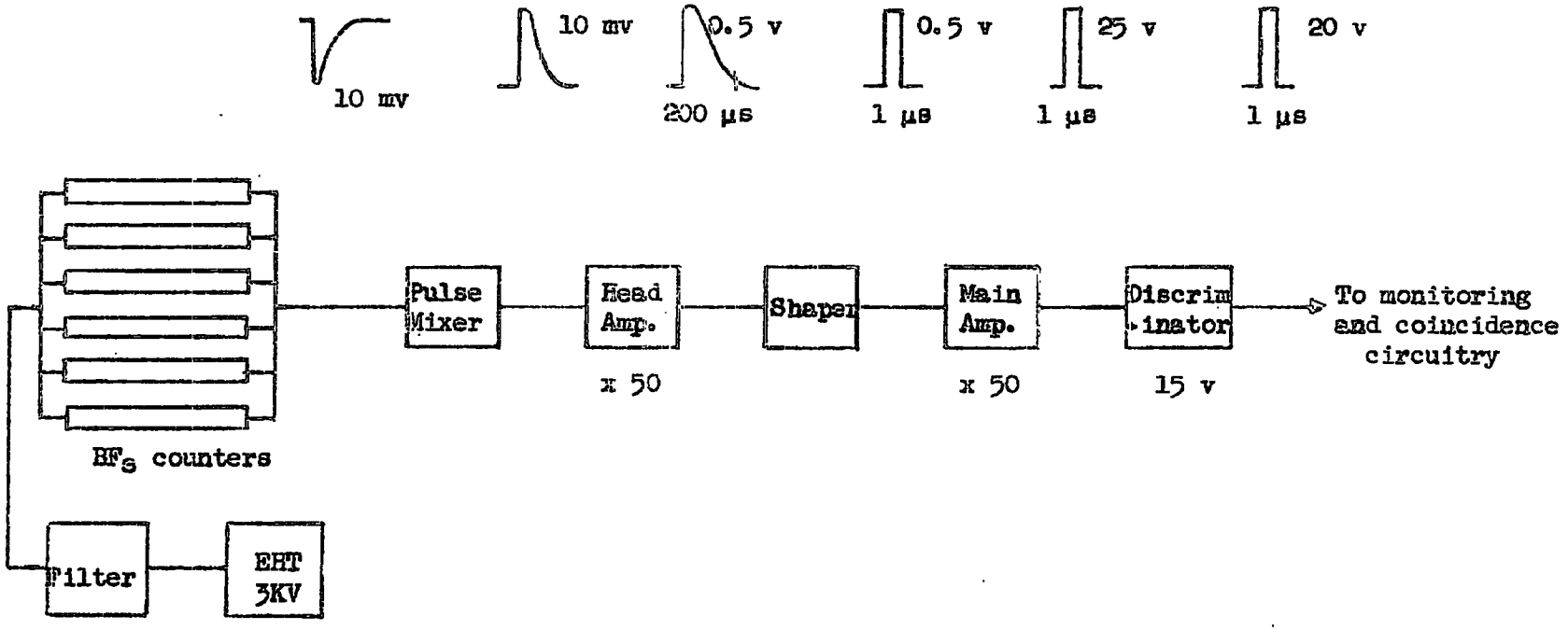

Block Diagram of Neutron Recording Circuitry

Fig. 4.4

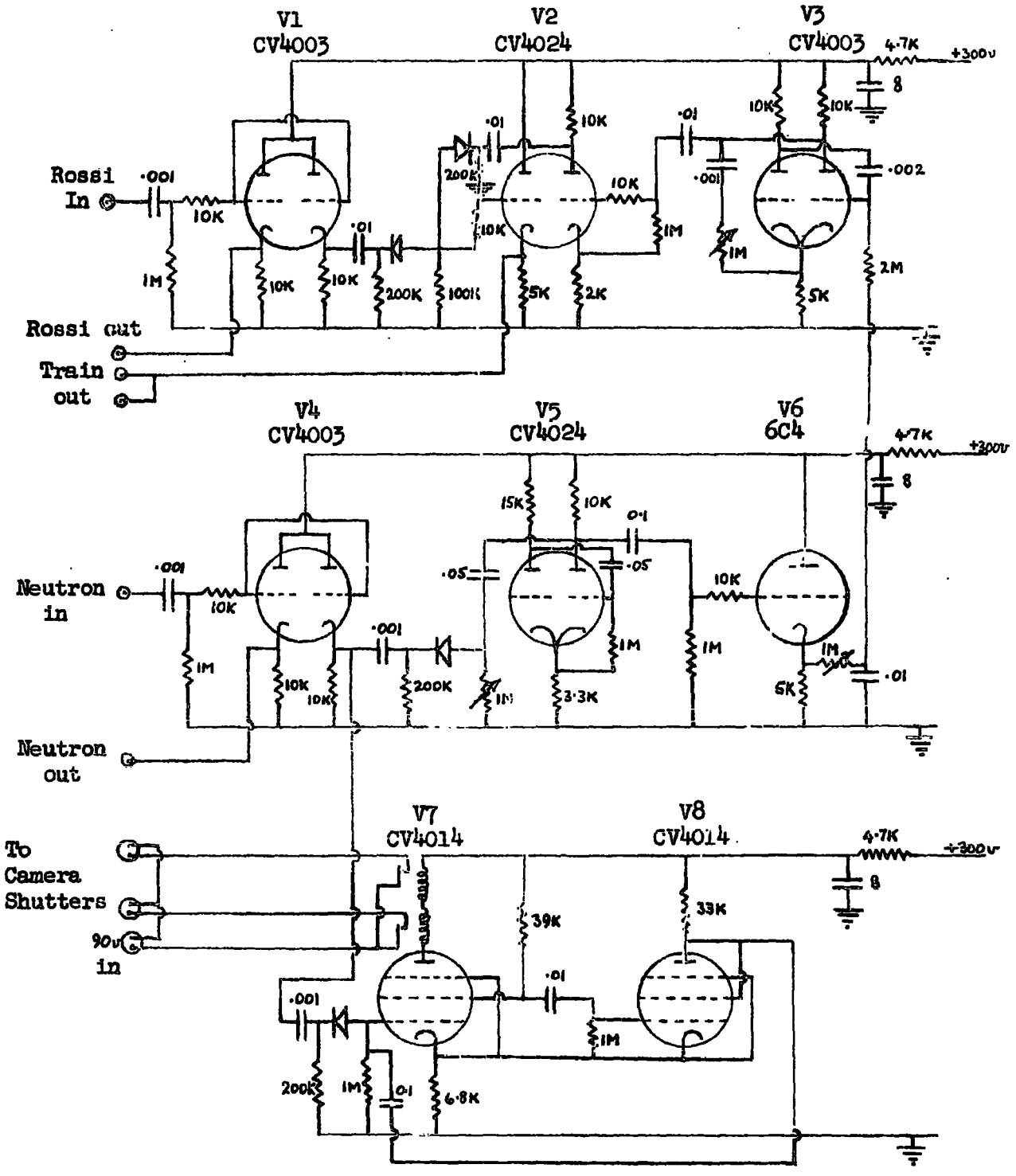

The Multiple Pulsing Unit

Fig. 4.5

Coincidence pulses from the Rossi circuit are split by two cathode followers (Valve V_1). One output opens gate I in the neutron recording circuitry and the other passes via the mixing valve V_2 to the H.V. pulsing unit. Pulses from the neutron circuitry which show that one or more neutrons have been detected in the gate interval are applied to two cathode followers (valve V_4). The output from one of these triggers the "cycling system", i.e. illuminates the reference bulbs in each flash-tube array and after a short mechanical delay winds on the cameras. The output from the other cathode follower operates a unistable multivibrator, valve V_5. The output from this, taken via a cathode follower V_6, biasses valve V_3 so that it becomes a free-running multivibrator. The length of time for which V_3 is allowed to oscillate is adjustable by means of a potentiometer in the V_5 stage. The train of pulses from V_3 is inverted by V_2 and passes from there to the H.V. pulsing unit. The separation of the pulses in this train can be adjusted by varying the time constant of V_3. The camera shutters are operated by valves V_7 and V_8 arranged as a unistable multivibrator with a relay as the anode load of V_7 which is normally biassed off. A pulse taken from V_4 triggers the multivibrator and causes the camera shutters to be opened.

4.5. The Analysis of the Data

Approximately 50% of the photographs taken in both the S and H series were of events in which there was a shower in one or more of the flash-tube arrays A, B and C. These events were rejected. For the remaining events, the observed neutron multiplicity and the number of tracks in flash-tube array D were noted. The trajectory positions at levels A, B and C were measured by the projection method. From these measurements the angular deflection and also the position of the trajectory at the level of the neutron counters were computed for each event. Particles which would not have passed through the producer lead were rejected. The positions of particles which had deflections less than 0.01 radians were remeasured using the track simulator.

The events were of four types:-

1) Interactions of protons.
2) Interactions of positive or negative pions.
3) Interactions of positive or negative muons.
4) Chance coincidences between a 5-fold Geiger counter tray coincidence produced by a positive or negative muon and a detected neutron.

The behaviour of the protons was found from the difference in the observed results for positive and negative particles.

For each series particles were divided into momentum cells, positive and negative particles being treated separately. Within each cell the distribution in observed neutron multiplicity was found. The distribution in each momentum cell for negative particles was then multiplied by the appropriate positive-negative ratio for muons and the result subtracted from the distribution in observed neutron multiplicity for positive particles in the same momentum cell. This gave the distribution in observed neutron multiplicity from proton interactions in each momentum interval, assuming the positive-negative ratio for pions to be the same as that for muons at the same momentum.

4.6 The Mean Numbers of Neutrons Produced

As the efficiency of detecting neutrons is low, the probability of detecting m out of ν neutrons produced in an interaction follows a binomial distribution. If an exponential multiplicity spectrum is assumed for production of neutrons in an interaction of the form:-

$$I(\nu) = (e^{a} - 1)\, e^{-a\nu} \qquad 4.1$$

where $\sum_{1}^{\infty} I(\nu) = 1$ and a is a constant. Then, following Geiger, (1956),

$$R_m = Q \frac{(e^a - 1)\epsilon^m e^{-am}}{[1 - (1 - \epsilon)e^{-a}]^{(m+1)}} \qquad 4.2$$

and

$$\bar{\nu} = \frac{1}{1 - e^{-a}} \qquad 4.3$$

where R_m is the rate of observing m neutrons from an interaction

ϵ is the gate efficiency times the monitor efficiency with infinite gate

$\bar{\nu}$ is the mean number of neutrons produced in an interaction

Q is the rate of the interactions

From equation 4.3,

$$e^{-a} = 1 - \frac{1}{\bar{\nu}} \qquad 4.4$$

From equation 4.2 the mean number of neutrons observed in an interaction,

$$\bar{m} = \frac{\sum_{m=1}^{\infty} R_m \cdot m}{\sum_{m=1}^{\infty} R_m}$$

or

$$\bar{m} = \frac{1}{1 - \frac{\epsilon e^{-a}}{1-(1-\epsilon)e^{-a}}} \qquad 4.5$$

Substituting for e^{-a} from equation 4.4:-

$$\bar{m} = \frac{1}{1 - \frac{\epsilon(1-1/\bar{\nu})}{1-(1-\epsilon)(1-1/\bar{\nu})}}$$

$$= \bar{\nu}\epsilon + 1 - \epsilon$$

or

$$(\bar{\nu} - 1) = \frac{(\bar{m} - 1)}{\epsilon} \qquad 4.6$$

The mean numbers of neutrons produced were calculated using equation 4.6 from the observed neutron multiplicity distributions from protons for each momentum cell in both the S and H series. The results are given in Table 4.1.

Momentum Cell GeV/c	$\bar{\nu}$ S series	$\bar{\nu}$ H series
0.7-1.5	12.6 ± 1.5	11.65 ± 2.1
1.5-3.0	24.2 ± 2.4	21.0 ± 2.2
3.0-7.0	43.7 ± 5.1	36.1 ± 5.4
7.0-15	74.2 ± 15.7	56.4 ± 14.4
15 - 50	55.4 ± 21.1	157.5 ± 57.7
50 - 150	-	142.0 ± 110.0

Table 4.1

The intensities of protons were calculated separately for each series, values of $\bar{\nu}$ found from the same series being used.

4.7 Derivation of the Proton Intensity

If $I(p)\Delta p$ = the number of protons with momentum p to $(p + \Delta p)$ incident on the instrument per second,

$A(p)$ = the acceptance of the instrument in units of sterad cm^2 for particles of momentum p,

$\bar{\nu}$ = the mean number of neutrons produced in the interaction of a proton of momentum p,

σ = probability of a proton interacting in the producer,

ϵ = gate efficiency x efficiency of neutron pile with infinite gate,

r = probability of a particle passing through the spectrograph and giving a 5-fold coincidence in Geiger counter trays A, B, G, C, S,

then the number of neutrons detected from the interactions of protons with momenta between p and $p^{+}\Delta p$ per second,

$$R(n) = I(p).\Delta p.A(p).r.\sigma.\bar{\nu}.\epsilon \qquad 4.7$$

or

$$I(p)dp = \frac{R(n).dp}{\Delta p.A(p).r.\sigma.\bar{\nu}.\epsilon.} \qquad 4.8$$

The derivation of A(p) is given in Appendix 1.

The average thickness of lead in the neutron monitor was 13.2 cm. With an interaction length of 16 cm for protons in lead, see Chapter 3, section 4, the probability of a proton interacting in the lead of the neutron monitor was 0.563.

ϵ is equal to 0.0287 for the S-series and 0.0213 for the H-series. The evaluation of r is described in Chapter 5, section 2.

4.8 Scattering in the Spectrograph

The ratio of the r.m.s. error in the measurements of particle deflections to the magnetic deflection was $\frac{0.267}{\beta}$ for the S-series, and $\frac{0.0965}{\beta}$ for the H-series, where β is the velocity of the particle in units of c.

In these experiments, the proton intensity was found from the numbers of neutrons produced by proton interactions. Consequently, a proton scattered so as to appear to have higher momentum would not contribute as much to the calculated intensity at the higher momentum as a proton which had that momentum, since it would on the average produce fewer neutrons. Similarly, a proton scattered so as to appear to have a lower momentum would give a large contribution to the calculated intensity.

The deflection spectrum found from the AP-series and corrected for scattering was used to calculate the effect of scattering on the S and H-series results. The spectrum was divided into twenty-four cells and the number of particles for each of these, which due to scattering would have appeared to have some chosen deflection, was calculated, for the percentage of scattering in each series. Each contribution was then multiplied by the ratio of $\bar{\nu}$ for the cell from which it had been scattered to $\bar{\nu}$ for the cell in which it appeared. The results were summed for each point on the spectrum which had been considered. The ratio of the height of the original unscattered curve to the heights of the scattered curves gave the correction factors tobe applied to the S and H-series results, the mean value for the correction factor being taken for each momentum cell of the measured proton spectrum.

CHAPTER 5
THE VERTICAL PROTON MOMENTUM SPECTRUM

5.1 The Probability of Secondary Particles emerging from the Absorber

In the P and AP series the efficiency of detecting protons was reduced for protons with momenta too high to be stopped in the absorber by ionization loss alone. The probabilities for nuclear interactions in the two series were calculated and corrections applied to the observed intensities for this. However, a further reduction in detection efficiency was caused by secondary particles from the interactions penetrating the absorber and being observed in flash-tube array D with the consequent rejection of the event.

Exactly the same amount and geometry of lead was present for the P, S, and H-series and since in the S and H-series no account was taken of the number of tracks in flash-tube array D in selecting events, the correction factors to be applied to the P-series results could be found from the behaviour of the particles selected in the S and H-series.

For each of the momentum cells into which the P-series results had been divided, the number of events in the S and H-series in which there was no track in flash-tube array D and the number with

one or more tracks were found. The numbers of negative particles with and without tracks in flash-tube array D were multiplied by the positive-negative ratio for muons and subtracted from the numbers of positive particles with and without track in array D. This gave the behaviour of proton interactions in the absorber and hence the correction factors to be applied to the P-series results, the ratio of the total number of proton interactions to the number of interactions with no track in array D, were calculated.

The correction factors to be applied to the AP-series were estimated from those for the P-series. Due to the possible error in estimating these factors, particles with momenta greater than 4 GeV/c were rejected in the AP-series. The correction factor for the highest momentum cell accepted corresponded to a 12% increase in the observed intensity.

5.2 The Normalization of the Proton Intensities

The rate of particles observed using the spectrograph is equal to the incident intensity of particles multiplied by the acceptance of the instrument, A(p), the probability of a particle which has passed through all the required Geiger counter trays discharging one counter in each tray P(g), and the probability of the photograph of an event having single, measureable tracks in each flash-tube array, P(t).

P(g) and P(t) have the same values for all types of particle and are not momentum dependent. P(t) was evaluated by taking 1000 photographs of events in which a five-fold Rossi coincidence ABGC and S was recorded and finding the percentage of the photographs which had measurable tracks in each flash-tube array. The value found was 85.8%.

For each series, P(g) was found by comparing the observed Rossi coincidence rate A, B, G, C, S, during the series with the rate of muons passing through the instrument predicted by multiplying the muon momentum spectrum of Gardener et al. (1962) 0.4 - 10 GeV/c and Hayman and Wolfendale (1962) 5 - 1000 GeV/c by the geometrical acceptance of trays A, B, G, C and S at each momentum and integrating.

The spectrum of Gardener et al. has been normalized to the intensity given by Rossi (1948) at 1 GeV/c, and the spectrum of Hayman and Wolfendale has been normalized to the spectrum of Gardener et al. in the range 1 - 10 GeV/c.

The values of P(g) found for each series are given in Table 5.1.

The rates observed in each series were divided by P(t) and by the value of P(g) for the series, giving proton intensities normalized to the muon intensity at 1 GeV/c given by Rossi. No further normalization has been carried out between the different series.

Series	P(g)
P	0.341
AP	0.503
S	0.375
H	0.409

Table 5.1

5.3 The Sea-Level Proton Momentum Spectrum

The intensities measured in the present experiments are of protons arriving at ground level within 0.2 radians of the vertical. The variation in the thickness of the atmosphere over this range of angles is ~2%, see Appendix 2, and as this is small compared with the statistical accuracy of the experiments no correction was applied to the observed intensities: these were taken to be the vertical intensities of cosmic ray protons.

The bias in the measured intensities as a function of momentum, due to the rejection of events in which two or more particles were incident on the spectrograph simultaneously, is thought to be negligible.

The absolute values of the intensities of protons given are subject to any error in the muon intensity at 1 GeV/c of $2.45.10^{-3}$ $sec^{-1}cm^{-2}sterad^{-1}$ $(GeV/c)^{-1}$ given by Rossi (1948).

The intensities of protons measured in each of the four series are presented in Tables 5.2(a), (b), (c) and (d). These four independent measurements of the sea-level proton spectrum have been combined according to the statistical accuracy of the measurements in each series and these figures are given in Table 5.3.

The combined experimental results are shown in Fig. 5.1. The maximum of the spectrum lies between 600 and 800 MeV/c. If the spectrum in the range 3 - 150 GeV/c is represented by the form:- $N(p)dp = K\, p^{-\gamma}\, dp$, γ has a value of 2.6 ± 0.1. Below a few GeV/c, the exponent decreases rapidly with decreasing momentum due to ionization loss by the protons in passing through the atmosphere.

5.4 Protons as a Percentage of the Sea-Level Ionizing Particle Intensity

Due to possible errors introduced by normalizing the proton intensity to the intensity of muons at 1 GeV/c, the most accurate way in which the measurements of proton intensities can be presented is as a percentage of the single ionizing particle intensity. This is shown in Fig. 5.2 where the proton intensity is expressed as a percentage of the muon intensity measured using the Durham cosmic-ray spectrograph. The maximum percentage of protons observed is at 700 MeV/c. The percentage of protons

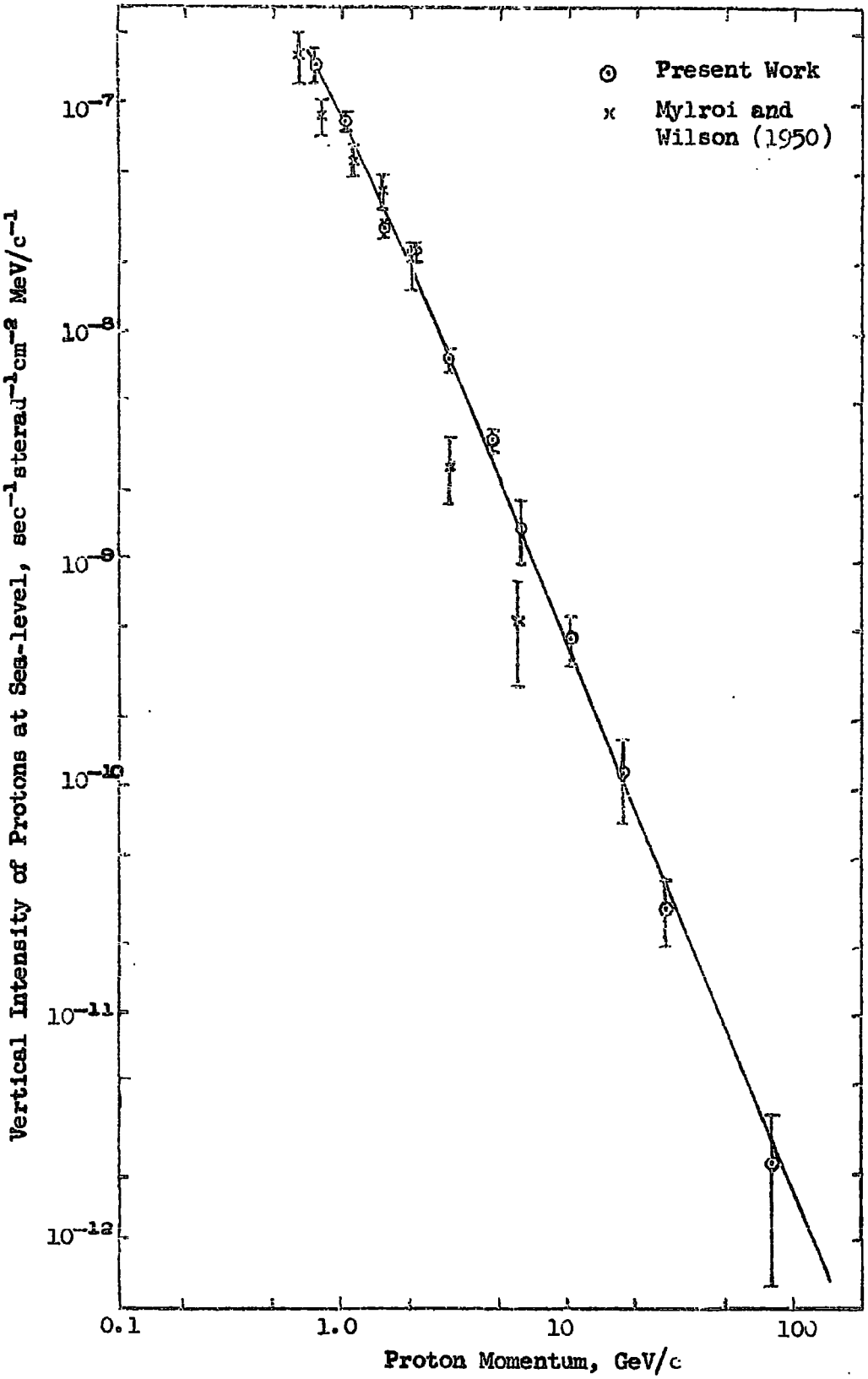

The Vertical Sea-Level Proton Momentum Spectrum

Fig. 5.1

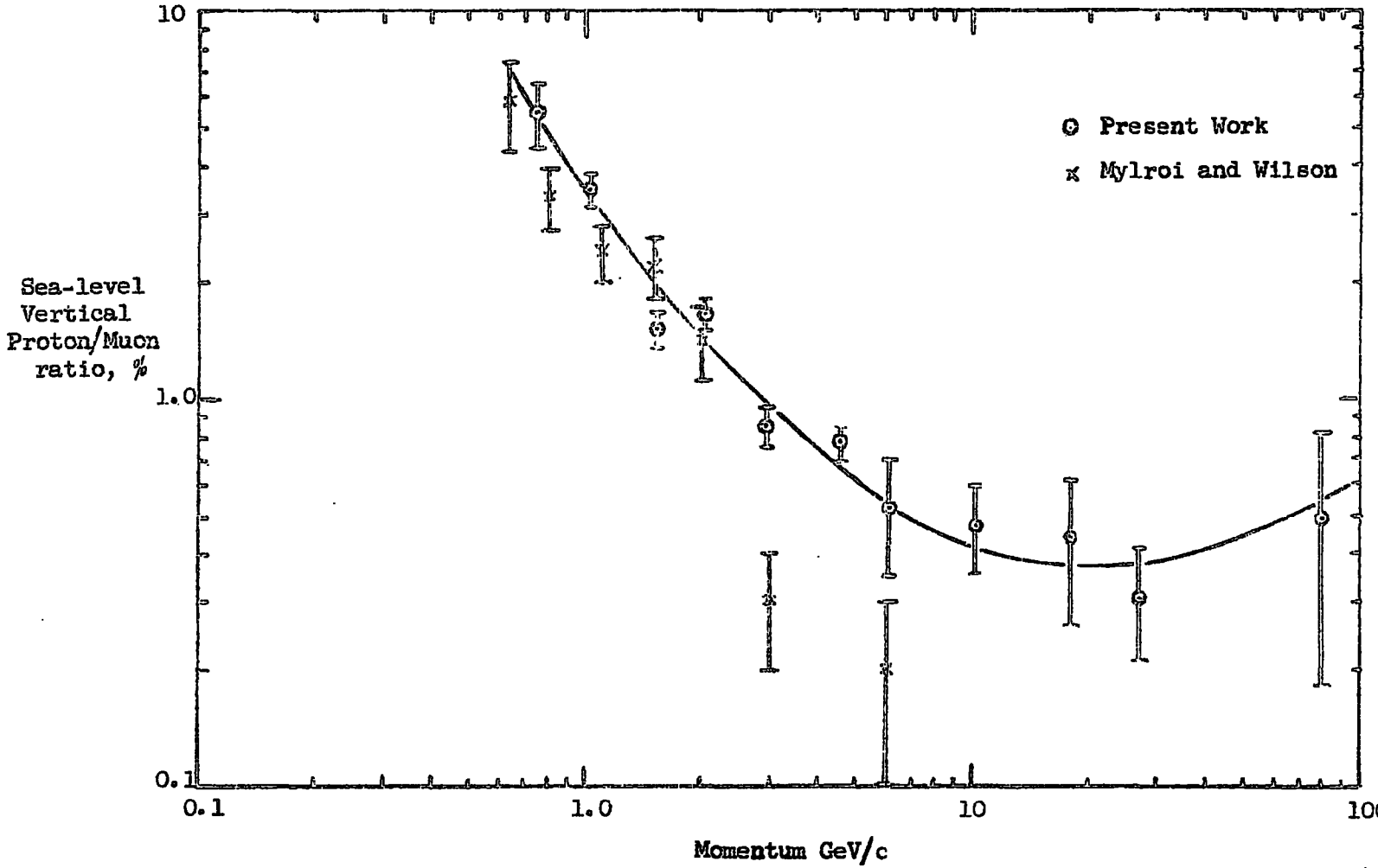

The Sea-Level Proton/Muon Ratio as a Function of Momentum

Fig. 5.2

Proton Momentum GeV/c	Sea-level proton intensity $sec^{-1}sterad^{-1}cm^{-2}$. MeV/c^{-1}	Proton/muon ratio %
0.79	$(1.37 \pm 0.51)10^{-7}$	5.08 ± 1.89
1.06	$(8.04 \pm 1.55)10^{-8}$	3.35 ± 0.65
1.56	$(2.72 \pm 0.37)10^{-8}$	1.47 ± 0.20
2.97	$(7.30 \pm 0.85)10^{-9}$	0.82 ± 0.10
6.16	$(1.40 \pm 0.46)10^{-9}$	0.53 ± 0.17
18.0	$(1.17 \pm 0.47)10^{-10}$	0.44 ± 0.18

P-series

Table 5.2(a)

Proton Momentum GeV/c	Sea-level proton intensity $sec^{-1}sterad^{-1}cm^{-2}$. MeV/c^{-1}	Proton/muon ratio %
0.70	$(1.62 \pm 0.29)10^{-7}$	5.79 ± 1.03
1.00	$(9.50 \pm 1.30)10^{-8}$	3.88 ± 0.53
1.50	$(2.97 \pm 0.47)10^{-8}$	1.55 ± 0.25
2.90	$(7.98 \pm 1.25)10^{-9}$	0.87 ± 0.125

AP-series

Table 5.2(b)

Proton Momentum GeV/c	Sea-level proton intensity $sec^{-1}sterad^{-1}cm^{-2}$. MeV/c^{-1}	Proton/muon ratio %
1.03	$(7.60 \pm 1.67)10^{-8}$	3.13 ± 0.69
2.12	$(2.78 \pm 0.36)10^{-8}$	2.01 ± 0.26
4.60	$(3.77 \pm 0.58)10^{-9}$	0.856 ± 0.132
10.3	$(5.24 \pm 1.63)10^{-10}$	0.545 ± 1.170
27.5	$(2.37 \pm 1.07)10^{-11}$	0.261 ± 0.118
79.0	$(2.28 \pm 1.45)10^{-12}$	0.496 ± 0.315

H-series

Table 5.2(c)

Proton Momentum GeV/c	Sea-level proton intensity $sec^{-1}sterad^{-1}cm^{-2}$. MeV/c^{-1}	Proton/muon ratio %
1.03	$(8.45 \pm 1.22)10^{-8}$	3.48 ± 0.50
2.12	$(1.73 \pm 0.21)10^{-8}$	1.25 ± 0.15
4.60	$(3.04 \pm 0.42)10^{-9}$	0.69 ± 0.10
10.3	$(3.90 \pm 0.93)10^{-10}$	0.41 ± 0.10
27.5	$(3.53 \pm 1.56)10^{-11}$	0.388 ± 0.177

S-series

Table 5.2(d)

Proton Momentum GeV/c	Sea-level proton intensity $sec^{-1}sterad^{-1}cm^{-2}$. MeV/c^{-1}	Proton/muon ratio %
0.75	$(1.50 \pm 0.28)10^{-7}$	5.44 ± 1.01
1.03	$(8.40 \pm 0.75)10^{-8}$	3.46 ± 0.31
1.53	$(2.85 \pm 0.30)10^{-8}$	1.51 ± 0.16
2.12	$(2.26 \pm 0.20)10^{-8}$	1.64 ± 0.15
2.94	$(7.64 \pm 0.88)10^{-9}$	0.848 ± 0.098
4.60	$(3.40 \pm 0.36)10^{-9}$	0.772 ± 0.082
6.16	$(1.40 \pm 0.46)10^{-9}$	0.528 ± 0.174
10.3	$(4.57 \pm 1.17)10^{-10}$	0.475 ± 0.122
18.0	$(1.17 \pm 0.47)10^{-10}$	0.441 ± 0.177
27.5	$(2.95 \pm 0.94)10^{-11}$	0.324 ± 0.103
79.0	$(2.28 \pm 1.45)10^{-12}$	0.496 ± 0.315

The combined intensities from the present work

Table 5.3

falls with increasing momentum, the measured value at 79 GeV/c being $0.50 \pm 0.32\%$.

5.5 Comparison with other work

The only previous measurement of the sea-level proton intensity over a wide momentum range is that of Mylroi and Wilson (1951) which covers the range 0.6 - 12 GeV/c. In that experiment protons were identified by absorption in 20 cm of lead which was sufficient to stop protons with momenta less than 1.05 GeV/c by ionization loss. At higher momenta the assumption made, that protons which interacted in the lead were absorbed, would lead to an underestimate of the proton intensity. This is due to secondary particles from an interaction emerging from the absorber, the event not then being recognized as an incident proton. Since the number and momentum of secondary particles increases with increasing momentum of the incident particle, the probability of one or more of the secondaries emerging from the absorber will also increase with momentum.

As expected from the above discussion, the results of Mylroi and Wilson agree with the present measurements up to 2 GeV/c, but at higher momenta their measurements fall increasingly below the results from the present experiments. The percentages of protons in the sea-level single particle intensity as measured by Mylroi and Wilson are shown in Fig. 5.2.

Pak and Greisen (1962) have identified protons with a median momentum of 22 GeV/c in the sea-level cosmic ray flux by means of their interaction in lead in a multiplate cloud chamber. They obtain a value for the proton intensity expressed as a percentage of the sea-level muon intensity of 1.6%, in the vertical direction, higher than that found in the present experiments. However, the error in the measurement by Pak and Greisen is 70% and their result can not be regarded as inconsistent with the present work.

At lower momenta, there is good agreement with the results of McDiarmid (1959) at 728 and 774 MeV/c, found using plastic scintillators and thin absorbing layers of aluminium in a cloud chamber. There is also good agreement with the proton intensities measured by Ballam and Lichtenstein (1954), using carbon absorber and a cloud chamber, at 800 and 914 MeV/c whilst their points at higher momenta are consistent with the present results. Also in agreement are the values measured by Rozen (1954), Merkle et al. (1950), Ogilvie (1955) and York (1952) in the range 0.80 to 1.0 GeV/c. The measurements of Filthüth (1955) at 730 and 890 MeV/c are lower by a factor of approximately two and are not consistent with the present work.

The measurements by the above authors of the differential sea-level proton intensity in the momentum range 0.70 to 1.0 GeV/c are shown in Fig. 5.3.

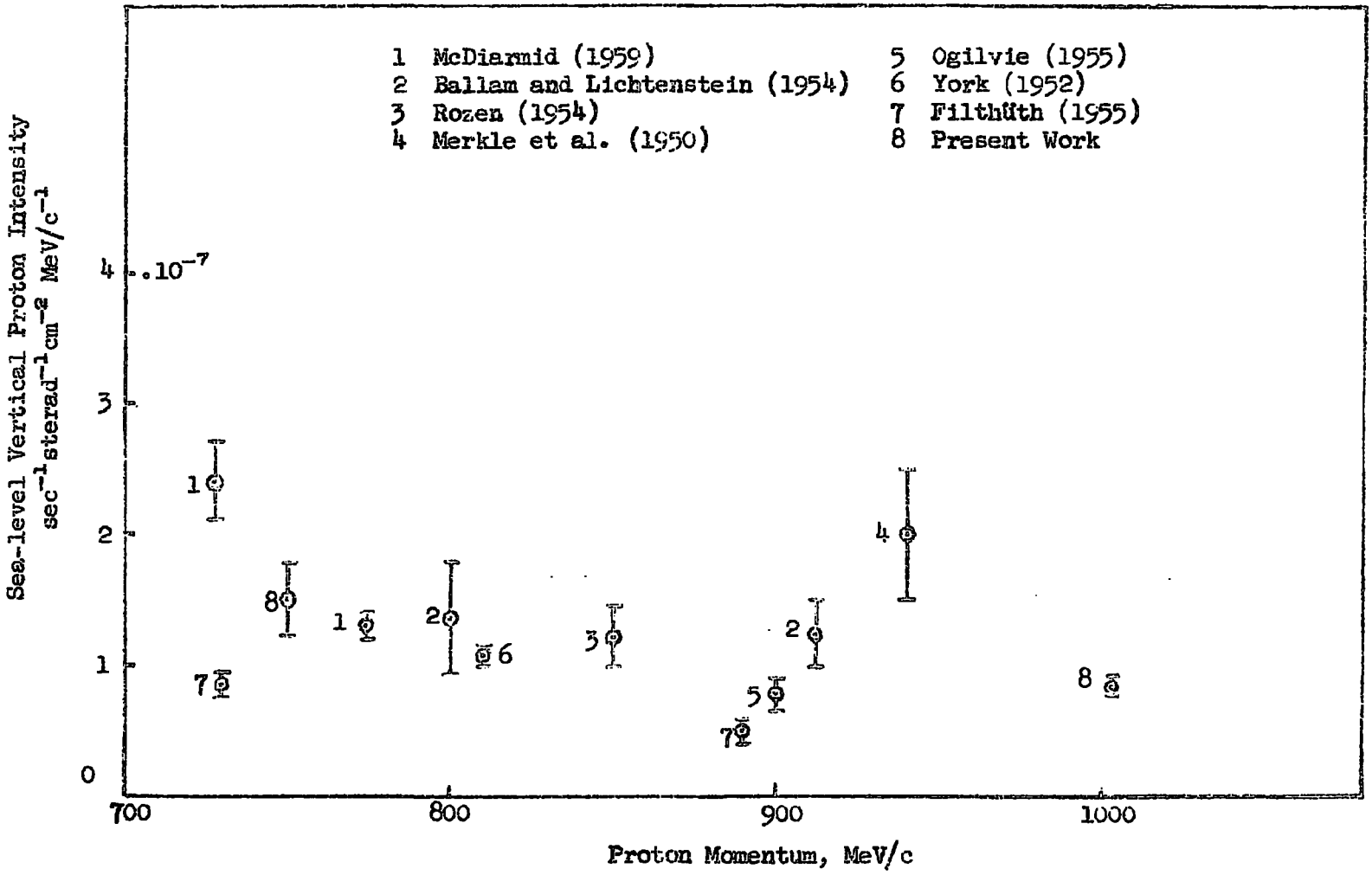

Other Measurements of Low Energy Proton Intensities

Fig. 5.3

CHAPTER 6

COMPARISON OF THE SEA LEVEL PROTON SPECTRUM WITH THE "M. I. T." PRIMARY SPECTRUM

6.1 Introduction

It has been found by many authors that, on average, in high energy nuclear interactions, the incident nucleons retain an appreciable fraction of their initial energy after their interactions. The fraction of the available energy retained by an incident nucleon is known as the elasticity, f, of the interaction. Values of elasticity have been obtained by direct observation of individual nuclear interactions using nuclear emulsions, in cloud-chambers or bubble-chambers, and also indirectly from studies of the rate of attenuation of the cosmic ray nucleon intensities in the atmosphere. Using the latter method, the sea-level proton spectrum obtained from the present experiments together with the primary cosmic ray spectrum enables an estimate to be made of the mean elasticity of nucleon-air nucleus collisions. The elasticity calculated by this method is not the arithmetic mean value but a function, which depends on the exponent of the primary spectrum, of the distribution in elasticity values. This distribution is discussed in detail in Chapter 8. In the present chapter, for a trial spectrum, the intensities of primary nuclei given by Linsley et al. (1962), the so-called "M. I. T." spectrum, will be assumed.

6.2 The sea-level proton energy spectrum

In the calculations which follow, the kinetic energy spectrum of protons at sea-level is required. Experimentally, the proton momentum spectrum was measured. The relation between E_K, the kinetic energy of a proton, and p, its momentum is given by the relativistic expression:-

$$E_K = (p^2 + m_o{}^2c^4)^{\frac{1}{2}} - m_oc^2 \qquad 6.1$$

where m_oc^2 is the rest energy of a proton in units of eV,
p is the momentum of a proton in units of eV/c, and
E_K is in units of eV.

Also, since the total intensity of protons at sea-level must be the same irrespective of whether the results are expressed as a momentum or energy spectrum:-

$$N(E_K)dE_K = N(p)dp \qquad 6.2$$

where $N(E_K)dE_K$ = intensity of protons with kinetic energy between E_K and $E_K + dE_K$

and $N(p)dp$ = intensity of protons with momentum between p and $p + dp$.

From equations 6.1 and 6.2:-

$$N(E_K) = N(p).\frac{1}{\beta} \qquad 6.3$$

where β = velocity of the proton expressed as a fraction of the velocity of light. The sea-level proton kinetic energy spectrum calculated from the combined results of the four series of experiments is shown in Figure 6.1, the experimentally measured intensities of protons being given in Table 6.1.

6.3 The "M.I.T." Primary Energy Spectrum

It is observed that, in the interactions of heavy nuclei, the nucleus behaves as a group of separate nucleons. For example, McEwen (1959) observed an interaction in emulsion of an alpha-particle, the secondary particles from which showed a marked separation into inner and outer cones. In the inner cone, a further interaction was observed of a neutron, with incident energy close to the value of 8000 GeV/nucleon found for the incident α-particle. This suggests that the neutron came from the original α-particle and that it did not take part in the interaction of the α-particle. Consequently the primary flux of nuclei may be considered to consist of separate nucleons in studying the propagation of the nucleon component in the atmosphere.

The nucleon energy spectrum has been calculated from the "M.I.T." spectrum of primary nuclei in the following way. In the energy region below 10^{15} eV, the particle spectrum given by Linsley et al. has been corrected for the presence of α-particles to give the

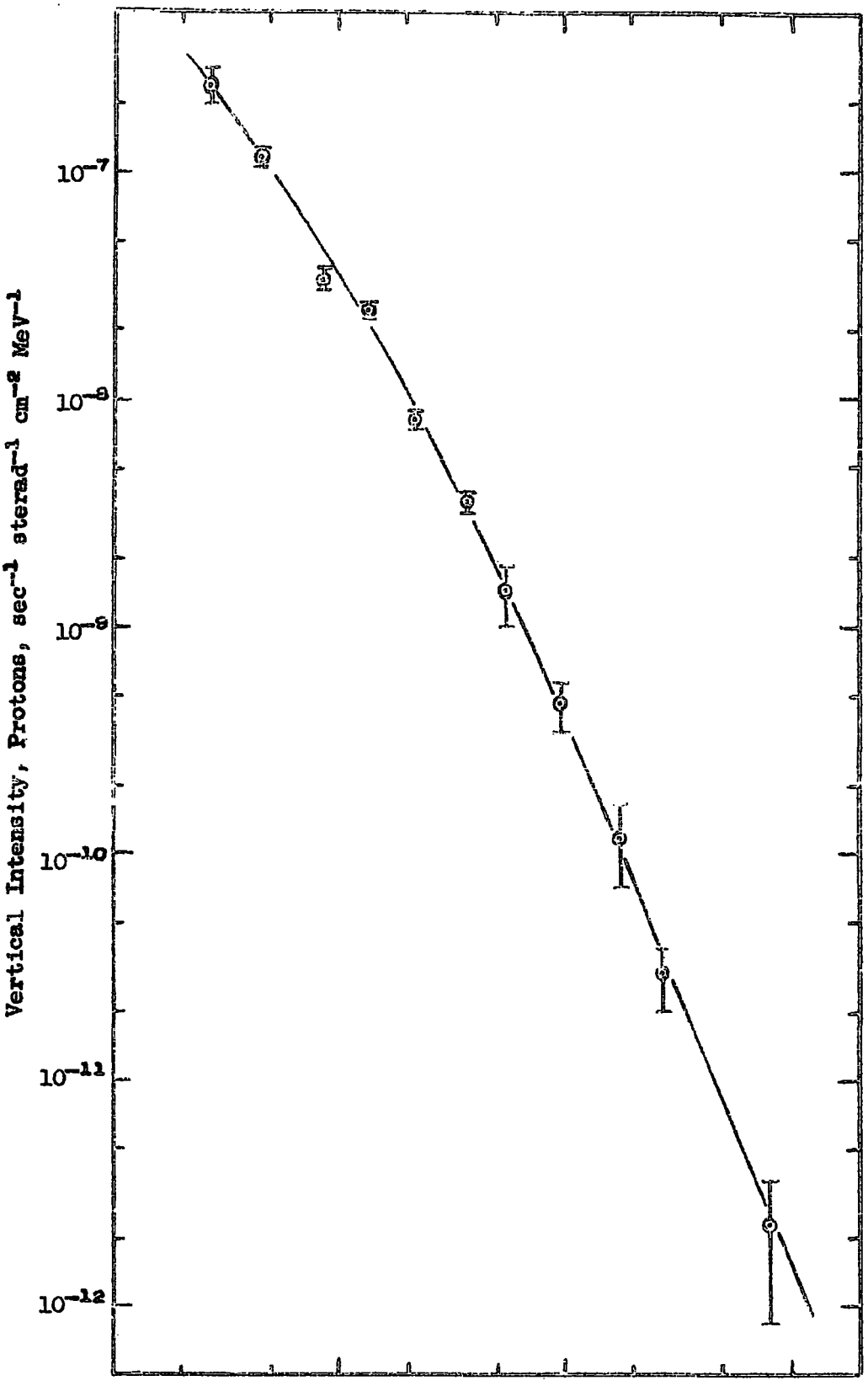

The Vertical Differential Energy Spectrum of Protons at Sea level

Fig. 6.1

Kinetic Energy (GeV)	Vertical Sea-level Proton Intensity ($cm^{-2} sec^{-1} sterad^{-1} MeV^{-1}$)	$p/\mu^{\pm}$ ratio (%)
0.27	$(2.40 \pm 0.45)10^{-7}$	9.40 ± 1.80
0.46	$(1.14 \pm 0.10)10^{-7}$	3.90 ± 0.34
0.85	$(3.33 \pm 0.35)10^{-8}$	1.32 ± 0.14
1.35	$(2.48 \pm 0.22)10^{-8}$	1.27 ± 0.11
2.13	$(8.03 \pm 0.93)10^{-9}$	0.627 ± 0.073
3.7	$(3.47 \pm 0.37)10^{-9}$	0.570 ± 0.061
5.4	$(1.42 \pm 0.46)10^{-9}$	0.444 ± 0.144
9.5	$(4.57 \pm 1.17)10^{-10}$	0.401 ± 0.103
17.5	$(1.17 \pm 0.47)10^{-10}$	0.441 ± 0.177
27.0	$(2.95 \pm 0.94)10^{-11}$	0.311 ± 0.099
79.0	$(2.28 \pm 1.45)10^{-12}$	0.496 ± 0.315

The Combined Intensities from the Present Work

Table 6.1.

spectrum of primary nucleons. Nuclei heavier than α-particles in the primary radiation have been ignored since in the measurement by Lal (1953) of the integral primary intensity above $1.6.10^{12}$ eV, only protons were observed and in the measurement by Kaplon and Ritson (1952) of the integral primary intensity above $4.5.10^{12}$ eV, no incident particles other than protons and α-particles were observed. The ratio of the intensity of the primary nucleon energy spectrum to the intensity of the primary nuclei energy spectrum at the same energy is therefore given by :-

$$R = \frac{[(1 - C_\alpha) + C_\alpha . 2^{(2-\gamma)}]}{[1 - C_\alpha) + C_\alpha . 2^{\gamma}]} ,$$

where C_α is the percentage of α-particles present above a constant rigidity and γ is the exponent of the primary integral spectrum . See Appendix 6.

Waddington (1960) gives the abundances by number of nuclei of the primary cosmic radiation as 85.9% protons, 12.7% α-particles and 1.4% heavier nuclei above a constant rigidity of 4.5 GV . The work of McDonald, reported by Van Allen (1960), shows that the ratio of the intensity of protons to the intensity of α-particles in the primary radiation is independent of time variations and is also independent of energy, at least up to 20 GeV. Taking a mean value of 1.5 for γ and with C_α = 12.7%, then R = 88.5%.

Linsley and Scarsi (1962), from a study of the fraction of the particles in extensive air showers which are muons, and also from the variation in shower age at a given depth, conclude that in the energy range 10^{17} to 10^{18} eV the primary particle flux consists almost entirely of protons. Consequently, the "M.I.T." spectrum above 10^{18} eV has been taken to represent the primary nucleon spectrum.

For an integral spectrum of the form:-

$$N(>E) = K.E^{-\gamma}, \quad \text{where } \gamma \text{ is constant,}$$

the corresponding differential spectrum is given by:-

$$N(E)dE = \frac{\gamma.N(>E)}{E}\, dE \qquad 6.4$$

The exponent, γ, of the "M.I.T." primary cosmic ray spectrum is not constant, but a function of the primary energy (Figure 6.2). However, $\frac{d\gamma}{dE}$ is so small that equation 6.4 can be used to a very good approximation.

The derived differential and integral primary nucleon energy spectra are given in Figure 6.3.

6.4 The Interaction Length for Nucleons in Air

In order to make calculations on the nucleon cascade in the atmosphere and to deduce values for the elasticity of nuclear

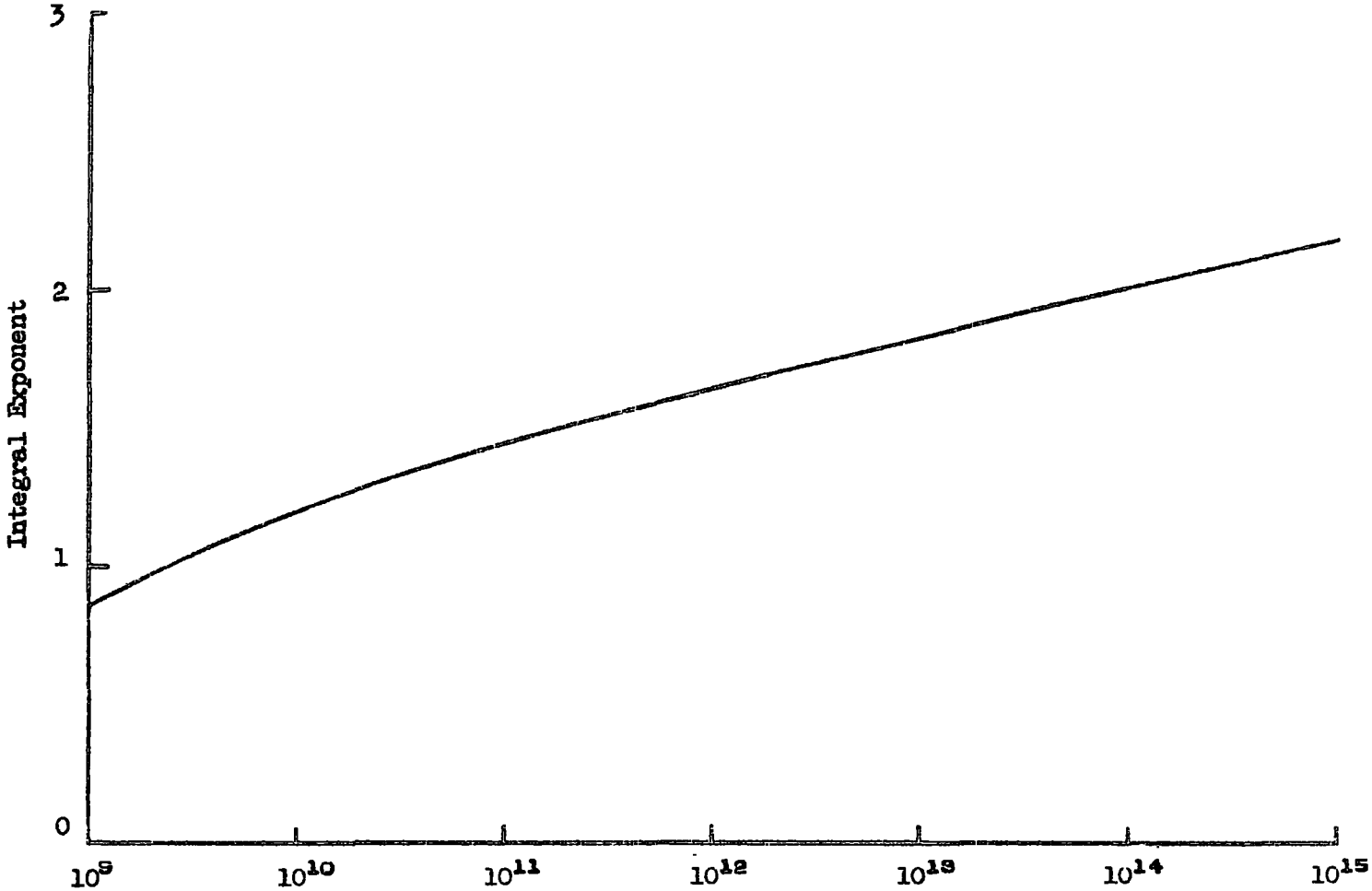

The Integral Exponent of the "MIT" Primary Spectrum

Fig. 6.2

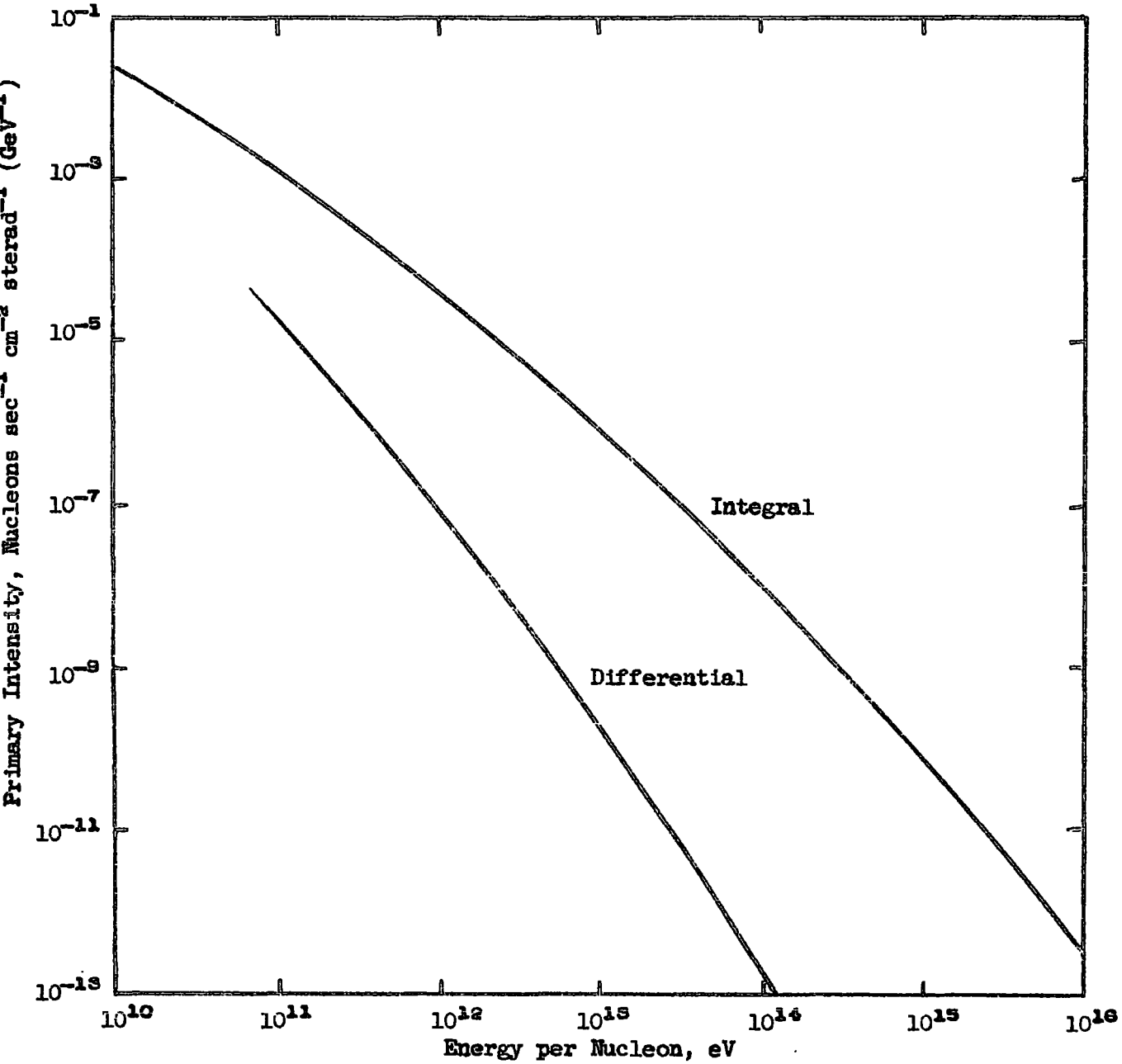

The "MIT" Primary Nucleon Spectrum

Fig. 6.3

interactions, it is necessary to know the probability of a nucleon undergoing a given number of interactions in traversing the atmosphere. Since this is a random process the probability distribution will be Poissonian, depending on the mean number of interactions undergone by a nucleon in the atmosphere. The mean number of interactions in turn depends on the interaction length for nucleons in air, the value of which is therefore required for the calculations which follow.

There are up to the present time no direct measurements of the nucleon interaction length, λ_i, in air. Calculations by Williams (1960) and by Alexander and Yekutieli (1961) of λ_i in terms of the elementary nucleon-nucleon cross-section, taking the value of 32 mb measured at CERN for the inelastic cross-section for 24 GeV protons in Hydrogen (Cocconi, 1961), give 93 gm.cm^{-2} for air. However, it is expected from theoretical considerations that at higher energies the inelastic cross-section for nucleon-nucleon interactions is equal to the total cross-section and also that the total (i.e. elastic plus inelastic) cross-section is independent of energy. The value reported by Cocconi for the total proton-proton cross-section is 43 ± 3 mb, leading to a value for λ_i in air of $\sim$80 gm.cm^{-2} according to the above mentioned calculations. This would apply to nucleon-air nucleus collisions where the incident proton energy is greater than a few hundred GeV.

The atomic number of carbon is close to the mean atomic number for air nuclei and, since the interaction length varies with atomic number A as approximately $A^{-\frac{1}{3}}$, the values of λ_I found experimentally for nucleons in carbon can be taken to apply also to nucleon interactions in air. Walker et al. (1950), working at an altitude of 4260 metres measured the mean free path in carbon of cosmic-ray particles, capable of producing a penetrating shower of three or more particles, to undergo an interaction which either made them incapable of producing such a shower or which gave rise to one or more penetrating secondaries. The value obtained, 81 ± 5 gm.cm^{-2}, is an upper limit to the inelastic interaction length, since interactions in which secondary particles were produced which were not capable of penetrating the carbon absorber, could not be detected by the experimental arrangement used.

Bozoki et al. (1962) have measured the inelastic interaction mean free path of cosmic ray neutrons, with mean energy ~30 GeV, in carbon and obtained a value of 73 ± 7 gm.cm^{-2}. The experimental arrangement selected showers, of two or more penetrating particles, produced in lead by uncharged particles which did not interact in layers of graphite placed between the above trays of geiger counters which were in anticoincidence.

Recent calculations by Udgaonkar and Gell-Mann (1962) of high energy nucleon-nucleon interaction cross-sections in terms of the

Regge pole hypothesis predict that at very high energies the total interaction cross-section for the collision of a nucleon with a nucleus of atomic number A, σ_A, should be $A.\sigma_{NN}$, where σ_{NN} is the elementary nucleon-nucleon cross-section. In this theory the radius and transparency of a nucleon increase with energy in such a way that σ_{NN} remains constant. It is expected that σ_A should tend very slowly to the limit $A.\sigma_{NN}$. For carbon, for example, at laboratory energies of 10, 10^3, 10^6 and 10^9 GeV, $\sigma_A/\sigma_{geom.}$ is respectively 0.98, 1.10, 1.22 and 1.33. For the energy range which is of interest in the present work, ~10 - 10^4 GeV, the interaction length of nucleons in air should be close to the value of 70 $gm.cm^{-2}$ corresponding to a geometrical cross-section. However, a value for the nucleon-nucleon cross-section has been used in these calculations which is appreciably larger than the experimental value. Consequently, it is probable that the derived cross-sections in carbon are too high.

The experimental values for λ_i in air, which have been mentioned previously, i.e. 73 ± 7 $g.cm^{-2}$ and 81 ± 5 $g.cm^{-2}$ are both consistent with a value of $\lambda_i = 80$ $g.cm^{-2}$. Theoretical values for λ_i vary from approximately 70 $g.cm^{-2}$ to 90 $g.cm^{-2}$, but taken together also indicate a value close to 80 $g.cm^{-2}$. The best estimate of the interaction length for nucleons in air which can be made at the present time is thus $\lambda_i = 80$ $g.cm^{-2}$.

In view of the appreciable differences in the values for λ_i in air found experimentally and theoretically, the calculations in this chapter have been performed for the extreme limiting values of λ_i, 70 and 93 g.cm^{-2}, in addition to the most likely value of 80 g.cm^{-2}.

6.5 The Elasticity of Nucleon-Air Nucleus Interactions

6.5.1 A Simple Propagation Model - Constant Exponent of Primary Spectrum

Following Cranshaw and Hillas (1960), it is assumed that:-

a) the primary integral cosmic ray spectrum is of the form $N_o(>E) = AE^{-\gamma}$, where γ is constant,

b) ionization loss is negligible,

c) the fraction of the initial energy retained by the incident nucleon after an interaction, i.e. the elasticity f, is constant,

and d) only one high energy nucleon emerges from each interaction.

Then if λ_i and λ_a are the interaction and absorption lengths for nucleons in the atmosphere, for an atmospheric depth t the mean number of interactions $m = \frac{t}{\lambda_i}$. The probability of i collisions follows a Poisson distribution and is given by:- $e^{-m}.\frac{m^i}{i!}$. At a depth t, the number of nucleons with energy greater than E which have made i collisions is given by:-

$$N_t(>E) = A. \left(\frac{E}{f^i}\right)^{-\gamma} . e^{-m} . \frac{m^i}{i!} \qquad 6.5$$

and therefore the total number of nucleons with energy greater than E is:-

$$N_t(>E) = AE^{-\gamma} e^{-m} \sum_{\text{all } i} \frac{f^{i\gamma} m^i}{i!} \qquad 6.6$$

or

$$N_t(>E) = N_o(>E). e^{-t/\lambda_i}. \exp\left(\frac{f^\gamma t}{\lambda_i}\right) \qquad 6.7$$

By definition

$$\frac{N_t(>E)}{N_o(>E)} = e^{-t/\lambda_a} \qquad 6.8$$

and from equation 6.7 this is equal to $\exp\left\{(f^\gamma - 1).t/\lambda_i\right\}$

or

$$-\frac{t}{\lambda_a} = \frac{t}{\lambda_i}(f^\gamma - 1)$$

$$\frac{\lambda_i}{\lambda_a} = (1 - f^\gamma) \qquad 6.9$$

Since it is the intensities of protons at sea-level which have to be found experimentally, the proton to neutron ratio at sea-level is required in order to calculate the attenuation length for nucleons in air. Experimentally it has been found by Guseva et al. (1962) working at an altitude of 3860 m, that half of the jets observed in

LiH were produced by neutral particles. The effective mean energy for the particles producing these jets was ~250 GeV. Perkins (1963) found for the Bristol measurements on jets in nuclear emulsions, averaged over all energies, that the charged to uncharged ratio for the fastest emergent particle was unity. These experimental results support the assumption that the probability of charge exchange is 50% at the energies at which the first interactions take place ($\gtrsim$50% GeV), of cosmic ray nucleons capable of reaching sea-level with energies above a few GeV. Then, ignoring ionization loss in the atmosphere, the sea-level nucleon intensity is twice the sea-level proton intensity at the same energy. Values of λ_a calculated from the measured integral sea-level proton spectrum and the "M.I.T." primary nucleon spectrum are given in Table 6.2, together with the values for the elasticity, f, obtained using equation 6.9.

Sea-level energy GeV.	λ_a g.cm^{-2}	Exponent of integral primary spectrum, γ	Elasticity, f % λ_i = 70 g.cm^{-2}	λ_i = 80 g.cm^{-2}	λ_i = 93 g.cm^{-2}
3	127.7	1.40	56.8	49.6	39.5
10	121.5	1.50	56.4	49.0	38.1
30	118.5	1.58	56.8	49.1	37.8
100	116.1	1.68	57.6	50.0	38.3

Table 6.2.

In Table 6.3 values calculated for f from equation 6.9 are given for different values of γ with $\lambda_i = 80$ g.cm^{-2} and $\lambda_a = 120$ g.cm^{-2}.

Primary exponent, γ	Elasticity, f, %
1.2	40.0
1.4	45.6
1.6	50.4
1.8	54.3
2.0	57.8

Table 6.3.

The deduced elasticity is seen to be strongly dependent on the value taken for γ. The assumption made in deducing equation 6.9, that the primary exponent is constant, is therefore probably not justified.

A study of the individual terms of the summation in equation 6.6 shows that the main contribution to the intensity of nucleons reaching sea-level with greater than a given energy comes from nucleons which have interacted between three and seven times in the atmosphere. Since the nucleon-air nucleus elasticity is approximately 50%, nucleons will arrive at sea-level with on average about

a twentieth of their initial energy at the top of the atmosphere. Consequently, the values for γ given in Table 6.2 are for primary energies of twenty times the stated sea-level energies.

6.5.2 A Propagation Model - Varying Primary Exponent

The exponent of the "M.I.T." primary spectrum is a function of energy, increasing with increasing energy. It has been shown in the preceeding section that the value deduced for the elasticity of nuclear interactions in air is very sensitive to the value assumed for the primary exponent. Consequently calculations have been performed, as follows, taking into account the variation of the exponent with energy.

If a nucleon of initial energy E_o makes i interactions in traversing t g.cm^{-2} of the atmosphere then, with assumptions b), c) and d) of section 6.5.1,

$$E_t = f^i E_o \qquad 6.10$$

If the probability of a particle making i interactions is P_i, the contribution to the sea-level nucleon intensity between energies E_t and $E_t + dE_t$ follows as:

$$n(E_t)dE_t = P_i N_o(E_o)dE_o$$

or

$$n(E_t) = P_i N_o(E_o) \frac{dE_o}{dE_t}$$

$$n(E_t) = P_i \cdot \frac{1}{f^i} N_o \left(\frac{E_t}{f^i}\right) \qquad 6.11$$

where $N_o(E)$ is the primary differential nucleon spectrum.

The expression $\frac{1}{f^i} N_o\left(\frac{E_t}{f^i}\right) \equiv \psi(f^i, E_t)$ is shown in Figure 6.4 for E_t = 10 GeV and 100 GeV, as a function of f^i.

Then the total intensity of nucleons at depth t, between energy E_t and $E_t + dE_t$ is:-

$$N_t(E_t)dE_t = \sum_{i=o}^{\infty} P_i \cdot \psi(f^i, E_t)dE_t \qquad 6.12$$

If $m = \frac{t}{\lambda_i}$, $P_i = e^{-m} \frac{m^i}{i!}$ i.e. a Poisson distribution (which is tabulated in Biometrika).

The differential intensities of nucleons expected at sea-level at energies of 10 and 100 GeV were calculated numerically from equation 6.11 for λ_i = 70, 80 and 93 g.cm^{-2} and for f = 30, 35, 40, 45, 50 and 55%. At both energies, for each value of interaction length, the value of f was found by interpolation from the expected intensities thus obtained, which gave the observed nucleon intensity at that energy. The sea-level nucleon intensity was taken to be twice the best estimate of the measured intensity, i.e. $6.8.10^{-10}$ nucleons sec^{-1} sterad^{-1} cm^{-2} MeV^{-1} at 10 GeV and $2.8.10^{-12}$ nucleons sec^{-1} sterad^{-1} cm^{-2} MeV^{-1} at 100 GeV.

The values for elasticity found by this method are presented in Table 6.4.

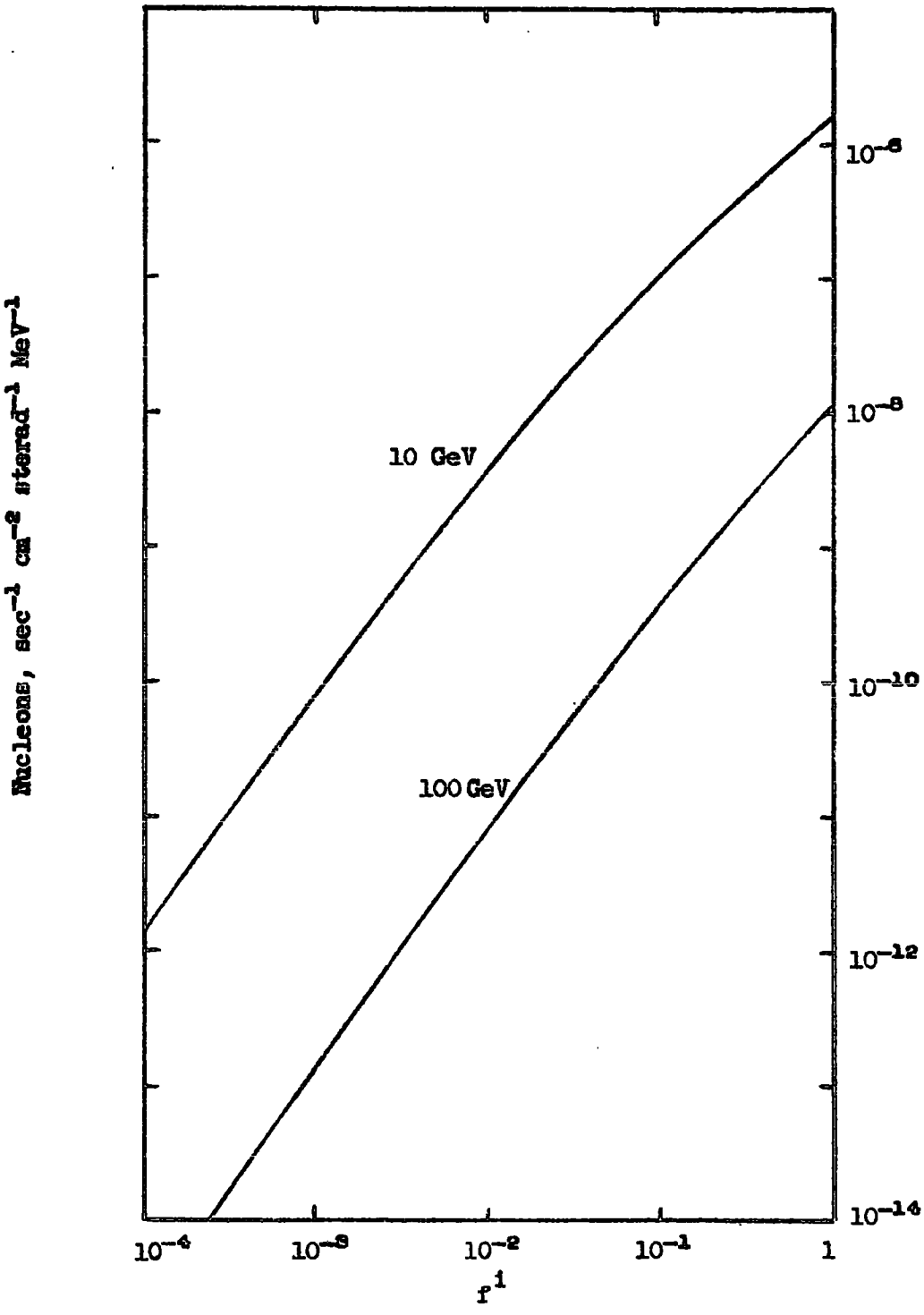
Nucleons, sec^{-1} cm^{-2} sterad^{-1} MeV^{-1}
10 GeV
100 GeV
10^{-6}
10^{-8}
10^{-10}
10^{-12}
10^{-14}
10^{-4}
10^{-3}
10^{-2}
10^{-1}
1
f^{1}

Fig. 6.4

Sea-level energy GeV.	Elasticity, f % $\lambda_i = 70$ g.cm^{-2}	$\lambda_i = 80$ g.cm^{-2}	$\lambda_i = 93$ g.cm^{-2}
10	52.0	42.5	32.0
100	55.0	46.0	33.0

Table 6.4

A comparison of these values with the values given in Table 6.2 shows that the assumption that the primary exponent is constant leads in general to an overestimate of the elasticity. This is true in spite of the use of the primary spectrum exponent at twenty times the sea-level energy in the earlier calculations in an attempt to allow for the variation of the exponent with energy. In addition, it can be seen that the constant exponent approximation leads to elasticity values which are not related in any simple manner to those deduced by the more accurate method.

CHAPTER 7

THE DERIVATION OF THE PRIMARY NUCLEON SPECTRUM

7.1 Introduction

The energy spectrum of nucleons which would be required to be incident at the top of the earth's atmosphere in order to give the measured intensities of nucleons at sea-level can be calculated as a function of K_T, the total fraction of energy lost by a nucleon in an interaction. Similarly, the primary nucleon energy spectrum can also be calculated in terms of the energy spectrum of pions at production (pion production spectrum) and K_π, the fraction of the available energy in an interaction going into the production of pions. If the relation between K_T and K_π is known, then the primary cosmic ray spectrum can be calculated.

This method is used in the calculations which follow, in which a particular model is assumed for high energy nuclear interactions. The best estimate of the interaction length of nucleons in air was taken to be 80 $g.cm^{-2}$, see Chapter 6, section 4.

7.2 The Pion Production Spectrum

The spectrum of charged pions at production is in general given by:-

$$F(E_\pi)dE_\pi = \int_{E=3E_\pi}^{\infty} [N(E_\pi)dE_\pi]_E \cdot n(E)dE \qquad 7.1$$

where $[N(E_\pi)dE_\pi]_E$ is the intensity of charged pions with energy E_π to $(E_\pi + dE_\pi)$ produced on average in a nuclear interaction of a nucleon of energy E. $n(E)dE$ is the rate at which interactions take place of nucleons with energy E to $(E + dE)$. The lower limit of the integral in equation 7.1 was assumed to be $E = 3E_\pi$.

The empirical model of Cocconi et al. (1961), (the "CKP" model) was used to describe the energy distribution in the laboratory system of charged pions produced in nucleon-air nucleus collisions, this being:-

$$N(E_\pi)dE_\pi = \frac{A}{T_P} \exp - \frac{E_\pi}{T_P} \cdot dE_\pi \qquad 7.2$$

where T_P is the mean pion energy given by:-

$$A\ T_P = \frac{2\ K_\pi E}{3} \cdot \qquad 7.3$$

A is the multiplicity of forward (in the centre of mass system) charged pions and is equal to $0.90\ E^{\frac{1}{4}}$, where E, the incident nucleon energy, is in units of GeV. The model is based on the experimental work of Baker et al. (1961) with a 29.5 proton beam incident on aluminium and beryllium targets. Consequently, it is considered that the model may be applied to nuclear interactions in air, which

has a mean atomic number between that of aluminium and beryllium, with negligible error. It is assumed that the model may be applied to the higher energies considered here.

If the primary differential nucleon spectrum is of the form:-

$$M_o(E)dE = B.E^{-\gamma}\ dE \qquad 7.4$$

and K_T is the total fraction of its energy lost by a nucleon in an interaction, then the spectrum of nucleons after each nucleon has interacted exactly n times is:-

$$M_n(E)dE = B.E^{-\gamma}\ (1-K_T)^{(\gamma-1)n}dE \qquad 7.5$$

The rate at which interactions occur at energies between E and (E + dE) is then approximately:-

$$n(E)dE = \sum_{n=0}^{\infty} M_n(E)dE$$

$$= \frac{B.E^{-\gamma}\ dE}{[1-(1-K_T)^{(\gamma-1)}]} \qquad 7.6$$

From equations 7.1, 7.2 and 7.6, the pion production spectrum is:-

$$F(E_\pi)dE_\pi = B.\int_{E=3E_\pi}^{\infty} \frac{\frac{A}{T_P}\exp\left(-\frac{E_\pi}{T_P}\right)dE_\pi.E^{-\gamma}\ dE}{[1-(1-K_T)^{(\gamma-1)}]} \qquad 7.7$$

The pion production spectrum is known from calculations based on the measured spectrum of muons at sea-level. Equation 7.7 therefore gives the intensity of the primary cosmic radiation in terms of the total and pion inelasticities as variable parameters.

7.3 The Relationship between Total and Pion Inelasticity

It has been found by many authors, e.g. Powell (1962), that the number of particles other than pions produced in nuclear interactions is small over a wide range of energies.

Although there are no direct measurements of the fraction of the available energy going into the production of particles other than pions, it is reasonable to assume that since the numbers of such particles are small, the fraction of the energy taken by them is also small.

According to Powell, about 75% of the secondary particles are π-mesons having altogether 30-45% of the available energy. The incident nucleon usually retains about 50% of its incident energy after a collision. The other 25% of the secondary particles must be K-mesons and baryons and they will share between them 5 - 20% of the available energy. The quantity "K_π" in equation 7.3 represents the fraction of the available energy which is taken by the forward pions and must therefore be slightly smaller than the fraction taken by all the pions. Consequently, the best estimate of $(K_T - K_\pi)$ has been taken to be 12%.

As there is a large degree of uncertainty about the above figure of 12%, the extreme case of $(K_T - K_\pi) = 0$ has also been considered. Physically this represents the condition that only pions are produced in nuclear interactions.

7.4 The Primary Spectrum

A trial primary nucleon spectrum was assumed of the form:-

$$N(E)dE = B.E^{-2.7}\ dE. \qquad 7.8$$

With $B = 9.43$ $(=B_o)$ and E in units of GeV, equation 7.8 agrees within 20% with the "M.I.T." nucleon spectrum in the energy range 2.10^2 - 10^5 GeV.

By the method described in Chapter 6, the value of the total inelasticity which would give the observed sea-level nucleon intensities was calculated for various values of B. It was assumed that K_T is not a function of incident energy.

From equation 7.7 for each of several chosen values of B, the value of K_π was calculated which gave the "measured" pion production spectrum. The pion production spectrum used was that given by Wolfendale (1962), which was calculated under the assumption that all muons reaching sea-level come from the decay of pions.

At each energy considered, the value of B was found such that the relation:- $K_T - K_\pi = 0.12$, was satisfied. The corresponding values obtained for K_T and K_π are respectively 0.47 and 0.35.

The best line was drawn through these calculated points on the differential primary spectrum, the corresponding integral spectrum of primary nucleons being shown in Figure 7.2. This satisfies the condition that $K_T - K_\pi = 0.12 \pm 0.04$, and represents the best estimate from the present work of the spectrum of primary nucleons. The intensity of this predicted integral spectrum, expressed as a fraction of the intensity of the "M.I.T." nucleon spectrum is shown in Figure 7.1. The intensities calculated under the assumption that the difference, $K_T - K_\pi$, is exactly 0.12 are also shown in this figure.

The lower limit for the primary intensities has also been calculated by the same method. This is the spectrum of primary nucleons which when compared with the sea-level proton spectrum and the pion production spectrum leads to the same value for K_T and for K_π i.e. all the available energy goes into the production of pions. The calculation of the lower limit to the primary intensities is the same as that for the best estimate except for the requirement that K_π be approximately equal to K_T instead of 12% less than K_T. The value of K_T and K_π obtained by this method is 0.43 ± 0.02. The integral spectrum is also shown in Figure 7.2, and in Figure 7.1 is given as a fraction of the "M.I.T." nucleon spectrum.

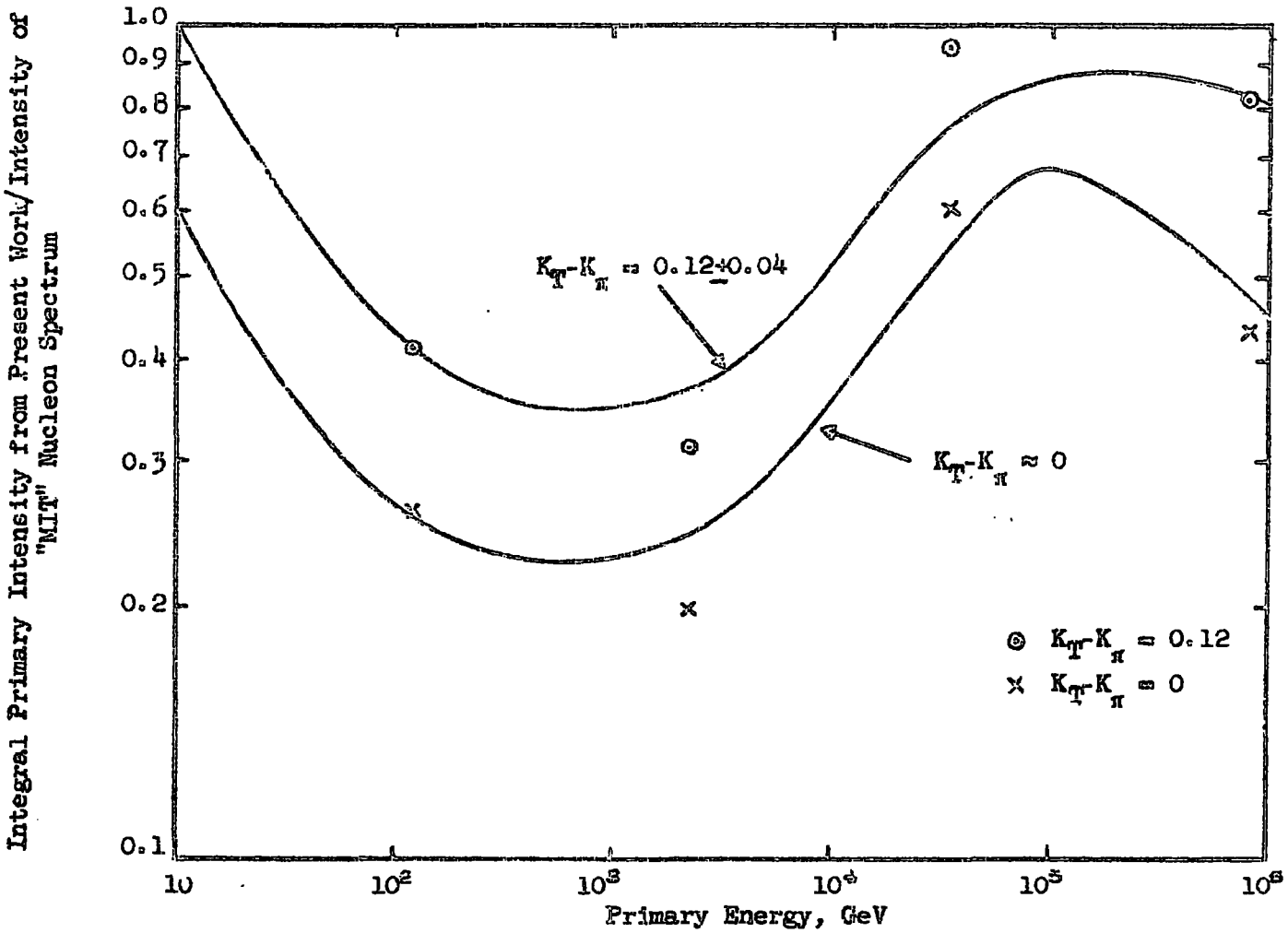
Integral Primary Intensity from Present Work/Intensity of "MIT" Nucleon Spectrum
1.0
0.9
0.8
0.7
0.6
0.5
0.4
0.3
0.2
0.1
$K_T-K_\pi = 0.12\pm0.04$
$K_T-K_\pi \approx 0$
$K_T-K_\pi = 0.12$
$K_T-K_\pi = 0$
10
10^2
10^3
10^4
10^5
10^6
Primary Energy, GeV

Fig. 7.1

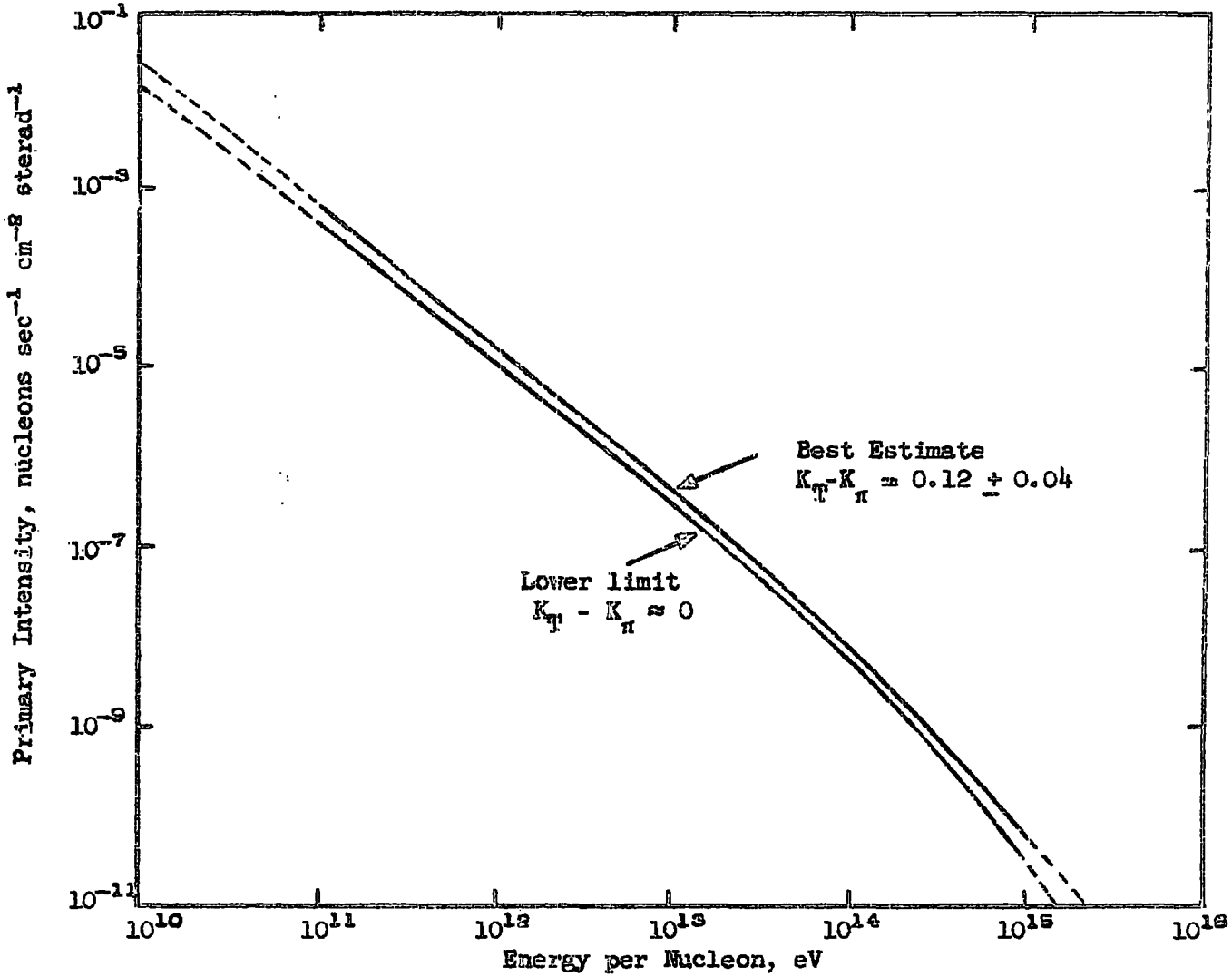

The Integral Primary Spectrum of Nucleons from the Present Work

Fig. 7.2

The values deduced for the primary intensities from the present calculations are compared with other recent measurements of primary cosmic ray intensities in Chapter 9.

CHAPTER 8

THE EFFECT OF FLUCTUATIONS IN ELASTICITY ON THE ANALYSIS

8.1 Observed fluctuations in Elasticity

Although it has been known for several years that the inelasticity of nuclear interactions is not constant, it is only recently that experiments have been performed to measure this variation without bias due to the experimental technique. Such experiments are possible with accelerators, since well collimated beams of particles of accurately known energies are available from them and an unbiassed sample of nuclear interactions can be observed by line scanning of bubble chamber photographs or nuclear emulsions.

Two experiments have been performed at C.E.R.N. using nuclear emulsions in a pulsed magnetic field. Major (1963), working at an energy of 13.5 GeV, measured the energies at the fastest emergent secondary in each of twenty eight interactions observed. In all except three of these, the most energetic secondary was positively charged. The elasticity distribution is shown in Figure 8.1 for the eighteen interactions in which all of the secondary tracks could be measured and in which the most energetic secondaries were considered to be the continuing proton primaries. Yash Pal et al. (1963), with a similar experimental arrangement but at an incident proton energy of 25 GeV, studied the particles emitted from 77 stars

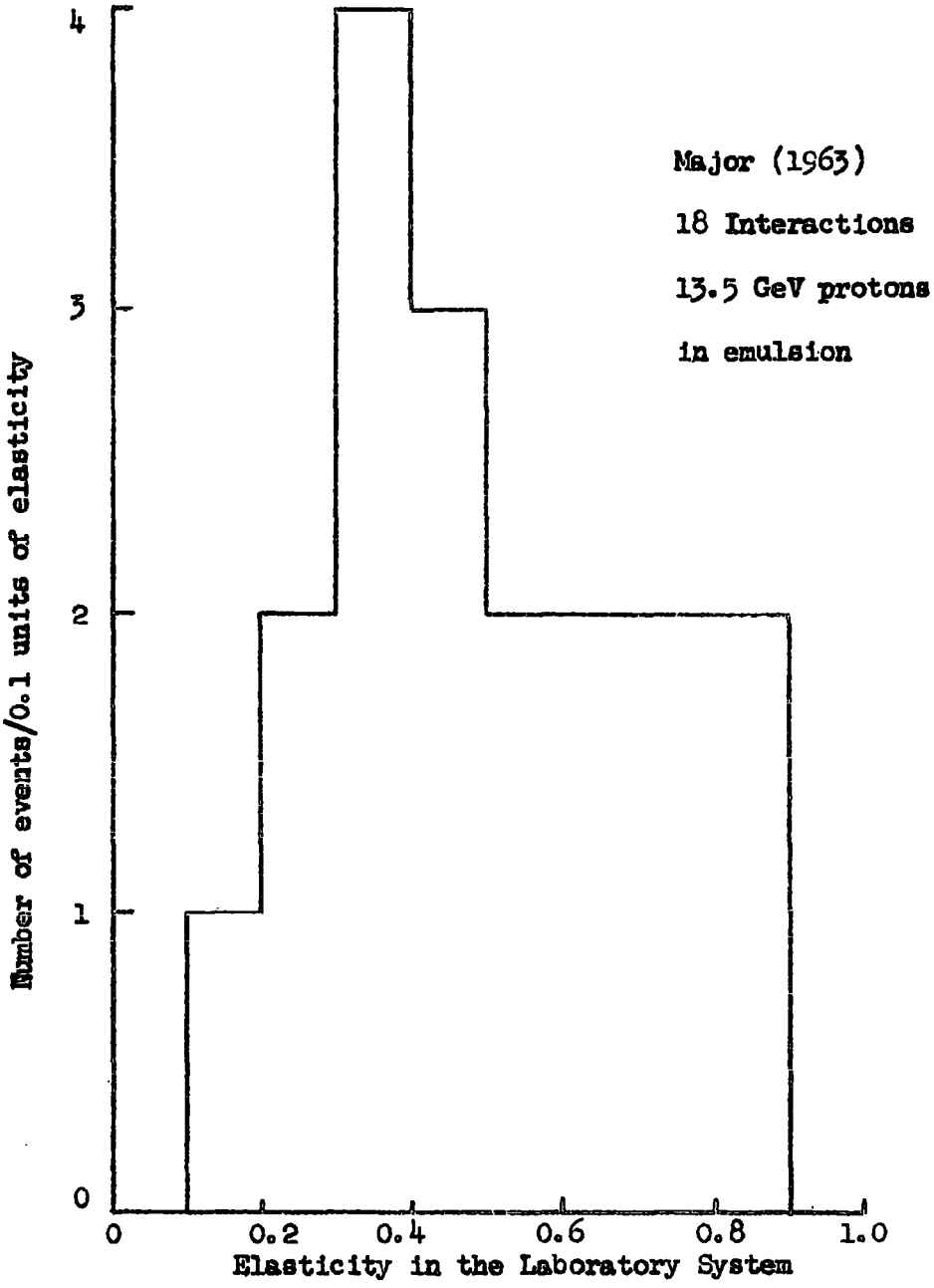
Major (1963)
18 Interactions
13.5 GeV protons
in emulsion
Number of events/0.1 units of elasticity
0
1
2
3
4
0
0.2
0.4
0.6
0.8
1.0
Elasticity in the Laboratory System

Fig. 8.1

within a forward angle of 5^{o}. In both experiments, the measured elasticities varied from zero to unity.

Dodd et al. (1961) measured the energy distribution of protons with laboratory energy <750 MeV, i.e. those emitted backwards in the centre of mass system, which emerged from interactions of 24 GeV protons in a hydrogen bubble chamber. Since proton-proton interactions are symmetrical in the centre of mass system, after interacting, the "target" protons will emerge backward with the same energy distribution as the "incident" protons have in the forward direction, and the elasticity distribution of the interactions can be calculated. This is shown in Figure 8.2 where the elasticity is calculated in the laboratory system. The elasticity values vary from unity to the minimum which was observable in that experiment. The distribution is based on 135 identified protons. However, the experimental distribution is biassed towards events with high elasticity as the condition that the target nucleon should have <750 MeV in the laboratory system leads to a lower energy limit in the centre of mass system which is dependent on the angle made by the secondary nucleon to the incident direction. As a result, there is a bias against observing events with low elasticity. This bias increases with decreasing elasticity and in this experiment it was impossible to observe interactions with elasticity in the laboratory system less than 36.5%. Nineteen of the protons shown (dotted) in

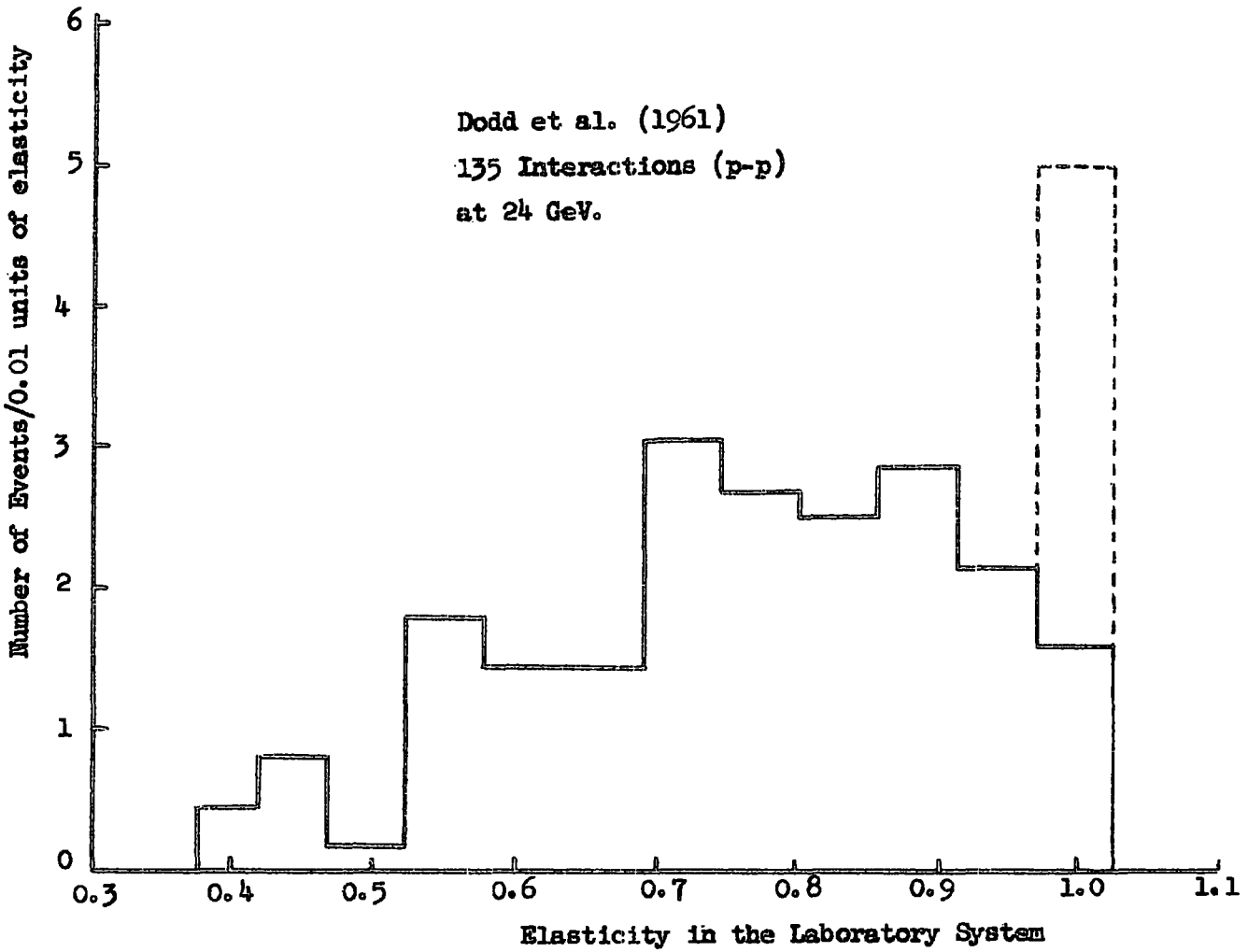
Dodd et al. (1961)
135 Interactions (p-p)
at 24 GeV.
Number of Events/0.01 units of elasticity
0
1
2
3
4
5
6
0.3
0.4
0.5
0.6
0.7
0.8
0.9
1.0
1.1
Elasticity in the Laboratory System

Fig. 8.2

the highest elasticity cell of the distribution had elasticity apparently greater than unity, presumably because of errors in measurement.

8.2 The Effect of Fluctuations in Elasticity on the Nucleon Intensities in the Atmosphere

Suppose that a nucleon retains a fraction f_n of its initial energy after it has undergone n nuclear interactions. Let $P(f_n)df_n$ be the probability that f_n lies between f_n and $f_n + df_n$.

For a primary spectrum of the form:-

$$N(E_p)dE_p = B\, E_p^{-\gamma} dE_p \,, \qquad 8.1$$

the intensity of nucleons reaching sea-level with energy between E and E + dE after making n interactions in the atmosphere is:-

$$n(E)dE = p(n) \int_{f_n=o}^{1} N\left(\frac{E}{f_n}\right) \cdot \frac{dE_p}{dE} \cdot dE \cdot P(f_n)df_n$$

or

$$n(E)dE = p(n)\, B\, E^{-\gamma} . dE \int_{o}^{1} P(f_n) \cdot f_n^{(\gamma-1)}\, df_n \qquad 8.2$$

where p(n) is the Poisson probability of a nucleon making n interactions in traversing the atmosphere. Then the ratio, R, of the total sea-level intensity of nucleons to the primary intensity at the same energy is:-

$$R = \sum_{n=0}^{\infty} p(n) \int_{0}^{1} P(f_n) \, f_n^{(\gamma-1)} \, df_n \qquad 8.3$$

If fluctuations in elasticity are ignored, equation 8.3 becomes:-

$$R = \sum_{n=0}^{\infty} p(n) \cdot f_{eff}^{n(\gamma-1)} \qquad 8.4$$

where f_{eff} is the unique value of elasticity for a single nucleon-air nucleus interaction. The relation between the distribution in elasticity and the unique value of elasticity which predict the same value of R is then:-

$$\sum_{n=0}^{\infty} p(n) \int_{0}^{1} P(f_n) \, f_n^{(\gamma-1)} \, df_n = \sum_{n=0}^{\infty} p(n) \, f_{eff}^{n(\gamma-1)} \, . \qquad 8.5$$

If

$$\int_{0}^{1} P(f_n) \, f_n^{(\gamma-1)} \, df_n = Y^n \, , \qquad 8.6$$

where Y is not a function of n, then the individual terms of equation 8.5 must be equal for each value of n, i.e.:-

$$f_{eff}^{n(\gamma-1)} = \int_{0}^{1} P(f_n) \cdot f_n^{(\gamma-1)} \cdot df_n \qquad 8.7$$

If the exponent of the primary differential spectrum, γ, is three, equation 8.7 means that the effective unique value of elasticity

after n interactions, f_{eff}^{n}, is equal to the root mean square value of the elasticity distribution after n interactions. However, for the range of primary energies of interest in the present calculations, γ is approximately 2.5 so that the effective unique values of elasticity calculated in Chapters 6 and 7 lie between the arithmetic mean and the root mean square values of the distribution in elasticity.

8.3 The Assumed Form of the Elasticity Distribution

The elasticity distributions which have been observed experimentally give values of f extending from 0 to 1. A probability distribution for the elasticity, f_1, of nucleon-air nucleus interactions of the form:-

$$P_1(f_1)df_1 = K f_1^{\alpha} \ell n f_1 \, df_1 \qquad 8.8$$

also extends from $f_1 = 0$ to 1 and for small values of α is sufficiently flat to approximate to the experimentally observed elasticity distributions. Equation 8.8 also has the advantages that a comparatively simple expression can be derived for the distribution in f_n, the fraction of the incident energy retained by a nucleon after it has made n interactions, and that the parameter α may be varied until the observed primary to sea-level nucleon intensity ratios are predicted.

Since f_1 must lie between 0 and 1,

$$\int_0^1 P_1(f_1)df_1 = 1$$

$$\therefore \quad K = -(1 + \alpha)^2, \qquad \text{see Appendix 7.}$$

The elasticity distribution for a single nucleon-air nucleus collision is therefore:-

$$P_1(f_1)df_1 = -(1 + \alpha)^2 \, f_1^{\alpha} \, \ell n \, f_1 \, df_1 \qquad 8.9$$

and this is shown in Figure 8.3 for $\alpha = 1$, 2 and 3.

The distribution in f_2 is given by:-

$$P_2(f_2)df_2 = \int_{f=f_2}^1 P_1(f).P_1\,(f_2/f)\,\frac{df}{f}\,df_2, \qquad \text{see Appendix 8}$$

$$= \frac{-(1 + \alpha)^4}{3!} \, f_2^{\alpha} \, (\ell n \, f_2)^3 \, df_2 \, . \qquad 8.10$$

Similarly, the distribution in f_n is:-

$$P_n(f_n)df_n = \int_{f = f_n}^1 P_1(f) \, P_{(n-1)}\left(\frac{f_n}{f}\right)\frac{df}{f}\,df_n$$

$$= \frac{-(1 + \alpha)^{2n}}{(2n-1)!} \, f_n^{\alpha} \, (\ell n \, f_n)^{(2n-1)} \, df_n \, . \qquad 8.11$$

The condition given in section 8.2, equation 8.6, such that the contribution to the sea-level intensity of nucleons from particles

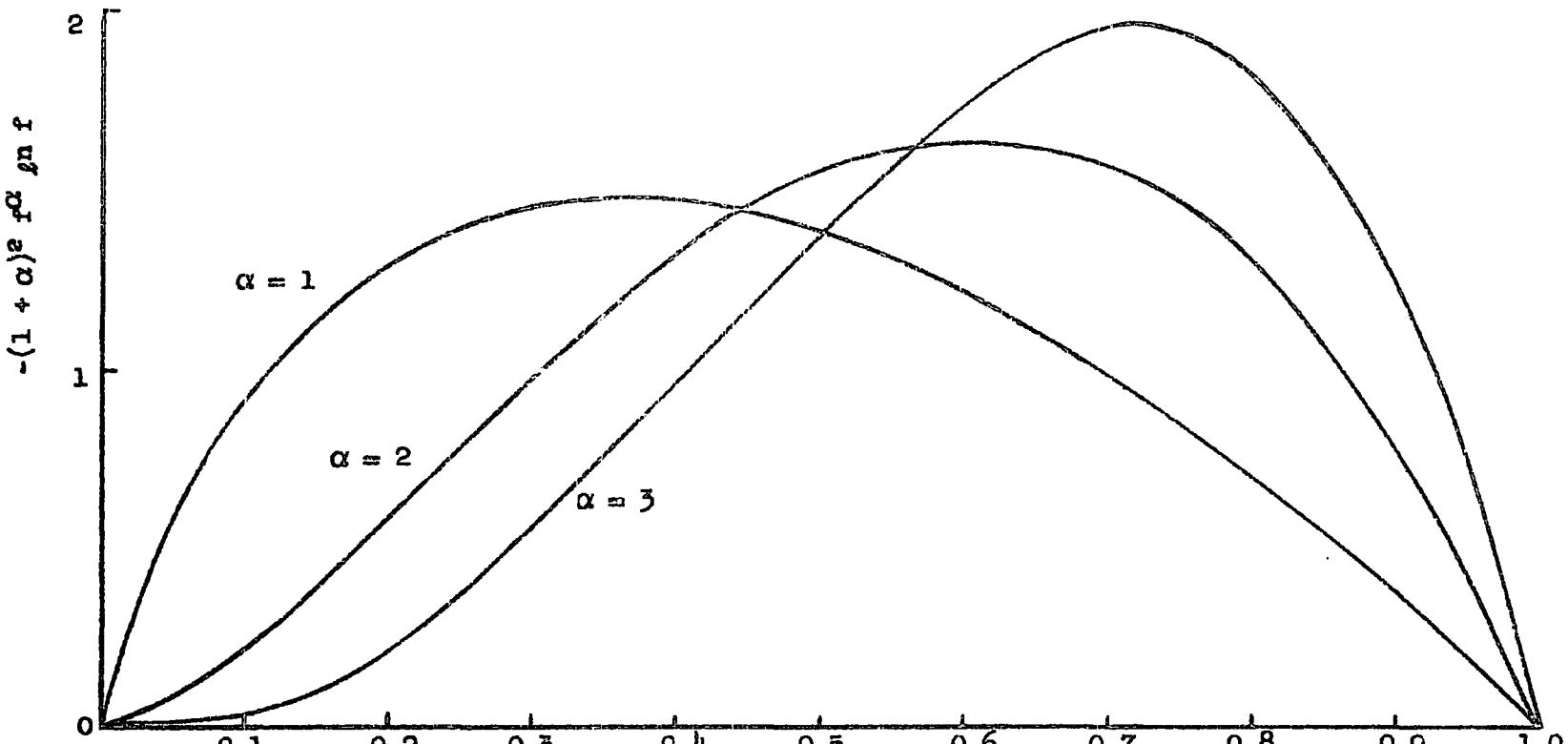

The Form of the Assumed Elasticity Distribution

Fig. 8.3

which have interacted n times can be made equal with and without fluctuations in elasticity for all values of n, is satisfied as:-

$$\int_0^1 P(f_n)\, f_n^{(\gamma-1)} df_n = \frac{-(1+\alpha)^{2n}}{(2n-1)!} \int_0^1 f_n^{(\alpha+\gamma-1)} (\ell n\, f_n)^{(2n-1)}\, df_n$$

$$= \left(\frac{1+\alpha}{\gamma+\alpha}\right)^{2n}, \qquad \text{from Appendix 7.}$$

Then substituting the above value in equation 8.7, the relation between the unique value of elasticity, f_{eff}, and the distribution in elasticity given in equation 8.9 so that the same ratio of sea-level to primary nucleon intensities is predicted, is:-

$$f_{eff}^{n(\gamma-1)} = \left(\frac{1+\alpha}{\gamma+\alpha}\right)^{2n} \qquad 8.12$$

or

$$\alpha = \left(1 - \gamma . f_{eff}^{\frac{1}{2}(\gamma-1)}\right) \Big/ \left(f_{eff}^{\frac{1}{2}(\gamma-1)} - 1\right) \qquad 8.13$$

The values of f_{eff} and γ found in Chapter 7 are 0.53 and 2.58 respectively giving $\alpha = 1.43$.

Therefore a nucleon-air nucleus elasticity distribution of the form:-

$$P(f)df = -5.9\, f^{1.43}\, \ell n\, f\, df \qquad 8.14$$

is consistent with the observed sea-level proton intensities and the primary nucleon spectrum calculated ignoring variations in elasticity. The arithmetic mean of this distribution is, from Appendix 7:-

$$\int_0^1 -5.9\, f^{2.43} \ln f \cdot df = \frac{5.9}{3.43^2} = 0.50$$

This is to be compared with the value of 0.53 found for no fluctuation in elasticity.

For a nucleon interaction length in air of 80 ± 10 g.cm^{-2} the mean number of interactions undergone by a nucleon in traversing the whole atmosphere is $12.9^{+1.8}_{-1.5}$. In Figure 8.4 the calculated contributions to the sea-level to primary nucleon intensity ratio are shown as a function of the number of interactions in the atmosphere, i.e. the individual terms of equation 8.3 with the distribution in elasticity of the form given in equation 8.9 and α = 1.0, 1.43, 2.0 and 3.0. The main contribution to the ratio for $\alpha = 1.43$ is seen to come from nucleons which have interacted between two and seven times in traversing the atmosphere. Consequently, the values of elasticity calculated refer to interactions over a wide range of incident energies, the mean being ~10 times the sea-level energy considered.

8.4 The Effect of Fluctuations in K_π

The C.K.P. model, which was used in Chapter 7 to calculate K_π in terms of the primary nucleon spectrum and the pion production spectrum, is based on the distribution in pion energies from a large number of individual interactions. Consequently, this model

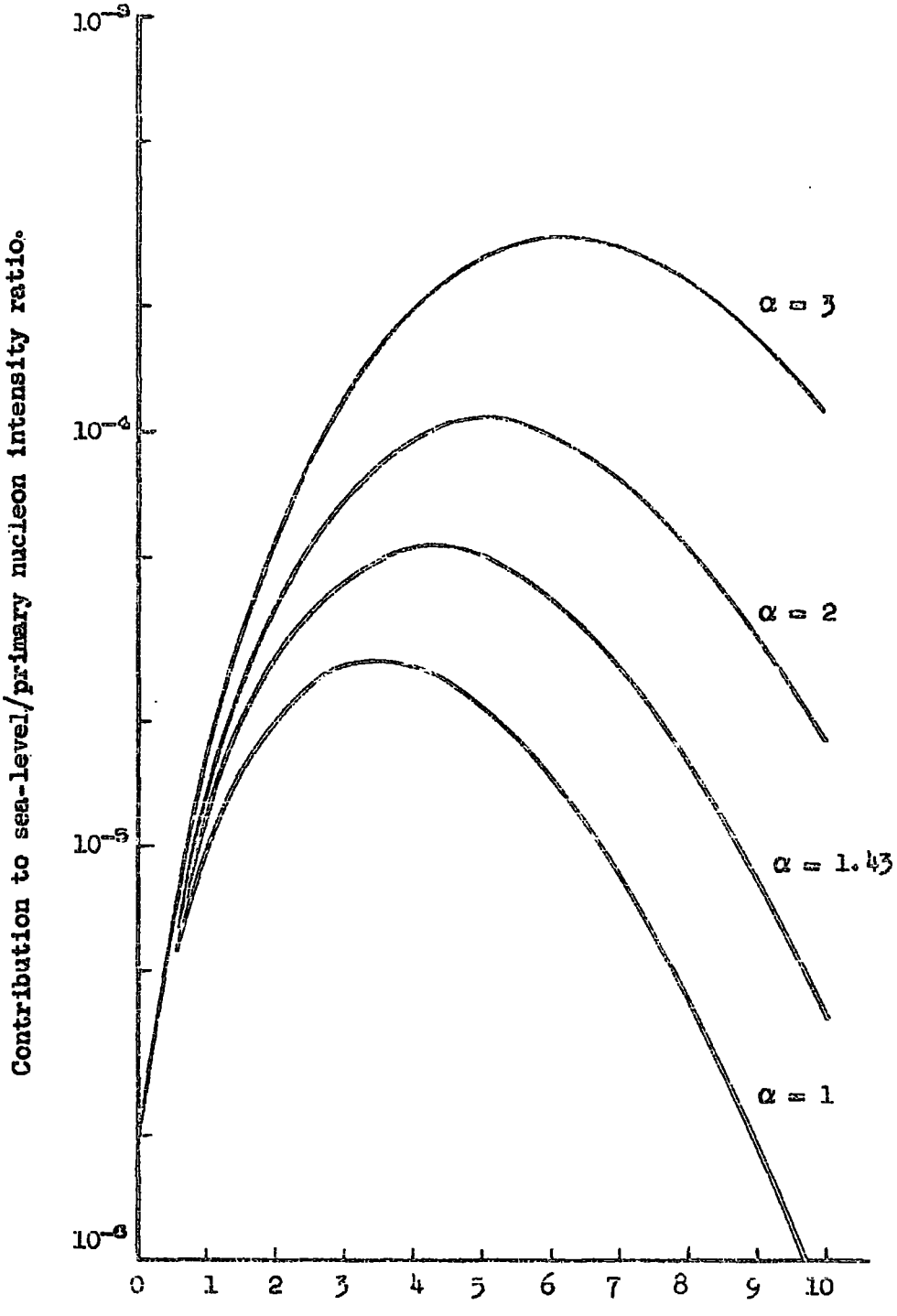

Contribution to the Sea-level/primary nucleon intensity ratio from nucleons which have interested n times in the atmosphere.

Fig. 8.4

includes to some extent the effect of variations in K_π and also in the numbers of pions produced. It is not possible to study one of these variations without knowing accurately the form of the other. In order to estimate the effect of fluctuation in K_π, a model has been assumed in which all pions produced in an interaction have equal energies in the laboratory system.

Using the same notation as in Chapter 7 section 2,

$$[N(E_\pi)dE_\pi]_E = A \quad \text{for } E_\pi = \frac{E\,K_\pi}{A} \qquad 8.15a$$

and

$$= 0 \quad \text{for } E_\pi \neq \frac{E\,K_\pi}{A} \qquad 8.15b$$

$$A = a\,E^{\frac{1}{4}}$$

so that from equations 7.1 and 7.6 the pion production spectrum is:-

$$F(E_\pi)dE_\pi = A\,n(E)\,\frac{dE}{dE_\pi}\cdot dE_\pi$$

$$= \frac{A \cdot B}{[1-(1-K_T)^{(\gamma-1)}]}\,\frac{4a}{3\,K_\pi}\left(\frac{AE_\pi}{K_\pi}\right)^{(\frac{1}{4}-\gamma)} dE_\pi$$

$$= \frac{\frac{4}{3}\,a^{\frac{4}{3}(2-\gamma)}\,B\cdot K_\pi^{\frac{1}{3}(4\gamma-5)}\cdot E_\pi^{\frac{4}{3}(\frac{1}{2}-\gamma)}\,dE_\pi}{[1-(1-K_T)^{(\gamma-1)}]} \qquad 8.16$$

With $\gamma = 2.58$, the pion production spectrum is proportional to $K_\pi^{1.77}$.

If the distribution in K_π is of the same form as that for the elasticity in a single nucleon-air nucleus interaction, then:-

$$P(K_\pi)dE_\pi = -(1+\alpha')^2 \ (1 - K_\pi)^{\alpha'} \ \ell n(1 - K_\pi)dK_\pi \qquad 8.17$$

The unique value, $\left(K_\pi\right)_{eff}$, in terms of the distribution in K_π which gives the same relation between the primary nucleon spectrum and the pion production spectrum is:-

$$\left(K_\pi\right)_{eff}^{1.77} = -(1+\alpha')^2 \int_0^1 K_\pi^{1.77} \ (1 - K_\pi)^{\alpha'} \ \ell n(1 - K_\pi)dK_\pi \ . \qquad 8.18$$

From Appendix 9

$$\left(K_\pi\right)_{eff}^{1.77} = (1+\alpha')^2 \sum_{m=0}^{\infty} (-1)^m \ \frac{1.77.0.77 \ \ldots \ (1.77-m+1)}{m!} \cdot \frac{1}{(m+\alpha'+1)^2} \qquad 8.19$$

For positive values of α', this series converges rapidly and only the first four terms need be considered. Inserting numerical values in equation 8.19 for $\left(K_\pi\right)_{eff} = 0.35$ as found in Chapter 7, $\alpha' = 3.6$; the arithmetic mean value for K_π for the distribution:-

$$P(K_\pi)dK_\pi = -21.1 \ (1 - K_\pi)^{3.6} \ \ell n(1 - K_\pi)dK_\pi \qquad 8.20$$

is $\overline{K}_\pi = 0.33$.

The difference in the value of K_π derived using the C.K.P. model and the mean value of K_π derived from a model in which large

variations in K_π are specifically included must therefore be less then 0.02.

8.5 Conclusions

The effect of allowing both K_T and K_π to have large variations in different interactions is to increase the difference, $\bar{K}_T - \bar{K}_\pi$, calculated from the best estimate of the primary spectrum shown in Figure 7.2 from 0.12 to not more than 0.17. The primary intensities should therefore be decreased by a small percentage below the previously calculated values in order to restore the required relation between the mean values of K_T and K_π. However, since many factors in the calculations are uncertain, in particular the exact form of the inelasticity variations and the interaction length for nucleons in air, and also as the effect is only of the order of a few percent, it is considered that it may be neglected.

The best estimate from the present work is that on average in a nucleon-air nucleus interaction, pions carry off $35 \pm 5\%$ of the available energy and the nucleon retains 53% of its initial energy, the remainder going into the production of other particles. These percentages are independent of incident energy in the energy range 10^9 - 10^{15} eV.

8.6 Comparison with other Measurements of Inelasticity

8.6.1 Total Inelasticity, K_T

Values have been given by many authors for the total inelasticity of nuclear interactions. Many of the earlier values were deduced from measured values for the absorption length of nucleons in air by means of expression 6.10 and are consequently inaccurate. Grigorov et al. (1959) using an ionization calorimeter to study interactions in the energy range 10^{11} - 10^{12} eV in Iron found that the mean inelasticity, $\bar{K}_{\pi}$, is greater than 50%. The statistical accuracy of the results was not sufficient to give a more accurate value.

Many individual nuclear interactions have been studied in nuclear emulsion. For most of these the incident nucleon energy has been estimated by the method due to Castagnoli et al. (1953) which uses the supposed symmetry of the angular distribution of the secondary particles in the centre of mass system. Then the "half angle" i.e. the angle to the direction of the incident particle within which half of the secondary particles appear in the laboratory system, can be related to the velocity of the centre of mass system with respect to the laboratorysystem. Hence, the velocity and therefore the energy of the primary particle can be found. It is now known that this method can lead to errors of up to a factor of three in the estimated energy in either direction, but usually to an overestimate. This has been shown by Aly et al. (1963) working at C.E.R.N. on 30 GeV proton interactions in nuclear

emulsions and by Lal et al. (1962) from a comparison of the energy measured with an ionization calorimeter with that calculated by the Castagnoli method.

The experiments described in section 1 of this Chapter give values of $\overline{K}_T = 49 \pm 12\%$, Major et al., and $\overline{K}_T = 59 \pm 5\%$ from the work of Yash Pal, both values being for proton-emulsion nuclei interactions.

The average total inelasticity of proton-proton interactions calculated from the work of Dodd et al. shown in Figure 8.2 is $\overline{K}_T = 23.5\%$, ignoring those events for which the measured elasticity is greater than unity, see section 1.

In order to compare the values of inelasticity found for different target nuclei, it is necessary to calculate from the measurements the corresponding values for nucleon-nucleon inelasticity.

In Appendix 5 the percentages of the interactions in air and in emulsion nuclei in which n nucleon-nucleon interactions occur are calculated using a statistical model of the nucleus. The results are given in Table 8.1.

Then, the relation between the mean elasticity of nucleon-nucleon interactions f_1 and the mean elasticity which would be observed in emulsion, f_E, is:-

No. of N-N interactions n	% of all interactions in which n N-N interactions occur, R(n)	
	Air	Emulsion
1	36.7	25.0
2	30.1	26.0
3	18.5	20.8
4	9.25	13.6
5	2.66	7.5
6	-	3.5
7	-	1.3

Table 8.1

$$f_E = \frac{\sum_{\text{all } n} R_E(n) \cdot f_1^n}{\sum_{\text{all } n} R_E(n)} \qquad 8.21$$

A similar relation applies for interactions in air. Taking a mean value of 45 ± 5% for the elasticity of nucleon-emulsion nucleus collisions, the mean elasticity of nucleon-nucleon interactions, from equation 8.21 is 71 ± 4%, i.e. $\bar{K}_T = 29 \pm 4\%$.

With a value for the interaction length in air of 80 g.cm^{-2}, the mean elasticity of nucleon-air nucleus collisions calculated from the present work, section 5, is 53%. Using the expression for air corresponding to equation 8.21 the nucleon-nucleon elasticity is found to be 71%, $\bar{K}_T = 29\%$, in good agreement with the value deduced from nuclear emulsion measurements.

These values for elasticity are lower than that obtained from the direct measurements of Dodd et al. as is to be expected due to the experimental bias in that work against interactions with low elasticity (see Section 8.1).

These results are summarized in Table 8.2.

	Measured Total Inelasticity %	Predicted nucleon-nucleon total inelasticity %
Proton-proton	23.5	23.5
Proton-air Nucleus	47.0	29.0
Proton-Emulsion Nucleus	55.0	29.0

Table 8.2.

8.6.2 Pion Inelasticity, K_π

Measurements of K_π for cosmic ray particle interactions in nuclear emulsions are in general not accurate due to the difficulty in determining the primary energy. Yash Pal and Rengarajan (1962), using nuclear emulsion to detect electron pairs produced by γ-rays from the decay of π^o-mesons which come from the interactions of 24 GeV protons (C.E.R.N., P.S.) in carbon, found $K_\pi = 43 \pm 7\%$. The value for K_π deduced from the work of Baker et al. (1961), with a 29.5 GeV proton beam at Brookhaven incident on targets of aluminium and beryllium, is 38%. Subrahmanyan (1962) has measured K_π for the interactions of nuclear active cosmic ray particles in carbon with a multiplate cloud chamber. The primary energy was determined by means of an ionization calorimeter (total absorption spectrometer) and K_π was found to be $33 \pm 8\%$. The distribution in

K_π obtained by Guseva et al. (1962) again with an ionization calorimeter but with a target of lithium hydride (LiH) is shown in Figure 8.5. The mean value of K_π calculated from this is $35 \pm 5\%$. Also shown in Figure 8.5 is the distribution assumed for K_π in the present calculations, equation 8.17, with α' equal to 3.6. This is the value for α' derived in section 8.4 from the best estimate of the primary spectrum and the pion production spectrum. The good agreement obtained between the experimental and theoretical distributions supports the use of the particular type of inelasticity distribution which has been assumed. The above values for K_π are all consistent with the value of $K_\pi = 35 \pm 5\%$, the best estimate from the present work.

These measurements of K_π in various light materials are summarized in Table 8.3.

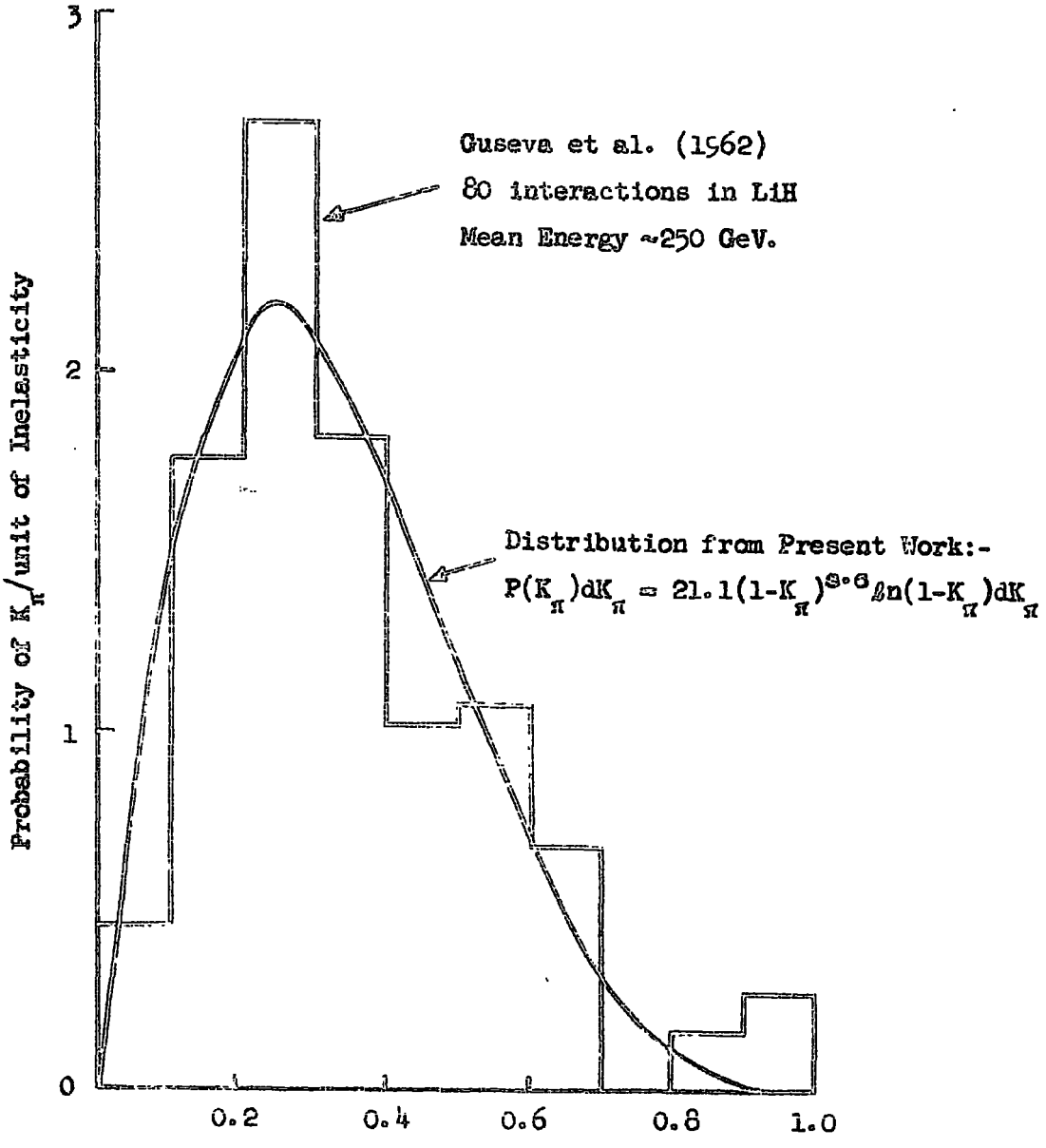

Pion Inelasticity in the Laboratory System, K_π

Fig. 8.5

Author	Nucleon Energy, GeV	K_π %	Material
Yash Pal & Rengarajan	24	43 ± 7	Carbon
Baker et al.	29.5	38	Aluminium Beryllium
Subrahmanyan	>30	33 ± 8	Carbon
Guseva et al.	>100	35 ± 5	Lithium hydride
Present work	$\gtrsim$100	35 ± 5	Air

Table 8.3.

CHAPTER 9

COMPARISON WITH OTHER MEASUREMENTS OF THE PRIMARY SPECTRUM AND THE PROTON SPECTRUM AT HIGH ALTITUDE

9.1 The Primary Spectrum

Recent measurements of the integral primary nucleon spectrum are shown in Figure 9.1, together with the best estimate from the present work. For ease of comparison, the intensities are shown multiplied by the square of the energy. The "M.I.T." spectrum is that given by Linsley et al. (1962). Below 10^{15} eV the intensities shown have been corrected for the presence of α-particles in the primary flux, see Appendix 6 and section 6.3. Above 10^{16} eV, the intensities given by Linsley et al. have been converted to a nucleon spectrum for three alternative assumptions: that the primary flux either

a) consists entirely of protons,

or b) consists of protons and α-particles and that the percentage of the nuclei with greater than a certain rigidity, which are α-particles is 12.7%,

or c) has the composition given by Waddington (1960) and that the composition of the primary rigidity spectrum is constant.

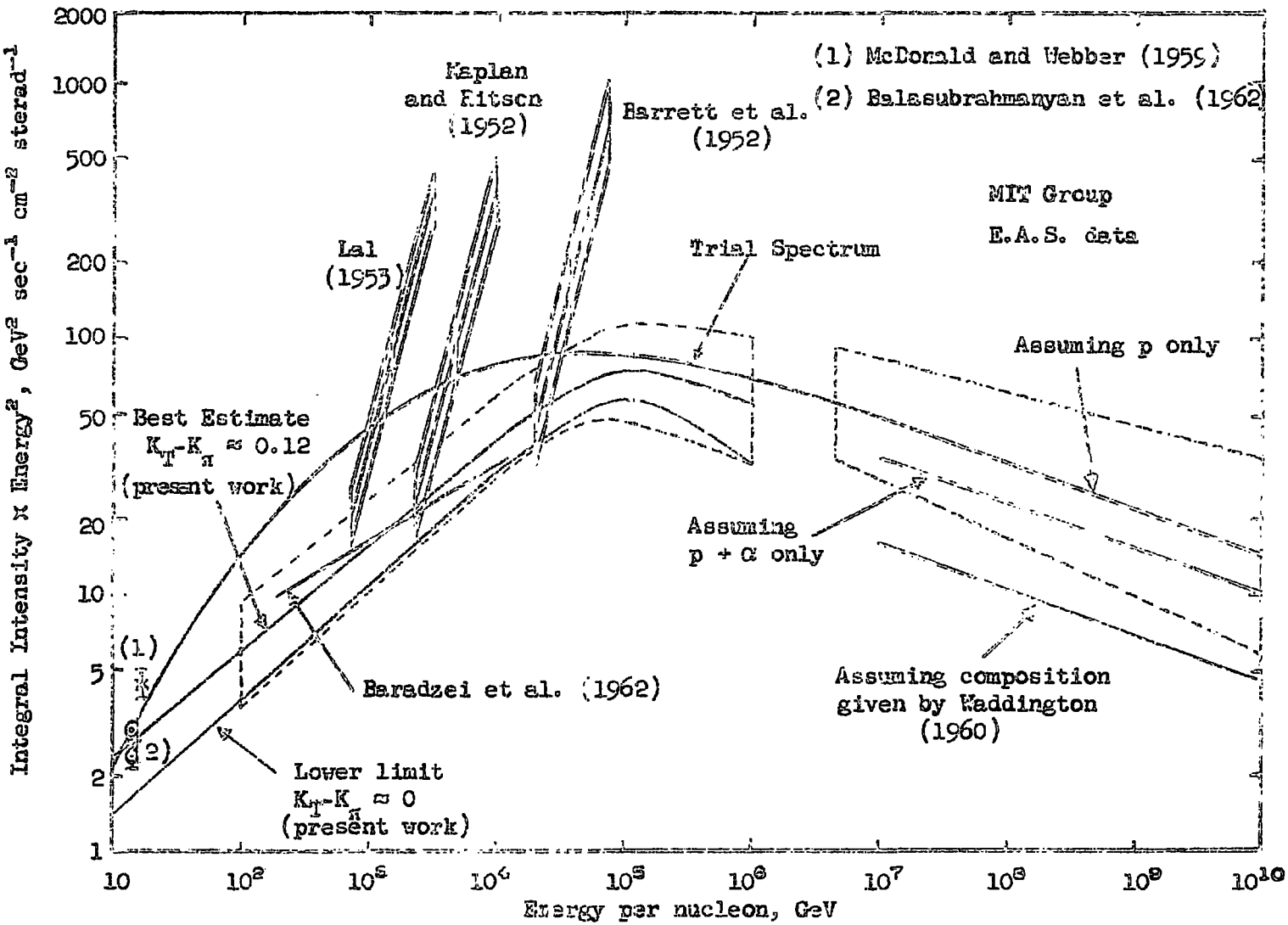

Recent measurements of the Integral Primary Nucleon Spectrum

Fig. 9.1

In the energy range 10^{12} to 10^{14} eV, the "M.I.T." spectrum is based on measurements with nuclear emulsions by Lal (1953) and Kaplon and Ritson (1952), both of these being of low statistical accuracy. In addition, in both of these experiments the energy of the incident particles was estimated by the method due to Castagnoli et al., see Chapter 8 section 8.6.1, which is now known to lead in general to an overestimate of the energy and consequently to an overestimate of the primary intensity by these authors. At energies between 10^{9} and 10^{10} eV the spectrum is based on early geomagnetic measurements, in which upward moving particles could not be identified as such.

More recently geomagnetic measurements have been made by Balasubrahmanyan et al. (1962) and McDonald and Webber (1959). In each case Geiger counters and Cerenkov detectors with good directional properties were used and it was possible to discriminate against albedo particles. As is to be expected, because of this, these measurements fall below the "M.I.T." spectrum. Baradzei et al. (1962), from a study of the energy spectra of cascades produced by nuclear active particles in a carbon block above an ionization chamber at atmospheric depths of 200, 300 and 1030 g.cm^{-2}, have calculated the integral primary spectrum in the energy range 2.10^{11} to 2.10^{13} eV.

They obtained an expression for the number of incident particles with energy greater than E eV:-

$$N(>E) = (600 \pm 150)\ (E/10^{12})^{-1.70\pm0.15}\ hr^{-1}m^{-2}sterad^{-1}$$

This spectrum is lower than the "M.I.T." spectrum by a factor of ~3 in the energy range 5.10^{11} to 10^{13} eV.

The estimate of the primary intensities in the energy range 2.10^{11} to 2.10^{13} eV made by Baradzei et al. does not differ by more than a factor of 1.25 from the best estimate of the primary intensities from the present work, being higher than the present estimate by this factor at an energy of 2.10^{11} eV and lower by this factor at 2.10^{13} eV.

The present best estimate of the primary spectrum is systematically below the "M.I.T." nucleon spectrum in the energy range 10^{11} to 10^{13} eV by a factor varying between 2 and 3 and is in agreement in the range 10^{14} to 10^{15} eV, i.e. the disagreement is confined to the part of the "M.I.T." spectrum which is not based on work performed by the "M.I.T." group, the results from the "M.I.T." air shower experiments being for primary energies above ~2.10^{15} eV.

The recent measurements in the range 10^{9} to 10^{10} eV mentioned above together with the present data lead to a best estimate primary nucleon spectrum with constant exponent in the range 10^{10} to 3.10^{13} eV/nucleon of the form:-

$$I(>E) = 0.87^{+0.52}_{-0.30}\ E^{-1.58}\ cm^{-2}sec^{-1}sterad^{-1},$$

with E in units of GeV.

9.2 The Proton Spectrum at 3200 metres Altitude

The proton spectrum at any depth in the atmosphere can be calculated from the primary nucleon spectrum and the model for the interactions of high energy nucleons deduced in Chapter 7. This method is equivalent to interpolating between the measured sea-level proton spectrum and the primary spectrum. The proton spectrum at an altitude of 3200 metres (710 $g.cm^{-2}$) has been calculated as two direct measurements of the proton spectrum have been made near to this altitude. Kocharian et al. (1959) operated a magnetic spectrograph at 3200 metres altitude and performed a series of experiments covering the energy range 0.10 - 66.0 GeV. Protons were identified at low energies by an absorption method and at high energies by their interaction in a layer of graphite above the spectrograph. The results of these experiments are shown in Figure 9.2.

Whittemore and Shutt (1952), using two cloud chambers, one above and the other below a magnet, calculated the proton spectrum in the range 0.125 - 5.2 GeV at an altitude of 3400 metres (685 $g.cm^{-2}$) from the difference in the positive-negative ratio at 3400 metres and sea-level. The intensity of their proton spectrum is normalized to the value for the total intensity of the penetrating

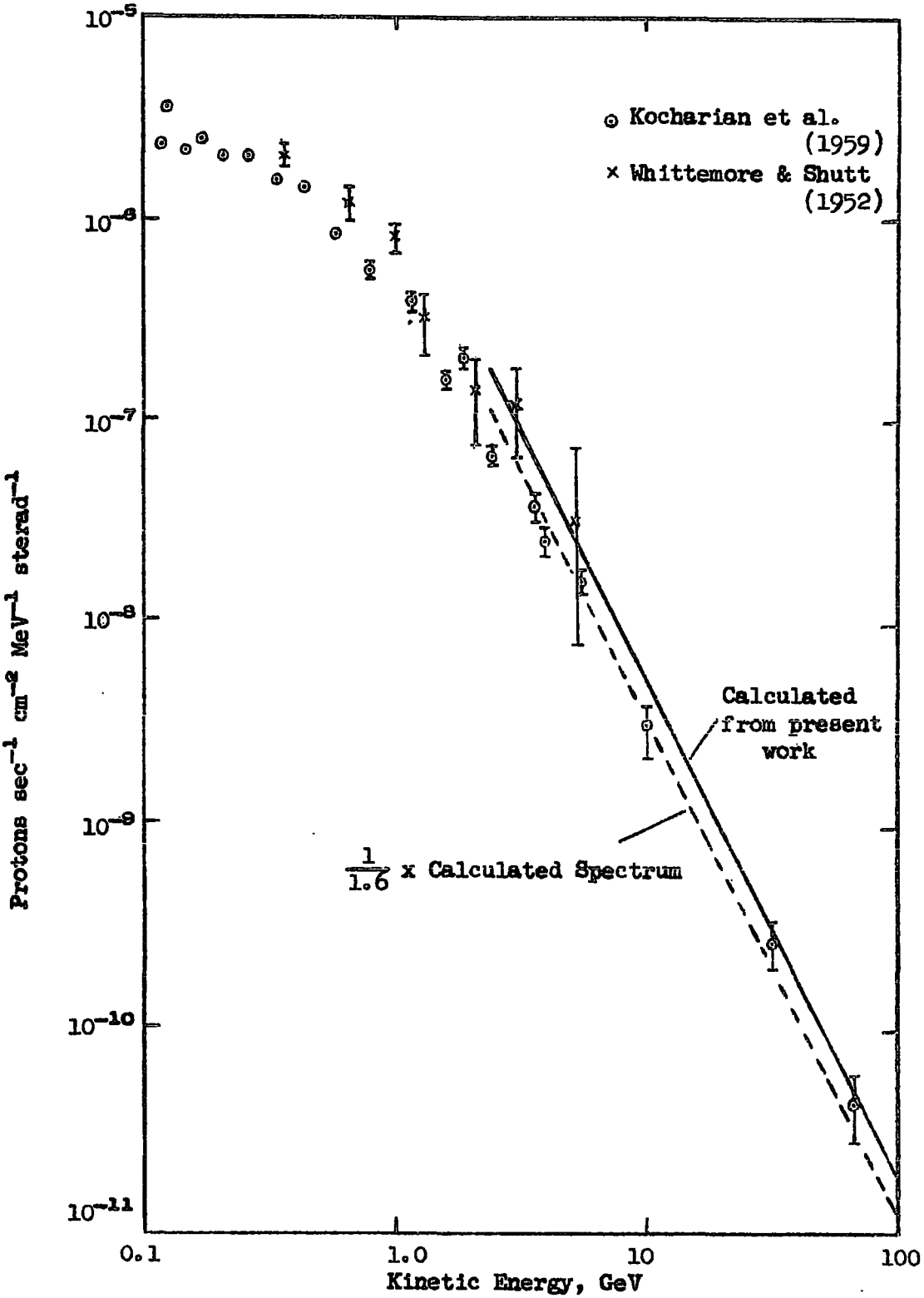

The Vertical Differential Energy Spectrum of Protons at 3200 m Altitude

Fig. 9.2

component at sea-level given by Greisen (1949). For comparison, these measured intensities have been multiplied by a factor:-

$$\exp - \Delta t/\lambda_a = 0.831$$

to give the proton spectrum at 3200 metres. These are also shown in Figure 9.2.

The proton spectrum at 3200 has been calculated from the primary nucleon spectrum derived in Chapter 7. The effective unique value for elasticity derived in that chapter with λ_i = 80 g.cm^{-2} was used in the calculation since it has been shown that the effect of fluctuations in elasticity are negligible. The calculated spectrum is shown in Figure 9.2 (full line) in the energy range 3.0 to 100 GeV. At lower energies, ionization loss becomes important and the simplified treatment can not be applied.

The calculated spectrum agrees with the measurements of Whittemore and Shutt, within the large statistical errors in that experiment. The measurements of Kocharian et al. in the region below 10 GeV, where the statistical errors are small are below the calculated spectrum. However, the normalization of these experimental results may be incorrect since the absolute proton intensities were found from a comparison with earlier work by Kocharian et al. (1956) in which an attempt was made to calculate the absolute acceptance of the apparatus. If the spectrum of Kocharian et al.

is renormalized to the measurements of Whittemore and Shutt by increasing the proton intensities given by 60%, this spectrum is then in agreement with the spectrum predicted from the present work; the mean deviation of the experimental points from the predicted spectrum is 25%, compared with statistical errors in the measurements of ~40%, see Figure 9.2.

9.3 The Attenuation Length for Nucleons in Air

The best value for the attenuation length for nucleons in air from the present work is 127 ± 4 g.cm^{-2} for nucleon energies $\gtrsim$2 GeV, see Figure 10.6. This value has been derived from the primary nucleon spectrum calculated in Chapter 7 for $K_T - K_\pi \approx 0.12$, and assuming that at sea-level the neutron intensity is equal to the proton intensity at the same energy. Values found by other authors for the nucleon attenuation length in the atmosphere are as follows. Bridge and Rediker (1952) obtained a value for λ_a of 119 ± 5 g.cm^{-2} for the nuclear active component of the cosmic radiation from measurements of the absorption of this component in lead at sea-level and 10600 ft. Bennett et al. (1962) have calculated from the zenith angle distributions of events, the absorption length for various sizes of extensive air showers. The best value for λ_a obtained was 121 ± 7 g.cm^{-2}. Coxell et al. (1963) obtained a value for λ_a of 117 ± 6 g.cm^{-2} from a study of the zenith angle distribution of air

showers of 10^5 - 10^6 particles. Cicchini and Chagaly (1961) operated a neutron monitor in a Comet IV aircraft and from a comparison of the counting rates at 1650 and 5650 metres found $\lambda_a = 149 \pm 5$ g.cm^{-2}. However, Hughes (1961) has shown that, for a standard I.G.Y. neutron monitor, approximately 75% of the countingrate is due to low energy ($\lesssim$ 1 GeV) neutrons, so that the attenuation length found by Cicchini and Chagaly refers to a lower mean energy than the other experiments. Duthie et al. (1962) found that $\lambda_a = 125$ g.cm^{-2} for energies $\geq$470 GeV.

With the exception of the work of Cicchini and Chagaly, the results of other work are in agreement with the present value for the nucleon attenuation length.

CHAPTER 10

THE SEA-LEVEL PION SPECTRUM

10.1 The Identification of Negative Pion Interactions

The negative particles detected in coincidence with neutrons in the S and H series (described in Chapter 4) were either pions or muons which interacted in the neutron monitor or muons in chance coincidence with random neutrons, assuming no anti-protons to be present in the cosmic ray flux at sea-level. Muons interact with nucleons only through their virtual photon fields and consequently the cross-section for muon-nucleus interactions is $\sim 10^{-4}$ times that for pion-nucleus interactions. Most of the muon-nucleus cross-section refers to interactions in which only a small momentum transfer takes place, as the probability of a particular momentum transfer falls rapidly as the momentum transfer increases. Most of the muon interactions therefore result in an angular scattering of the muon which is small compared with the large amount of scattering undergone by strongly interacting pions in an interaction.

The muon intensity at sea-level is approximately 10^3 times the pion intensity, so that ~10% of the interactions of negative particles are due to muons, but in only a small fraction of this 10% is the muon scattered to such an extent that it could simulate a pion interaction. In view of the following criterion b), the contribution of muon interactions to the total number of events classified as pion interactions has been neglected.

For each particle its momentum and the position, d', at level D through which it would have passed in the absence of scattering material in the spectrograph were computed from the measured positions at levels A, B and C. In addition, the root mean square displacement, σ_D, at level D due to scattering in the neutron monitor and layer of lead beneath the monitor was computed from the momentum of the particle. All events were rejected in which the particle would have passed nearer to the edge of array D than $1.5 \times \sigma_D$, in the deflection plane, according to the calculated value for d' and $1.0 \times \sigma_D$ in the back plane according to tray S hodoscope record.

The following criteria were used to identify negative pion interactions from the remaining events:-

a) No track observed in array D. Particles which stopped in the neutron monitor or in the layer of lead between it and flash-tube array D were pions if they had momenta >700 MeV/c since muons above this momenta could penetrate the absorber.

b) A single track observed in array D. The ratio of the distance of the observed position at level D, d, from the predicted position, d', to the r.m.s. displacement due to scattering, i.e. $\frac{|d-d'|}{\sigma_D}$ was calculated for each particle. Events with $\frac{|d-d'|}{\sigma_D} \leq 7$ were rejected as these were mainly muons in chance coincidence with

detected neutrons or muon interactions. The remaining events were pion interactions. The fraction of the pion interactions in which the pion emerged with $\frac{|d-d'|}{\sigma_D} < 7$ was predicted to be small from the distribution in this quantity for the identified pion interactions.

c) Two or more tracks observed in array D. The position of d_N the track nearest to the predicted position, d', at level D was measured. Events with $\frac{|d_N-d'|}{\sigma_D}$ less than or greater than seven were classified as muon electromagnetic interactions and pion nuclear interactions respectively.

10.2 The Sea-level Pion Spectrum

The intensity of charged pions with momenta between p and p+dp, using the same method as for protons (section 4.7), is given by:-

$$I_\pi(p)dp = \frac{R_\pi(n)\ dp\ [1 + C(p)]}{\Delta p.A(p).r.\sigma_\pi.\bar{\nu}.\epsilon} \qquad 10.1$$

where $R_\pi(n)$ is the number of neutrons detected from negative pions with momenta between p and p+Δp per unit time. σ_π is the probability of a pion interacting in the lead of the neutron monitor. With the negative pion-nucleon cross-section measured at CERN, Morrison (1963), Figure 10.1, the interaction length for negative pions in lead has

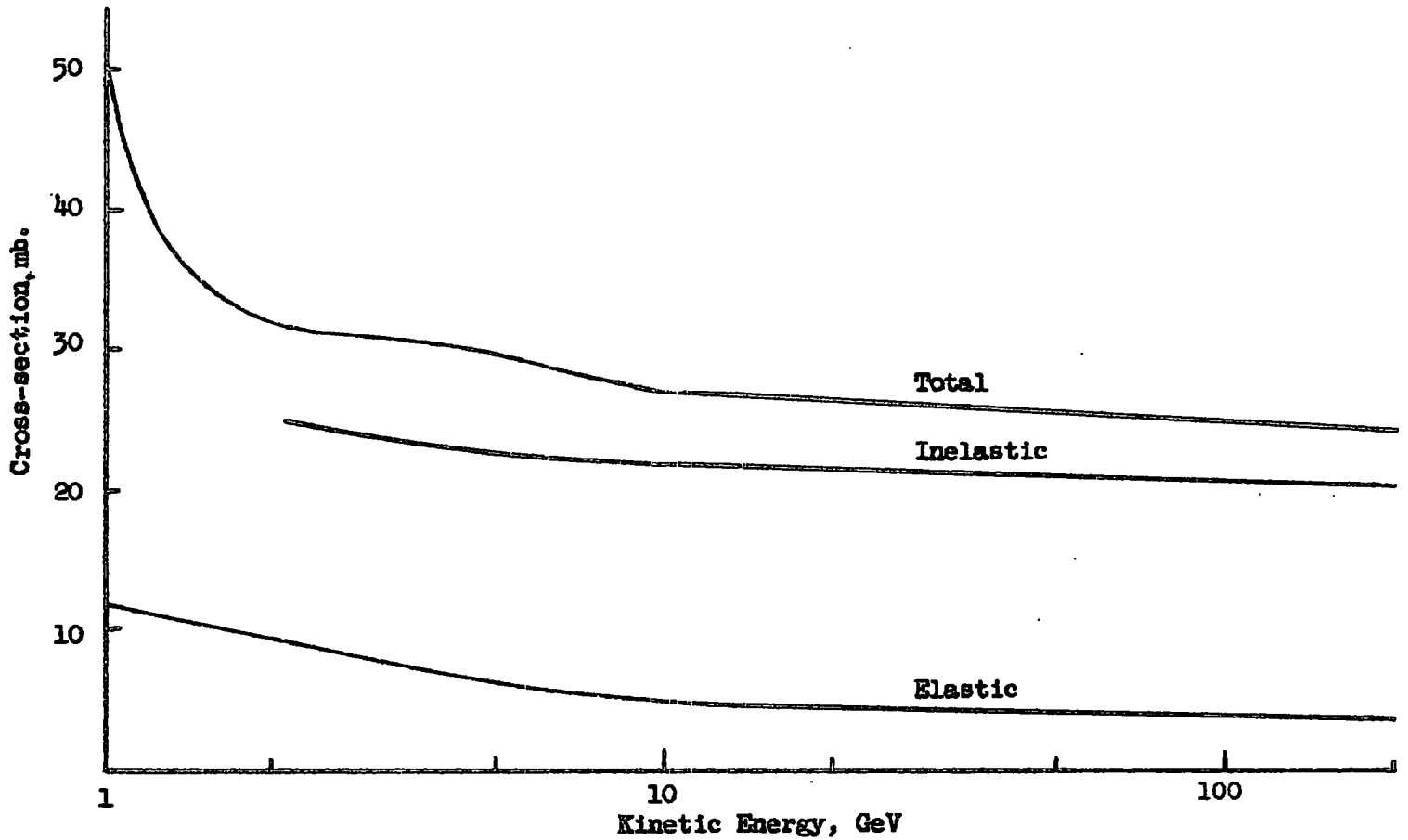

Negative Pion - Proton Cross-Sections (after Morrison, 1963)

Fig. 10.1

been calculated using the optical model (see Appendix 4) giving values from 15.6 cm of Pb ($\sigma_\pi = 0.570$) at 1 GeV to 17.8 cm of Pb ($\sigma_\pi = 0.525$) at 80 GeV. C(p) is the positive-negative ratio for pions with momentum p. This was taken to be unity, since the calculations of Taylor (1961) show that even for high energies at sea-level the majority of the surviving pions come from interactions at low altitudes where the proton-neutron ratio is unity and there is consequently no positive excess in the secondary pions. Due to the small numbers of pion interactions identified, it was not possible to accurately evaluate $\bar{\nu}$, the mean number of neutrons produced in the interactions of pions with momentum p. The sea-level pion spectrum was evaluated separately from the H and S series results, values for $\bar{\nu}$ calculated from the proton multiplicity distributions (Table 4.1) for the corresponding series were used. The measurements of the pion spectrum were corrected for scattering in the spectrograph by a method similar to that described in section 4.8. The two spectra were then combined to give the best estimate of the momentum spectrum of charged pions at sea-level which is shown in Figure 10.2. In Figure 10.3 the measurements are shown expressed as a kinetic energy spectrum. Also shown is the sea-level pion spectrum calculated by Taylor (1961) under the assumption:- nucleon attenuation length, λ_p = pion attenuation length, $\lambda_\pi = 120$ g.cm^{-2}.

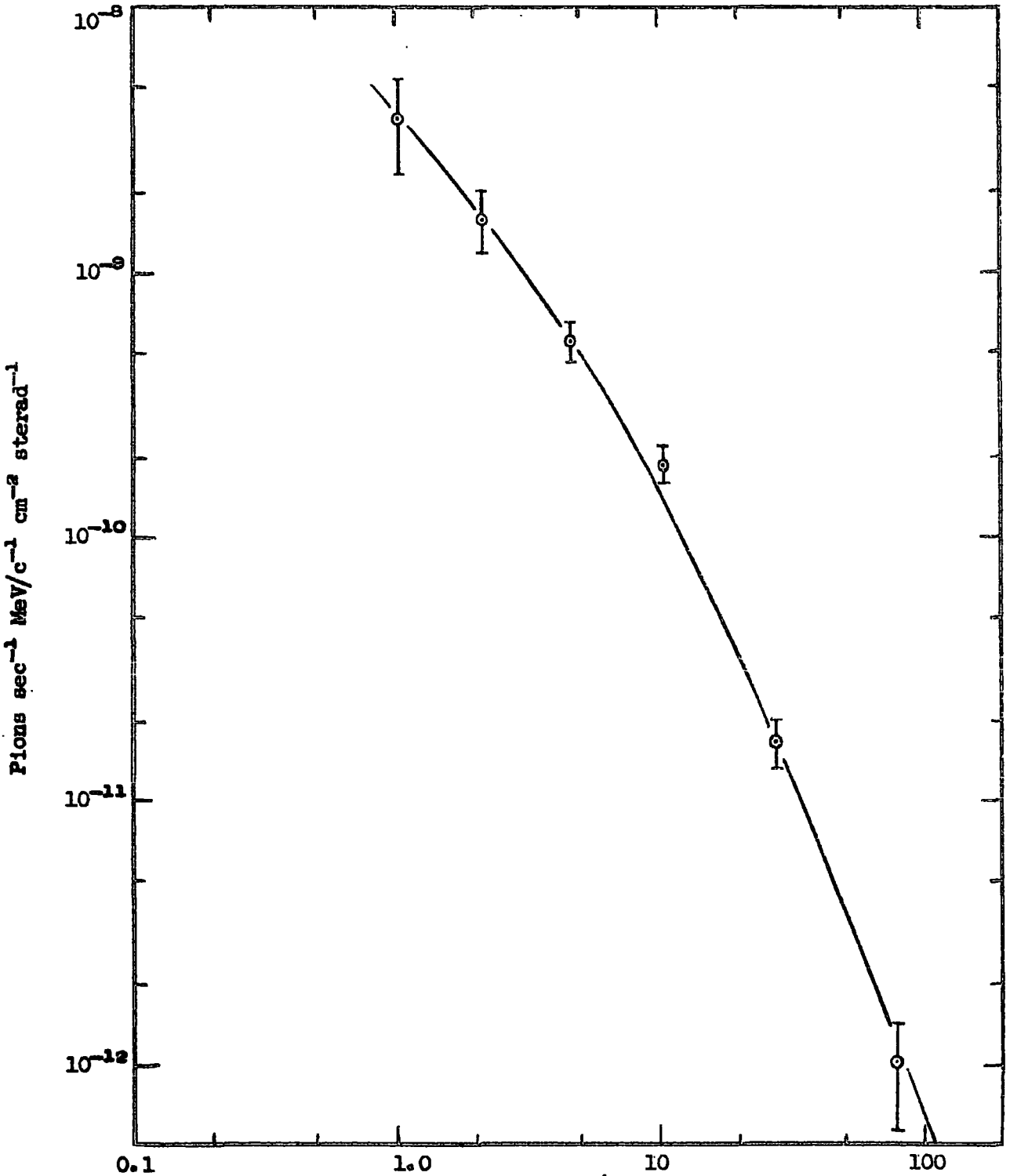

The Vertical Differential Momentum Spectrum of Pions at Sea Level

Fig. 10.2

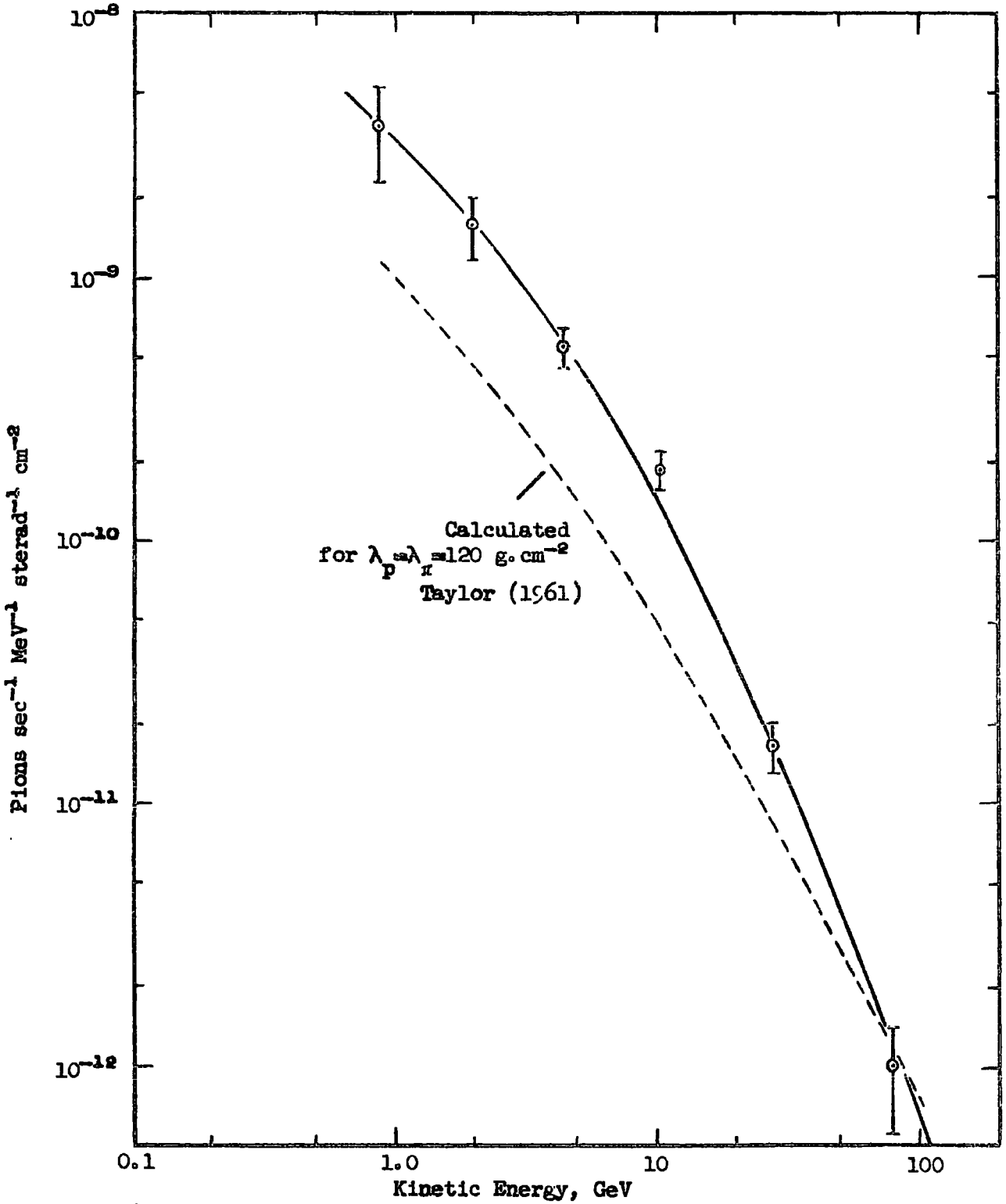

The Vertical Differential Energy Spectrum of Pions at Sea Level

Fig. 10.3

The ratio of the sea-level intensity of pions to that of muons is shown in Figure 10.4. The muon spectrum used for this comparison is that given by Gardener et al. (1962) and Hayman and Wolfendale (1962). The pion-muon ratio increases with increasing energy as would be expected since the probability of a pion reaching sea-level from any given depth in the atmosphere without decaying increases.

The pion spectrum has also been compared with the best estimate from the present work of the sea-level proton spectrum, Figure 10.5. The pion-proton ratio increases up to 10 GeV and above this energy becomes constant at ~49%. Subrahmanyan (1962) using a total absorption spectrometer at an altitude of 2200 metres (800 g.cm^{-2}) was able to measure the pion-proton ratio at 30 GeV from the change in the efficiency of an air Cerenkov counter compared with the spectrometer. The value obtained was 51.5 $\pm$ 9%, in good agreement with the results from the present work.

10.3 The Attenuation Length for Pions in the Atmosphere

It is clear, from the calculations of Taylor (1961) (Figure 10.3), that the propagation of pions in the atmosphere can not be described by a model in which the pion attenuation length is equal to that for protons, i.e. ~120 g.cm^{-2}. If the attenuation length for pions is not restricted to this value, then following Barrett et al. (1952), see Appendix 10, the following expression is obtained

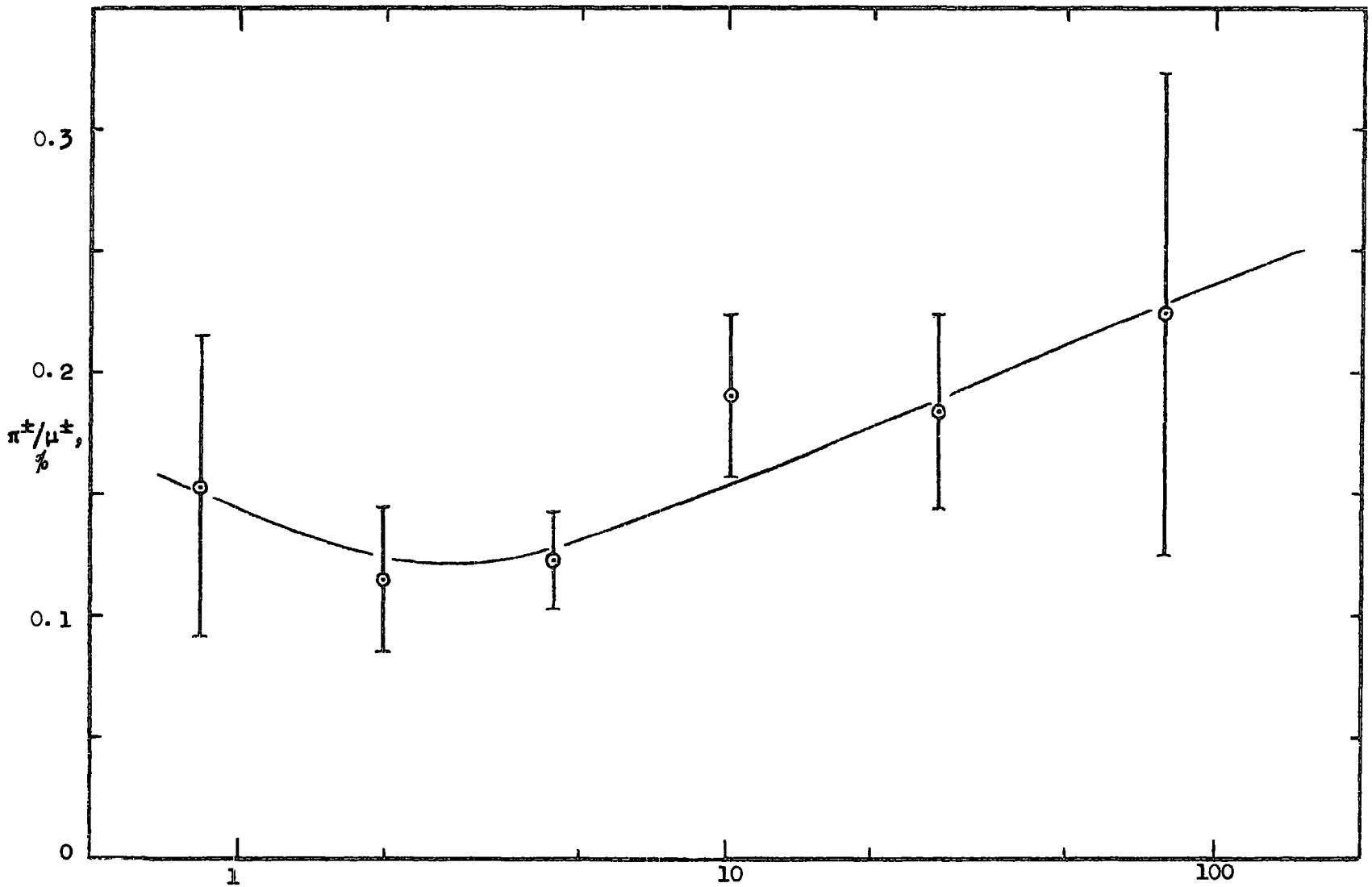

The Ratio of Charged Pions to Charged Muons at Sea Level

Fig. 10.4

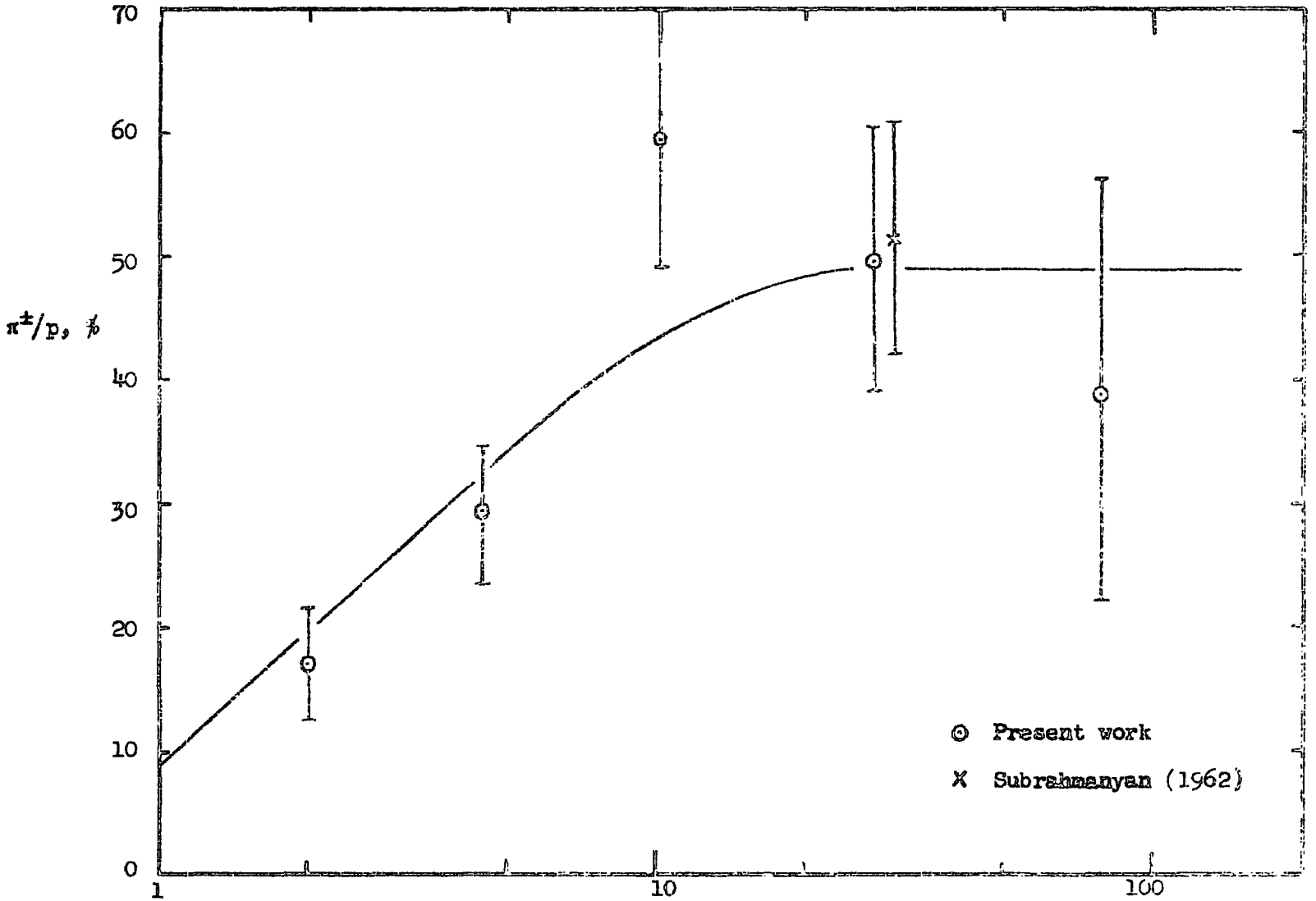

The Ratio of Charged Pions to Protons at Sea Level

Fig. 10.5

for pion intensities in the atmosphere:-

$$\pi(E,x,\theta)dE = [F(E)dE/\lambda_p]\ e^{-x/\lambda_\pi . x^{-(B/E\cos\theta)}} . \int_0^x e^{-x'/\lambda' . x', B/E\cos\theta} dx'$$

$$= F(E)dE\ e^{-x/\lambda_\pi} . \frac{x}{\lambda_p}\left\{\frac{1}{1+B/E\cos\theta} - \frac{x/\lambda'}{2+B/E\cos\theta} + \frac{1}{2!}\frac{(x/\lambda')^2}{3+B/E\cos\theta} - \ldots\right\}$$

10.2

where $\pi(E,x,\theta)dE$ = the intensity of pions with energy between E and E+dE at depth x in the atmosphere and at zenith angle θ, $F(E)dE$ = the spectrum of pions at production, calculated by Taylor (1961), λ_p = the differential absorption length for nucleons in the atmosphere, λ_π = the absorption length for pions in the atmosphere. In this case λ_π represents only the attenuation by collision of pion intensities, both decay of the pionsand the generation of further pions being taken into account separately in equation 10.2,

$$\frac{1}{\lambda'} = \frac{1}{\lambda_p} - \frac{1}{\lambda_\pi}$$

$$B = \frac{m_\pi c^2 H}{c\ \tau_o}$$

where $m_\pi c^2$ and τ_o are the rest energy and mean life of a pion, and H = the ratio of the atmospheric depth to the density of air. This quantity is given by Rossi (1952), values used in the present calculation varying from 8.35×10^5 cm (B = 153 GeV) to 8.04×10^5 cm (B = 148 GeV) for pions reaching sea-level with energies 1 and 100 GeV respectively, corresponding to the mean depths of production for such

pions calculated by Taylor. The differential attenuation length as a function of energy for nucleons in the atmosphere was calculated from the results of the present experiments at sea-level and the primary spectrum calculated in Chapter 7 and is shown in Figure 10.6. For each energy corresponding to a measured point on the pion spectrum, the vertical intensity of pions expected at sea-level was calculated from equation 10.2 for different values of λ_π. The values of λ_π found to give agreement with the observed pion intensities are shown in Figure 10.6, where it can be seen that the attenuation length for pions is ~ 30 g.cm^{-2} greater than that for protons at the same energy in the range 1 - 50 GeV.

10.4 The Elasticity of Pion Interactions

The expression derived in Chapter 6, equation 6.9 may be used to calculate the average elasticity of pion-air nucleus interactions from the attenuation length derived in section 10.3 if the exponent of the spectrum of pions produced at any given depth in the atmosphere is not a function of depth. This is so if the nucleon intensities are attenuated exponentially as a function of depth in the atmosphere. For the primary nucleon spectrum calculated in Chapter 7 which has a constant exponent in the energy range 10^{10} to 3.10^{13} eV this condition is satisfied. In addition, the exponent of the pion production spectrum over the energy range of interest is constant, (-1.64), so that no error is introduced by the use of

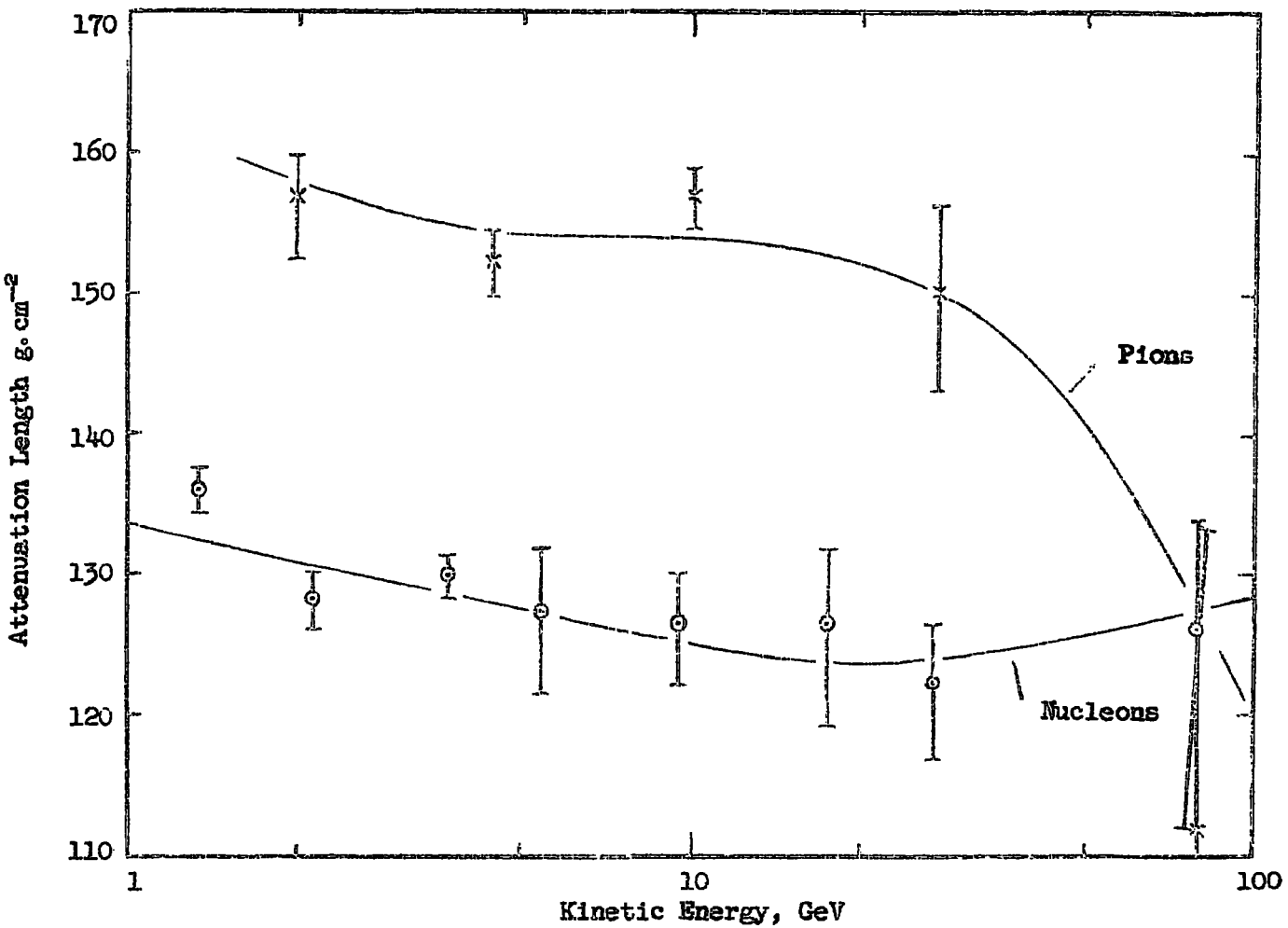

Differential Attenuation Length for Pions and Nucleons in Air

Fig. 10.6

equation 6.9. The mean free path for inelastic interactions of pions in air was calculated from the π-p cross-section given by Morrison (1963), using the optical model and is shown as a function of pion kinetic energy in Figure 10.7. The value obtained for the inelasticity of pion interactions are shown in Figure 10.8. In the energy range 2 - 10GeV the inelasticity increases from 55% to 60%. At an energy of 80 GeV, pion interactions are apparently completely inelastic but the statistical error in this measurement is large (~30%).

For pion interactions, the elasticity is to be interpreted as the fraction of the available energy carried off by the fastest pion emerging from the interaction, all other pions being assumed to have energies small compared with this.

10.5 Comparison with Other Work

The results of the present work show that, on average, pions lose a large fraction of their incident energy on interacting with an air nucleus. Experiments have been performed using pion beams from accelerators at energies up to 20 GeV. However, in these cases particular types of pion interaction have usually been studied e.g. quasi-elastic π-p collisions, strange particle production by pions, pion interactions in nuclear emulsion with large or small numbers of heavy tracks etc., whereas the results of the present cosmic ray measurements lead to average values of elasticity for all

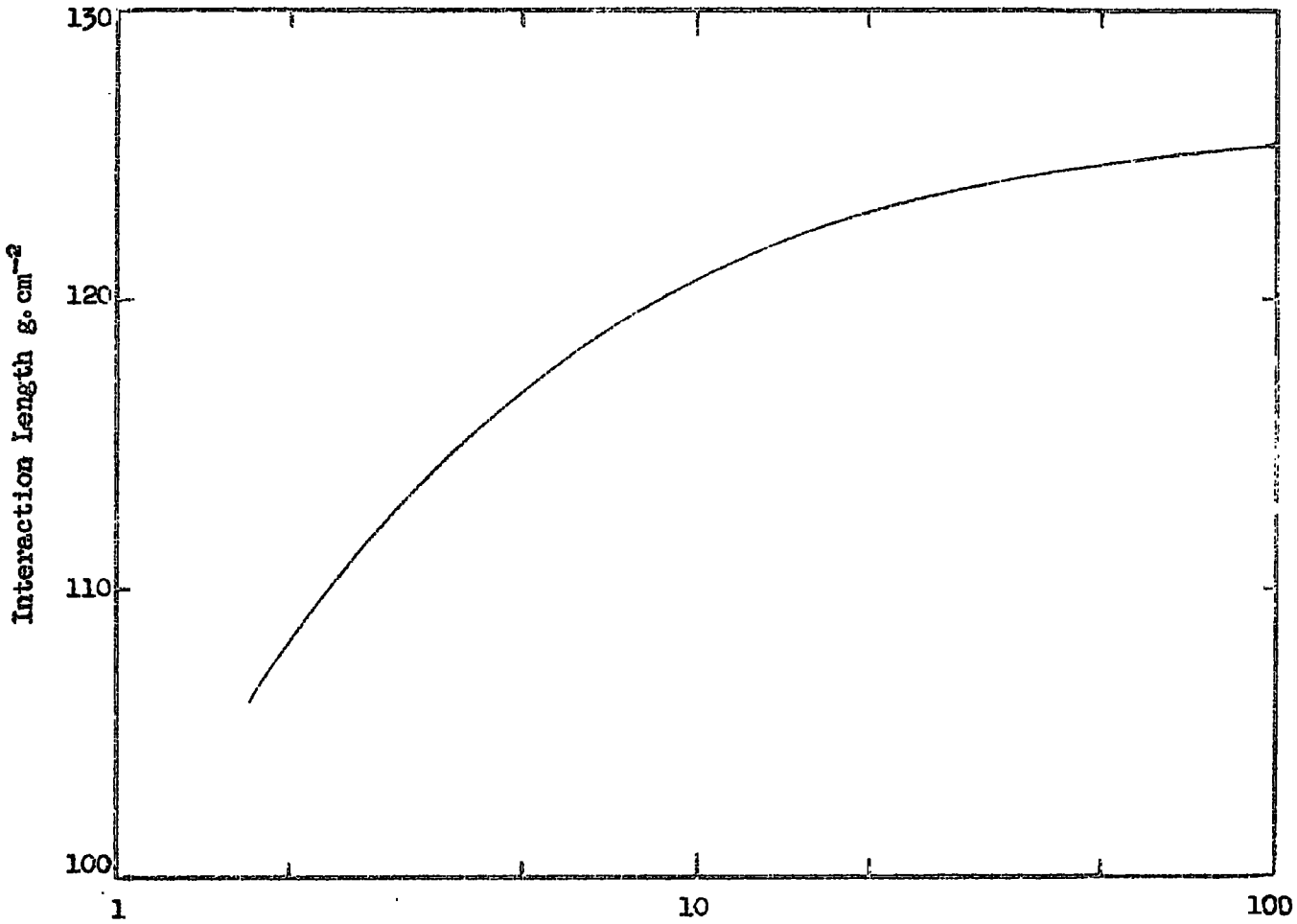

Interaction Length for Pions in Air

Fig. 10.7

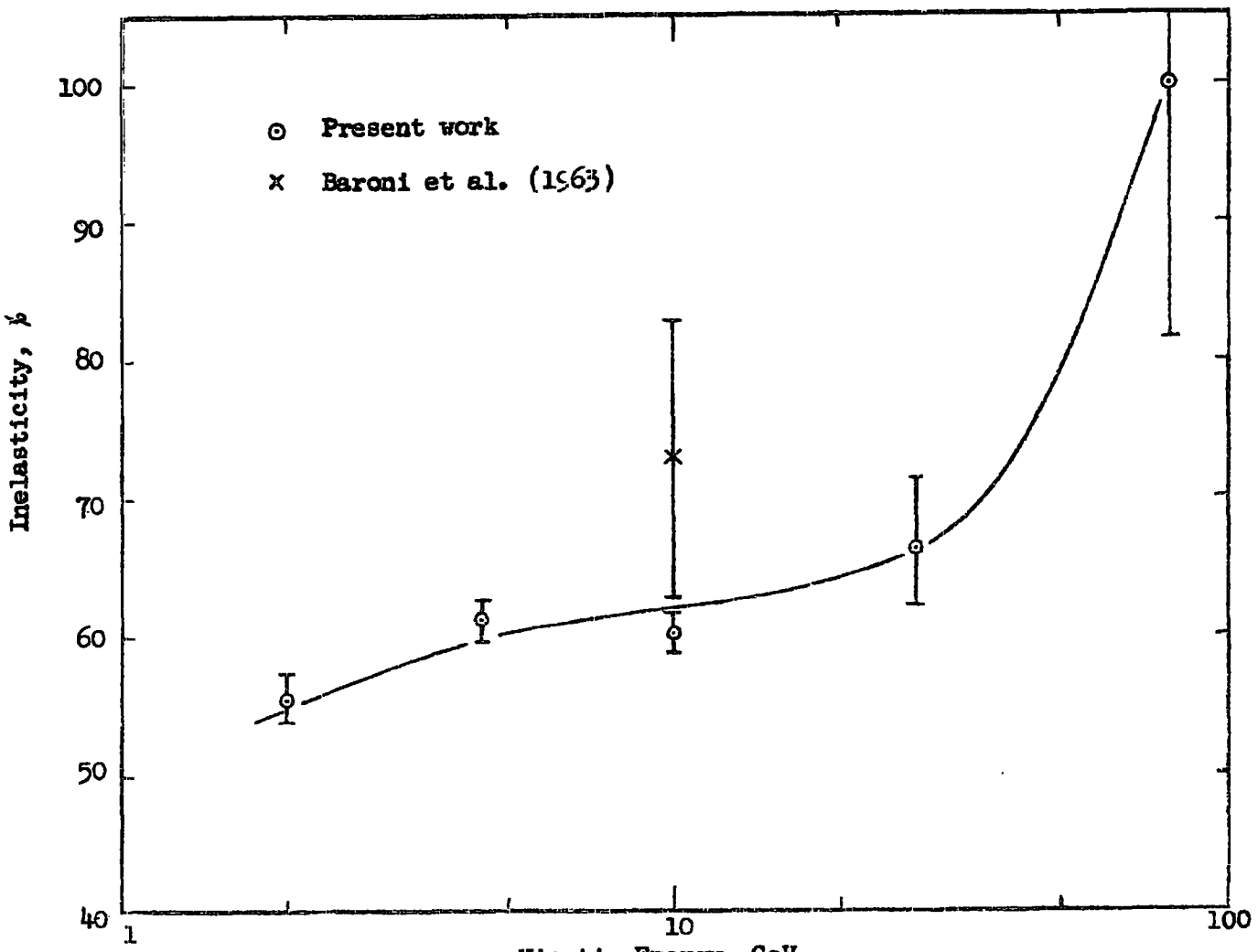

The Inelasticity of Pion Interactions

Fig. 10.8

types of inelastic pion interactions. The present results may be compared with the work of Baroni et al. (1963) in which the interactions in G5 emulsion of negative pions with momentum 10 GeV/c were studied. All events were included in which four or more charged particles emerged from the interaction. The mean inelasticity of these events was found to be 73 $\pm$ 10%, in agreement with the present work.

CHAPTER 11

CONCLUSIONS

It has been shown that a simple model for the nucleon cascade in the atmosphere may be used to describe the relation between the measured sea-level proton spectrum and the new estimate of primary nucleon intensities which has been made. In this model, the elasticity of nucleon-air nucleus collisions is not a function of the energy of the incident nucleon. The best estimate from the present work of the elasticity of such collisions is 53%.

The effect of considering large fluctuations in elasticity has been studied. It is found that for fluctuations of the particular form considered, the mean value of elasticity obtained is ~3% lower than the value obtained assuming the elasticity to have a unique value. This effect is negligible compared with the error introduced by the uncertainty in the interaction length for nucleons in air.

The new estimate of the primary nucleon spectrum, made under the assumption that ~12% of the available energy in a nucleon-air nucleus collision goes into the production of particles other than pions, may be expressed in the form:

$$I(>E) = 0.87^{+0.52}_{-0.30}\ E^{-1.58}\ \text{cm}^{-2}\ \text{sec}^{-1}\ \text{sterad}^{-1}$$

in the energy range 10^{10} to 3×10^{13} eV/nucleon, E being in units of GeV.

A constant exponent for the primary spectrum together with the fact that the elasticity is not a function of energy results in exponential attenuation of the nucleon component in the atmosphere. The best estimate from the present work of the attenuation length is 127 ± 4 g.cm^{-2}.

The direct measurement of the sea-level pion spectrum has enabled values to be obtained for the elasticity of pion interactions by considering the propagation of pions in the atmosphere. The attenuation length due to interaction, for pions in air, has been found to decrease with increasing pion energy from 157 ± 4 g.cm^{-2} at 2 GeV to 112 ± 22 g.cm^{-2} at 80 GeV. Measurements at CERN of the pion-proton inelastic cross-section (Morrison, 1963) lead to values for the interaction length in air which slowly increase with increasing pion energy. Consequently, the elasticity of pion interactions deduced from the relation between the interaction and attenuation lengths, ranges from 40% at 5 GeV to complete inelasticity at 80 GeV. This is in contrast to nucleon-air nucleus collisions, the elasticity of which has been found to be constant (53%) over the energy range considered.

ACKNOWLEDGMENTS

The author wishes to thank Professor G.D. Rochester for the provision of the facilities for this work and also for his continued support and interest.

The author is grateful to his supervisor, Dr. A.W. Wolfendale, for his help and guidance at all stages of the work. He would also like to thank Professor M.A. Meyer for his encouragement and for help with the operation of the neutron monitor.

Drs. P.J. Hayman and F.E. Taylor are thanked for help given through discussions on various aspects of the work. Thanks are also due to Dr. E.B. Hughes and Mr. A. Crispin for their assistance in the operation of the spectrograph and to Dr. Y. Kamiya for her help with the numerical calculations concerning the primary spectrum.

The technical staff of the Physics Department, in particular Mr. W. Threadgill, Mr. E. Lincoln, Mr. K. Tindale and Miss C. Guyll, are thanked for their willing help.

The assistance of Miss P.M. Hall with the preparation of this thesis is acknowledged with thanks.

Finally, the Department of Scientific and Industrial Research is thanked for the provision of a Research Studentship which enabled this work to be carried out, and also Durham University for the award of an Imperial Chemical Industries Fellowship.

REFERENCES

Alexander, G. and Yekutieli, G., 1961, Final Technical Report, AFCRL-1089, USAF Cambridge Research Center Contract No. AF 61(052) - 371.

Aly, H., Fisher, C.M. and Mason, A., 1963, Conference on Ultra High Energy Nuclear Physics, Bristol.

Ashmore, A., Cocconi, G., Diddens, A.N. and Wetherall, A.M., 1960, Phys. Rev. Letts., 5, 576.

Ashton, F., Kisdnasamy, S. and Wolfendale, A.W., 1958, Nuovo Cimento, Ser. X, 8, 615.

Baker, W.F., Cool, R.L., Jenkins, E.W., Kycia, T.F., Lindenbaum, S.J., Love, W.A., Lüers, D., Nüderer, J.A., Ozaki, S., Read, A.L., Russel, J.J. and Yuan, L.C.L., 1961, Phys. Rev. Letts., 7, 101.

Balasubrahmanyan, V.K., Ganguli, S.M., Gokhale, G.S., Kameswara Rao N., Kunte, P.K., Menon, M.G.K. and Swami, M.S., 1962, J. Phys. Soc. Japan, 17, Suppl. AIII, 433.

Ballam, J. and Lichtenstein, P.G., 1954, Phys. Rev., 93, 851.

Baradzei, L.T., Rubtsov, V.I., Smorodin, Y.A., Solovyov, M.V. and Tolkachev, B., 1962, J. Phys. Soc. Japan, 17, Suppl. AIII, 433.

Baroni, G., Conforto, B. and Manfredini, A., CERN Report EMC 63-16, 1963.

Barrett, P.H., Bollinger, L.M., Cocconi, G., Eisenberg, Y., and Greisen, K., 1952, Rev. Mod. Phys., 24, 133.

Bennett, S., Delvaille, J., Greisen, K. and Kendziorski, F., 1962, J. Phys. Soc. Japan, 17, Suppl. AIII, 196.

Biometrika Tables for Statisticians, Vol. I, 1958, Cambridge University Press.

Bozoki, G., Fenyves, E., and Janossy, L., 1962, Nucl. Phys., 33, 236.

Bridge, H.S. and Rediker, R.H., 1952, Phys. Rev,; 88, 206.

Brooke, G., Hayman, P.J., Taylor, F.E. and Wolfendale, A.W., 1962, J. Phys. Soc. Japan, 17, Suppl. AIII, 311.

Brooke, G., Hayman, P.J., Kamiya, Y., and Wolfendale, A.W., 1963, Nature, 198, 1293.

Castagnoli, C., Cortini, G., Franzinetti, C., Manfredini, A. and Moreno, D., 1953, Nuovo Cimento, 10, 1539.

Cicchini, A., and Chagaly, J., 1961, Phys. Rev., 124, 1201.

Cocconi, G., 1961, Int. Conf. on Theor. Aspects of Very High Energy Phenomena, CERN, 128.

Cocconi, G., Koester, L.J., and Perkins, D.H., 1961, Lawrence Rad. Lab. Rep., High Energy Phys. Study Seminars, No. 28, Part 2.

Conversi, M., Focardi, S., Franzinetti, C., Gozzoni, A., and Murtas, P., 1955, Suppl. Nuovo Cimento, 4, 234.

Coxell, H. and Wolfendale, A.W., 1960, Proc. Phys. Soc., 75, 378.

Coxell, H., Meyer, M.A., Scull, P.S. and Wolfendale, A.W., 1961, Suppl. Nuovo Cimento Ser. X, 21, 7.

Coxell, H., Scull, P.S. and Wolfendale, A.W., 1963, Proc. Phys. Soc., 81, 604.

Cranshaw, T.E. and Hillas, A.M., 1960, Proc. Moscow Cosmic Ray Conf., Vol. II, 210.

Dodd, P., Jobes, M., Kinson, J., Tallini, B., French, B.R., Sherman, H.J., Skillicorn, I.O., Davies, W.T., Derrick, M. and Radojicic, D., 1961, Aix-en-Provence Conf. Rep. Vol. 1, 433.

Duthie, J.G., Fowler, P.H., Kaddoura, A., Perkins, D.H., and Pinkau, K., 1962, Nuovo Cimento, 24, 122.

Fermi, E., 1949, Phys. Rev., 75, 1169.

Filthüth, H., 1955, Z. Naturforsch, Pt a, 10, 219.

Gardener, M., Kisdnasamy, S., Rössle, E. and Wolfendale, A.W., 1957, Proc. Phys. Soc. B70, 687.

Gardener, M., Jones, D.G., Taylor, F.E. and Wolfendale, A.W., 1962, Proc. Phys. Soc., 80, 697.

Geiger, K.W., 1956, Canad. Journal of Phys., 34, 288.

Greisen, K., 1949, Phys. Rev., 61, 212.

Grigorov, N.L., Murzin, V.S., Rapoport, I.D., 1959, J.E.T.P., 36(9), 759.

Guseva, W., Dobrotin, N.A., Zelevinskaya, N.G., Kotelnikov, K.A., Lebedev, A.M. and Slavatinsky, S.A., 1962, J. Phys. Soc. Japan, 17, Suppl. AIII, 375.

Hayman, P.J., 1962, Ph.D. Thesis, University of Durham.

Hayman, P.J. and Wolfendale, A.W., 1962, Proc. Phys. Soc., 80, 710.

Hughes, E.B., 1961, Ph.D. Thesis, University of Leeds.

Hughes, E.B., Marsden, P.L., Brooke, G., Meyer, M.A., and Wolfendale, A.W., To be published in Proc. Phys. Soc.

Hyams, B.D., Mylroi, M.G., Owen, B.G. and Wilson, J.G., 1950, Proc. Phys. Soc. A 63, 1053.

Jahnke, E. and Emde, F., 1945, Tables of Functions, Dover Publications, New York.

Jones, D.G., Taylor, F.E. and Wolfendale A.W., 1962, Proc. Phys. Soc., 80, 686.

Kaplon, M.F. and Ritson, D.M., 1952, Phys. Rev., 88, 386.

Kocharian, N.M., Aivazian, M.T., Kirakosian, Z.A. and Aleksanian, A.S., 1956, J.E.T.P., 3, 350.

Kocharian, N.M., Saakian, G.S. and Kirakosian, Z.A., 1959, J.E.T.P., 35(8), 933.

Lal, D., 1953, Proc. Indian Acad. Sci., 38, A, 93.

Lal, S., Raghavan, R., Sreekantan, B.V., Subrahmanyan, N.A. and Verma, S.D., 1962, J. Phys. Soc. Japan, 17, Suppl. AIII, 390.

Linsley, J. and Scarsi, L., 1962, Phys. Rev. Letts., 9, 123.

Linsley, J., Scarsi, L. and Rossi, B., 1962, J. Phys. Soc. Japan, 17, Suppl. AIII, 91.

Lloyd, J.L. and Wolfendale, A.W., 1957, Proc. Phys. Soc. A 70, 421.

Major, J.V., 1963, Private Communication.

McDiarmid, I.B., 1959, Canad. Journal of Phys., 37, 79.

McDonald, F.B. and Webber, W.R., 1959, Phys. Rev. 115, 194.

McEwan, J.G., 1959, Phys. Rev., 115, 1712.

Merkle, T.C., Goldwasser, E.L. and Brode, R.B., 1950, Phys. Rev., 79, 926.

Morrison, D.R.O., 1963, Conference on Ultra High Energy Nuclear Physics, Bristol.

Morrison, P., 1961, Handbuch der Physik, 46/1, 1.

Mylroi, M.G. and Wilson, J.G., 1951, Proc. Phys. Soc. A 64, 404.

Ogilvie, K.W., 1955, Canad. Journal of Phys., 33, 746.

Pak, W. and Greisen, K., 1962, Phys. Rev., 125, 1668.

Perkins, D.H., 1963, Conference on Ultra High Energy Nuclear Physics, Bristol.

Peters, B. and Yash Pal, 1963, Private Communication.

Powell, C.F., 1962, J. Phys. Soc., Japan, 17, Suppl. AIII, 492.

Rossi, B., 1948, Rev. Mod. Phys., 20, 537.

Rossi, B., 1952, "High Energy Particles", Prentice-Hall, U.S.A.

Rozen, A.Z., 1954, Phys. Rev., 93, 211.

Sternheimer, R.M., 1960, Phys. Rev. 118, 1045.

Subrahmanyan, N.A., 1962, Ph.D. Thesis, University of Madras.

Taylor, F.E., 1961, Ph.D. Thesis, University of Durham.

Udgaonkar, B.M. and Gell-Mann, M., 1962, Phys. Rev. Letts., 8, 346.

Van Allen, J.A., 1960, Proc. Moscow Cosmic Ray Conf., Vol. III, 153.

Waddington, C.J., 1960, Prog. Nucl. Phys., 8, 1.

Walker, W.D., Walker, S.P., and Greisen, K., 1950, Phys. Rev., 80, 546.

Whittemore, W.L. and Shutt, R.P., 1952, Phys. Rev., 86, 940.

Williams, R.W., 1960, Nuovo Cimento, 16, 762.

Wolfendale, A.W., 1962, J. Phys. Soc. Japan, 17, Suppl. AIII, 358.

Yash Pal and Rengarajan, T.N., 1962, J. Phys. Soc. Japan, 17, Suppl. AIII, 387.

Yash Pal, Ray, A.K. and Rengarajan, T.N., 1963, Nuovo Cimento, Vol. 28, 1177.

York, C.M., 1952, Proc. Phys. Soc. A 65, 559.

APPENDIX 1

THE ACCEPTANCE FUNCTION OF THE SPECTROGRAPH

A. The Acceptance Function for Geiger Counter Trays ABGCD

(i) Deflection Plane Acceptance, $A_1(\phi)$

In this case, the spectrograph is symmetrical about the centre of the magnetic field in the vertical direction. Trays B and C do not limit the acceptance of particles, limitations being imposed only by trays A, G and D.

The acceptance function in the deflection plane, $A_1(\phi)$, is equal to $\iint d\alpha dD$ for all trajectories passing through A, G and D. $d\alpha$ is the range of angles for which particles with deflection ϕ can pass through trays A, G and dD of tray D, see Figure A1.1(a).

It is assumed in the following calculations that angles are small and that there is negligible scattering and momentum loss for particles passing through the spectrograph.

a) $\phi = o$

For zero deflection the extreme trajectories are as shown in Figure A1.1(b). If the incident particles are isotropic the distribution of particles at C will then be as in Figure A1.1(d). Within $\pm$ (a - 2g) of the centre line the angular acceptance is limited by G and is equal to $2g/z$. From $\pm$ (a - 2g) to $\pm$ (a + 2g) respectively the acceptance falls linearly to zero.

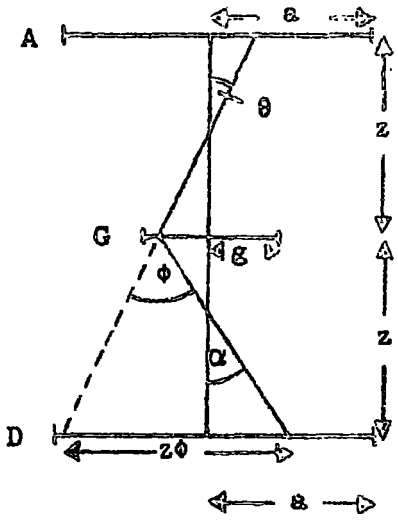

(a)

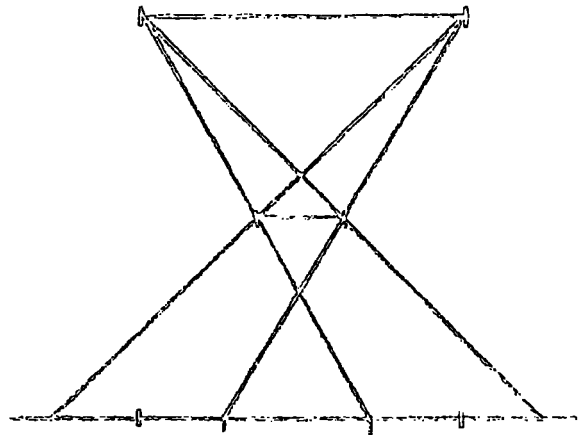

(b)

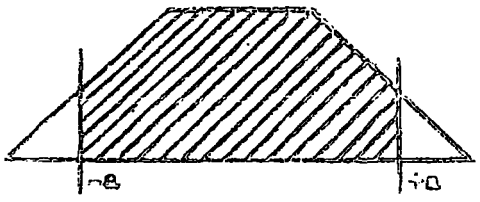

(c)

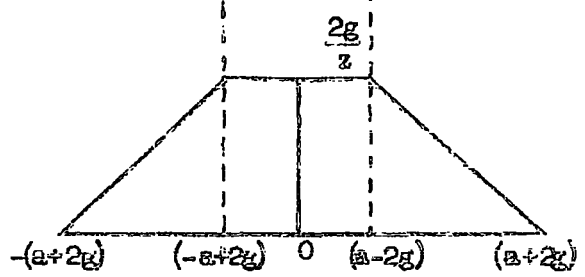

(d)

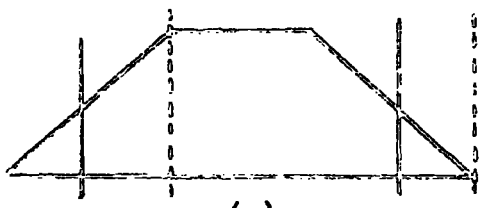

(e)

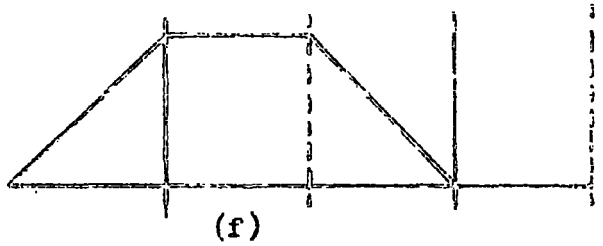

(f)

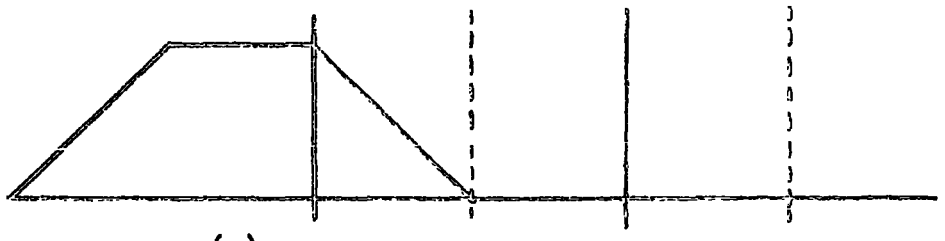

(g)

Fig. A1.1

Therefore, for zero deflection, $\iint d\alpha dD$ is the area under the curve between $\pm$ a, i.e. the limits of tray D, shown shaded in Figure A1.1(c).

Then $\iint d\theta dG = \frac{2a.2g}{z} - \frac{4g^2}{2z} = \frac{2g}{z}(2a-g)$, for $\phi = o$. A1.1

b) $\phi > o$

Imposing a deflection ϕ on the trajectory is equivalent to displacing D by a distance $z\phi$. Thus for deflection ϕ, $\iint d\alpha dD$ is the area under the curve between $(-a + z\phi)$ and $(+a + z\phi)$.

$\phi = o$ to $\phi = \phi_{max}$ can be covered by three regions shown in Figures A1.1(e), A1.1(f) and A1.1(g), where the full vertical lines indicate the displaced position of D for the smallest deflection and the 'dashed' lines the maximum displacement of D, in that region.

Region (i) $o \leqslant \phi \leqslant \frac{2g}{z}$,

$$\iint d\alpha dD = \frac{8ag - 4g^2 - z^2\phi^2}{2z} \quad \text{(Figure 1(e))} \qquad \text{A1.2(a)}$$

Region (ii) $\frac{2g}{z} \leqslant \phi \leqslant \frac{2(a-g)}{z}$,

$$\iint d\alpha dD = \frac{4ag - 2z\phi g}{z} \quad \text{(Figure 1(f))} \qquad \text{A1.2(b)}$$

Region (iii) $\frac{2(a-g)}{z} \leqslant \phi \leqslant \frac{2(a+g)}{z}$,

$$\iint d\alpha dD = \frac{(2g+2a-z\phi)^2}{4z} \quad \text{(Figure 1(g))} \qquad \text{A1.2(c)}$$

The values of $\iint d\alpha dD$ are given in Table A1.1 and plotted in Figure A1.2 for a = 47.26 cm, g = 12.52 cm and z = 265.1 cm.

c) Correction

In the calculation of $\iint d\alpha dD$ it has been assumed that the particles are deflected at a point which lies on G. In fact, the deflection takes place over a distance equal to the length of the magnetic field, as shown in Figure A1.3.

We have assumed that the trajectory is JKL (straight lines), when it is in fact JRKSL. The previous calculation gives the relation between $\iint d\alpha dD$ and $\phi (= \frac{LN}{z})$, but the true deflection

$$\phi' = LP/z = \frac{LN + NP}{z} = \phi + NP/z.$$

It is easily shown that NP = 2KM. The relation between KM and ϕ may be obtained as follows:-

Take rectangular axes (ℓ, y) with origin at the centre of the magnetic field and the ℓ axis along the direction of incidence of the particle, (Figure A1.5). The angular deflection when the particle moves from ℓ to $\ell - d\ell$ is $\frac{300\, H_\ell d\ell}{p}$ and this corresponds to a displacement at the centre of the field of $\frac{300}{p}\, \ell H_\ell d\ell$

$$\therefore KM = \frac{300}{p} \int_0^\infty \ell H_\ell d\ell$$

$$p = \frac{300\, z \int_{-\infty}^{+\infty} H d\ell}{z} \quad (z = \text{arm over which } \Delta \text{ is measured}).$$

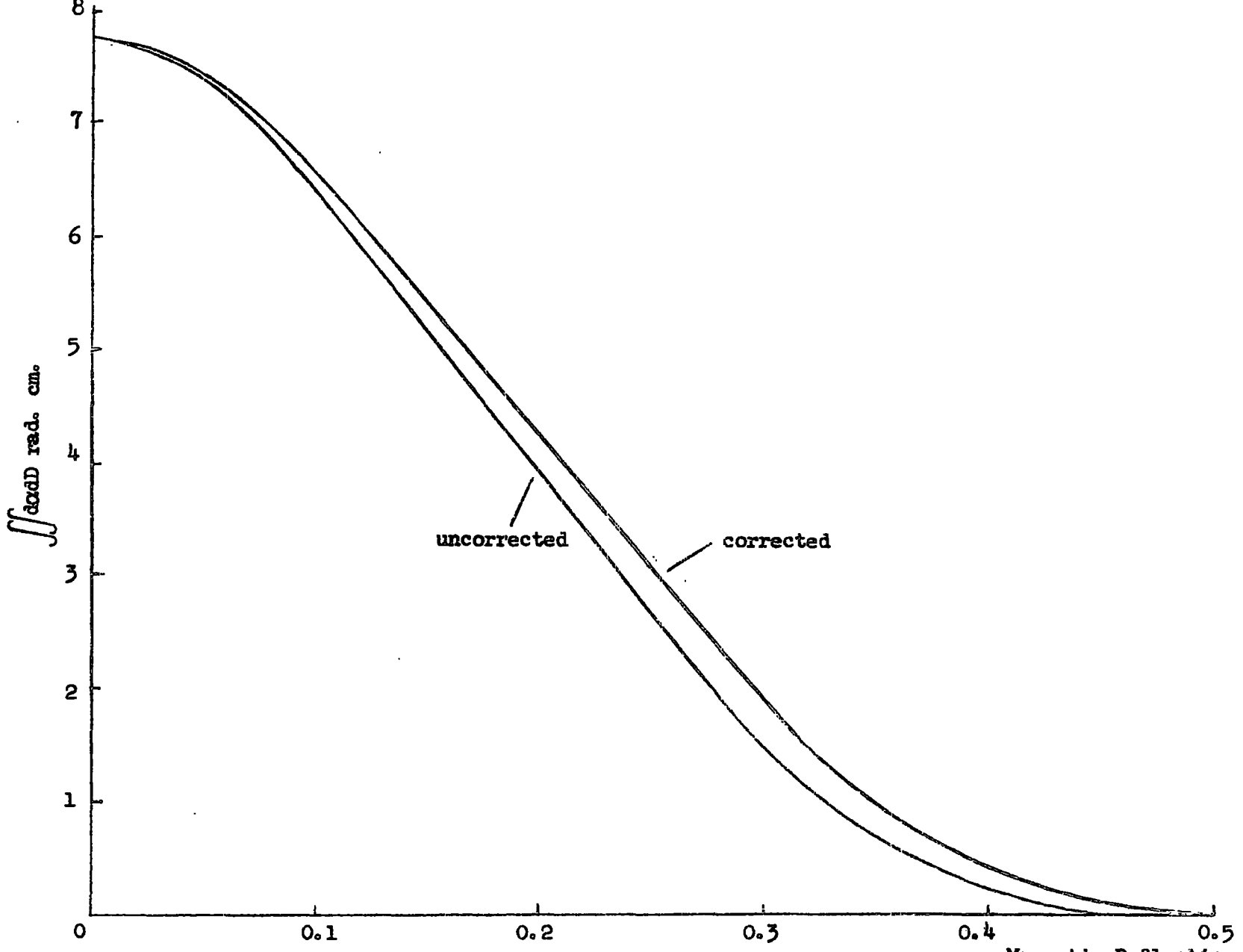

The Acceptance in the deflection plane for Geiger counter trays ABGCD
Fig. A1.2

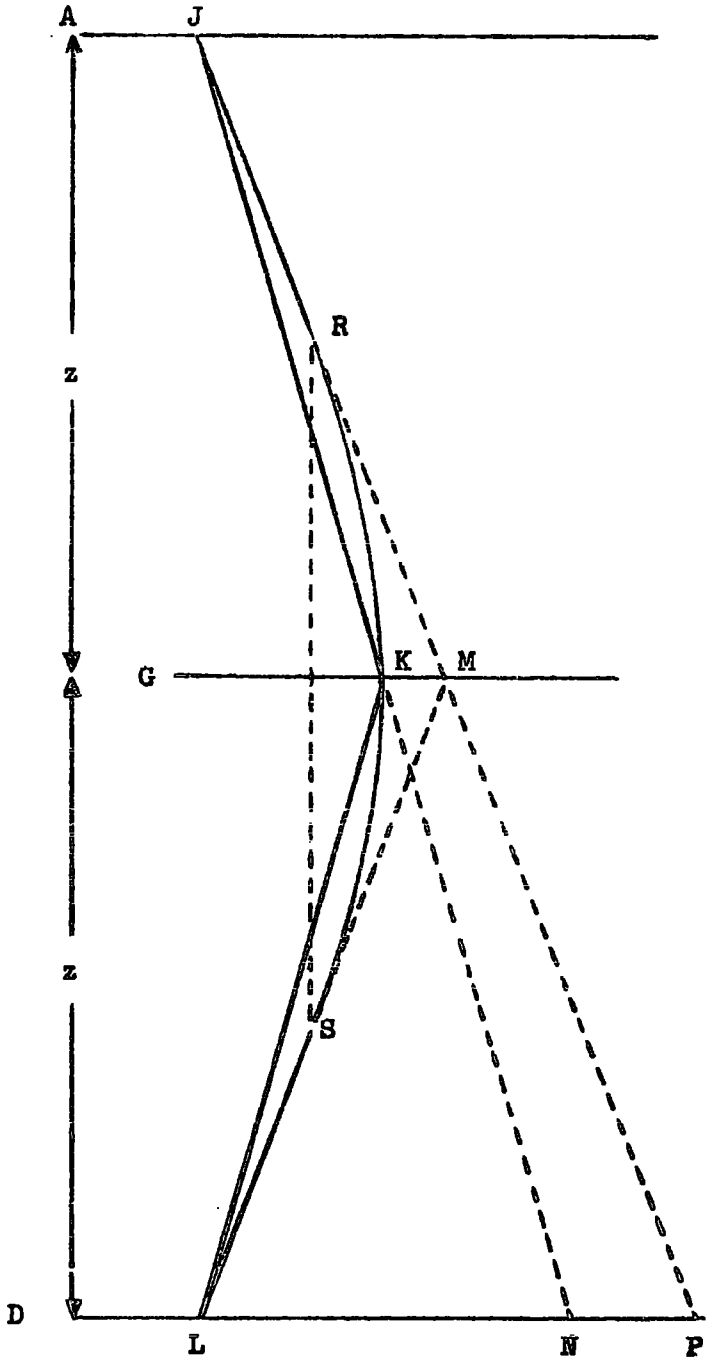

Fig. Al.3

In this particular case, the field distribution for a magnet current of 66.6A can be approximated to by:-

$$H = 12000 \text{ between } \ell = 0 \text{ and } 6 \text{ cm} \qquad \text{A1.3(a)}$$

$$H = 12000\left[1 - \frac{(\ell-6)^2}{800}\right] \text{ between } \ell = 6 \text{ and } 17 \text{ cm} \qquad \text{A1.3(b)}$$

$$H = 12000 \exp - \frac{(\ell-14)}{13} \text{ between } \ell = 17 \text{ and } 90 \text{ cm} \qquad \text{A1.3(c)}$$

and $H = 0$ for $\ell > 90$ cm (See Figure A1.4).

This gives a value of 5.30×10^6 Γ cm^2 for $\int_o^{\infty} \ell H d\ell$ and 6.4×10^5 Γ cm for $\int_{-\infty}^{+\infty} H d\ell$

$$\therefore \quad KM = \frac{z\phi \int_o^{\infty} \ell H d\ell}{z \int_{-\infty}^{+\infty} H d\ell} = \frac{5.30 \times 10^6}{265.1 \times 6.4 \times 10^5} z\phi = .0312\, z\phi \qquad \text{A1.4}$$

$\therefore \quad \phi' = \phi(1 + .0624)$.

Values of ϕ' are given in table A1.1 and the corrected acceptance in the deflection plane is plotted in Figure A1.2.

(ii) Back Plane Acceptance, A_2.

Since there is no deflection in the back plane of the spectrograph, the acceptance, A_2, is independent of particle deflection and is given by equation A1.1 with a = 30.0 cm, g = 5.45 cm and z = 265.1 cm. The value for A_2 thus obtained is 2.16 rad. cm.

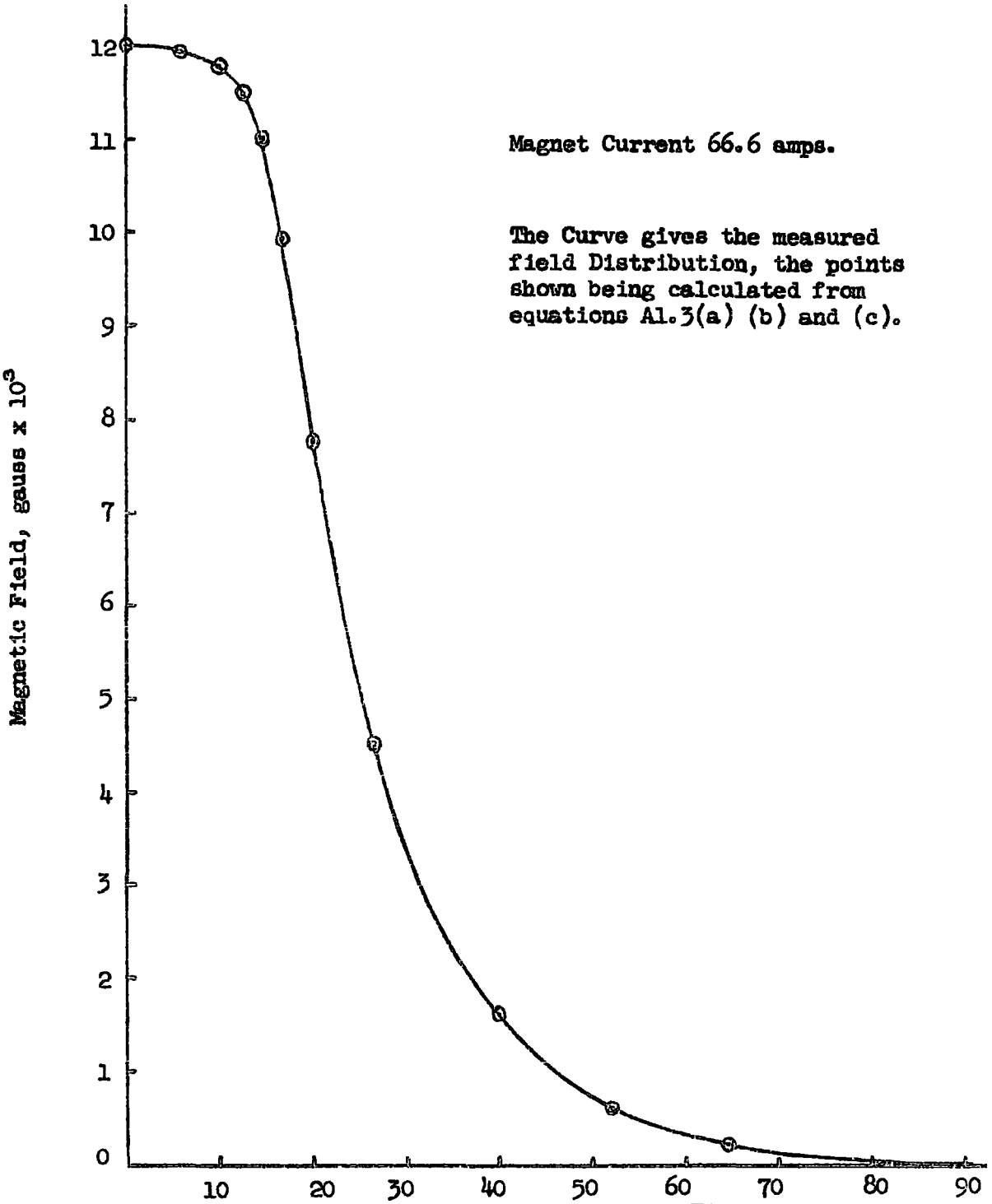

The Magnetic Field Distribution (Durham Cosmic Ray Spectrograph)
Fig. Al.4

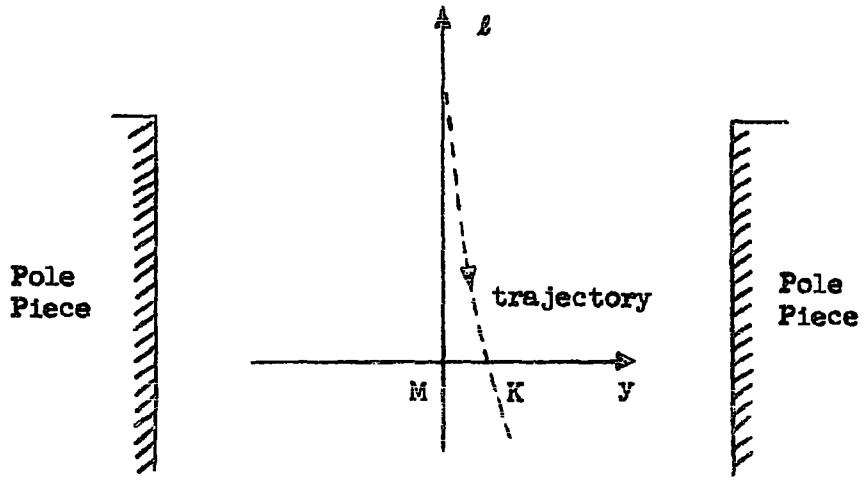

Fig. A1.5

B. The Acceptance Function for Geiger Counter Trays ABGCS

(i) Deflection Plane Acceptance $A_1(\phi)$

Since the spectrograph in this case is not symmetrical about the magnetic field, the method described in section A becomes complicated. $A_1(\phi)$ has therefore been evaluated graphically for each of the four experimental arrangements in the following manner. Templates were made for particle trajectories with various values of angular deflection, ranging from 0 to 0.35 radians, allowance being made according to equation A1.4 for the magnetic field distribution. On scale drawings of the spectrograph, $\iint d\alpha dD$ was found numerically. The limits on the positions at measuring level D between which particle trajectories were required to pass were marked on the scale drawings for each series for each deflection considered. In each case $\iint d\alpha dD$ was evaluated for deflections in both senses and the average value taken, in order to reduce the errors due to possible inaccuracies in the drawing of the spectrograph.

(ii) Back Plane Acceptance A_2

There is zero magnetic deflection in the back plane of the spectrograph. For any given Geiger counter arrangement in this plane the acceptance is not a function of the particle momentum. However, in series P, S and H the Geiger counters in tray S were

hodoscoped and minimum momenta were imposed for the acceptance of particles passing through any particular counter, leading to discontinuities in the acceptance functions at deflections corresponding to these momenta. A_2 was calculated graphically for the various tray S counter arrangements.

The acceptance functions, $A(\phi) = A_1(\phi).A_2$, for the P, AP, H and S series are shown in Figures A1.6(a) and (b).

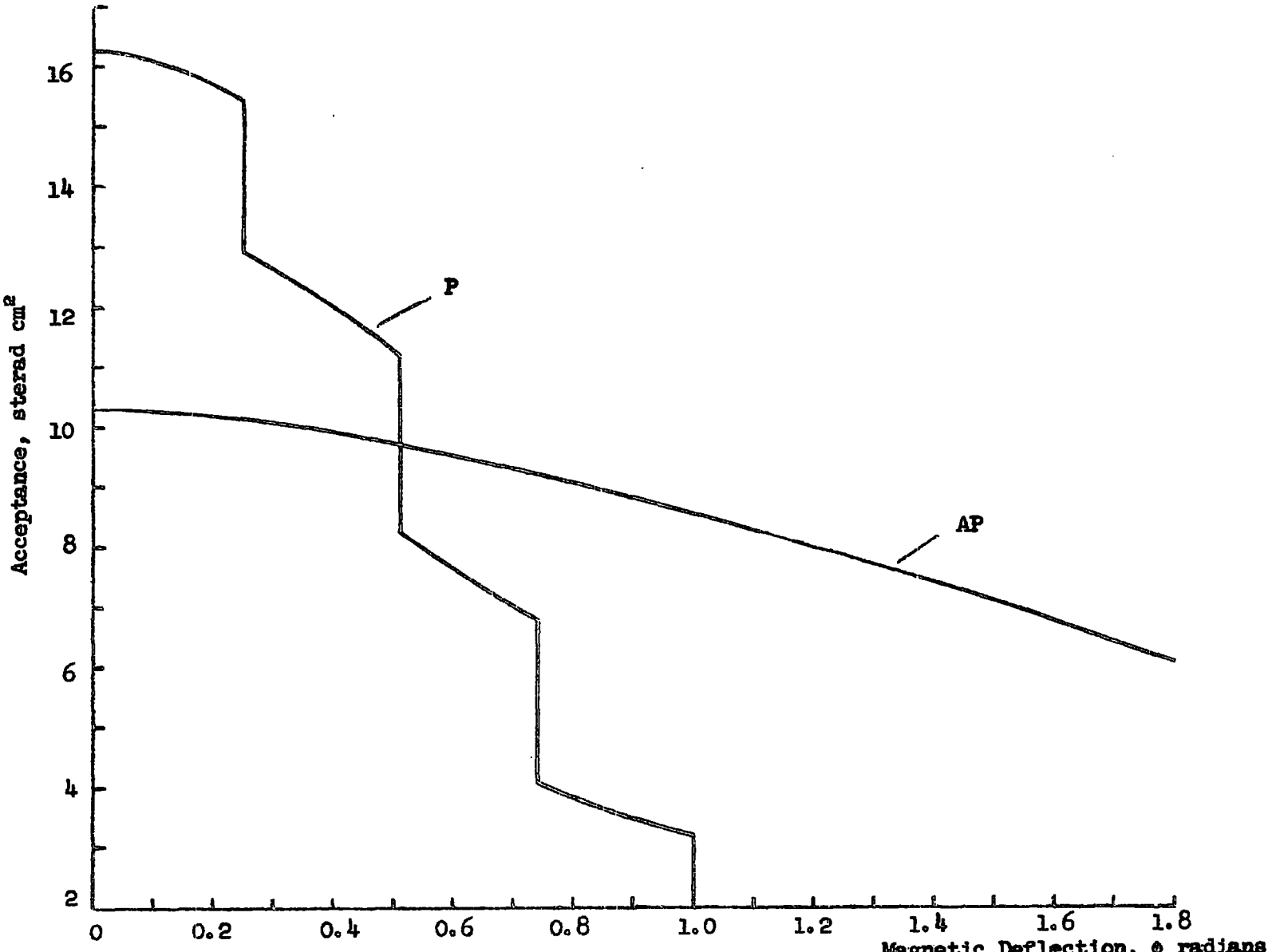

The Acceptance Functions for the P and AP Series
Fig. A1.6(a)

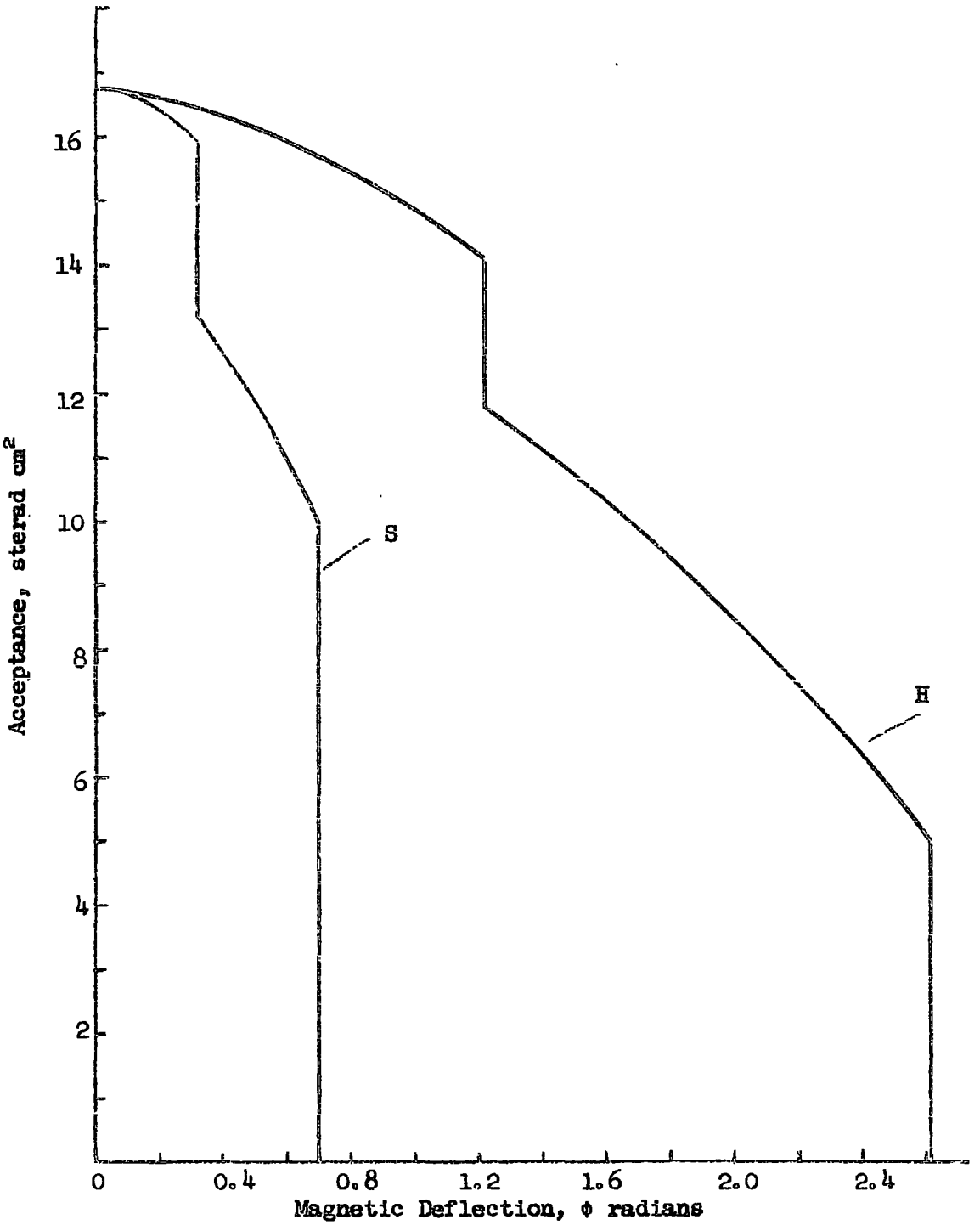

The Acceptance Functions for the S and H Series.

Fig. A1.6(b)

ϕ radians	$\iint d\alpha dD$ rad.-cms	ϕ' radians
0	7.75	0
0.0189	7.70	0.0201
0.0377	7.55	0.0401
0.0754	6.98	0.0801
0.0943	6.56	0.1002
0.113	6.10	0.120
0.151	5.15	0.160
0.189	4.21	0.201
0.226	3.26	0.240
0.264	2.32	0.280
0.302	1.47	0.321
0.339	0.824	0.360
0.377	0.360	0.401
0.415	0.086	0.441
0.450	0	0.478

The acceptance in the deflection plane $A_1(\phi) = \iint d\alpha dD$ for Geiger counter trays ABGC and D.

ϕ and ϕ' are respectively the uncorrected and corrected angular deflections.

Table A1.1

APPENDIX 2

THE GROSS TRANSFORMATION

The measurements of the sea-level proton and pion intensities described in this thesis are of average values of the intensities of particles within ~0.2 radians to the vertical. Since the thickness of atmosphere traversed by a particle in reaching sea-level increases with increasing angle of incidence, the angular distribution of particles at sea-level has a maximum in the vertical direction. Rossi (1952), under the assumptions that the primary flux is isotropic, that the direction of motion of the particles is unchanged in passing through the atmosphere and that the particles being considered are absorbed exponentially with an absorption length λ, gives the expression:-

$$2\pi J_o \epsilon_1 (x/L)$$

for the total integrated intensity at depth x. J_o is the incident intensity of particles per unit solid angle. The function $\epsilon_1(x)$ is defined as $x\int_x^\infty \frac{e^{-y}}{y^2}\,dy$, known as the Gold Integral. This function is extensively tabulated by, for example, Jahnke and Emde (1945) and also by Rossi.

In the case of the Durham spectrograph, the intensity of particles, integrated over all accepted angles is given by:-

$$2\pi\, J_o \int_x^{x_m} \frac{\exp(y/L)}{y^2}\, dy$$

$$= 2\pi\, J_o \left[\int_x^{\infty} \frac{\exp(-y/L)}{y^2}\, dy - \int_{x_m}^{\infty} \frac{\exp(-y/L)}{y^2}\, dy \right]$$

$$= 2\pi\, J_o \left[\epsilon_1\left(x/L\right) - x/x_m\, \epsilon_1\left(\frac{x_m}{L}\right) \right] \qquad \text{A2.1}$$

where x_m is the thickness of atmosphere traversed by particles at the maximum angle to the vertical accepted by the spectrograph.

With $L = 120$ g.cm^{-2}, equation A2.1 gives a value of $2.26.10^{-5}.J_o$ for the integrated intensity.

If it is assumed that all particles have traversed only the vertical thickness of the atmosphere, the integrated intensity is $2.31.10^{-5}.J_o$ showing that in this particular case the measured intensities can be taken to be the vertical intensities at sea-level.

APPENDIX 3

MOMENTUM CELL WIDTH CORRECTION

Suppose that the momentum spectrum being measured is of the form:-

$$N(p)dp = K.p^{-\gamma}dp, \qquad A3.1$$

where K and γ are constants.

The quantity required from the measurements is N(p) as a function of p, i.e. the intensity of particles with momenta between p and p + dp. In practice a finite momentum cell width must be taken.

Let the limits of the momentum cell be p_1 and p_2 $(p_1 < p_2)$.

Then, the number of particles in the cell $= \int_{p_1}^{p_2} N(p)dp$

$$= \int_{p_1}^{p_2} K.p^{-\gamma}dp$$

$$= \frac{K[p_2^{1-\gamma} - p_1^{1-\gamma}]}{(1-\gamma)} \qquad A3.2$$

The intensity of particles per unit momentum interval is then:-

$$\frac{K[p_2^{1-\gamma} - p_1^{1-\gamma}]}{(1-\gamma)\ (p_2 - p_1)} \qquad A3.3$$

The momentum, p_o, to which this intensity refers is, from equation A3.1, given by:-

$$p_o^{-\gamma} = \frac{[p_2^{1-\gamma} - p_1^{1-\gamma}]}{(1-\gamma)(p_2 - p_1)} ,$$

i.e. p_o is the momentum at which the intensity should be plotted.

In figure A3.1, p_o, expressed as a fraction of the arithmetic mean momentum, is shown as a function of p_2/p_1 for $\gamma = 2.5$.

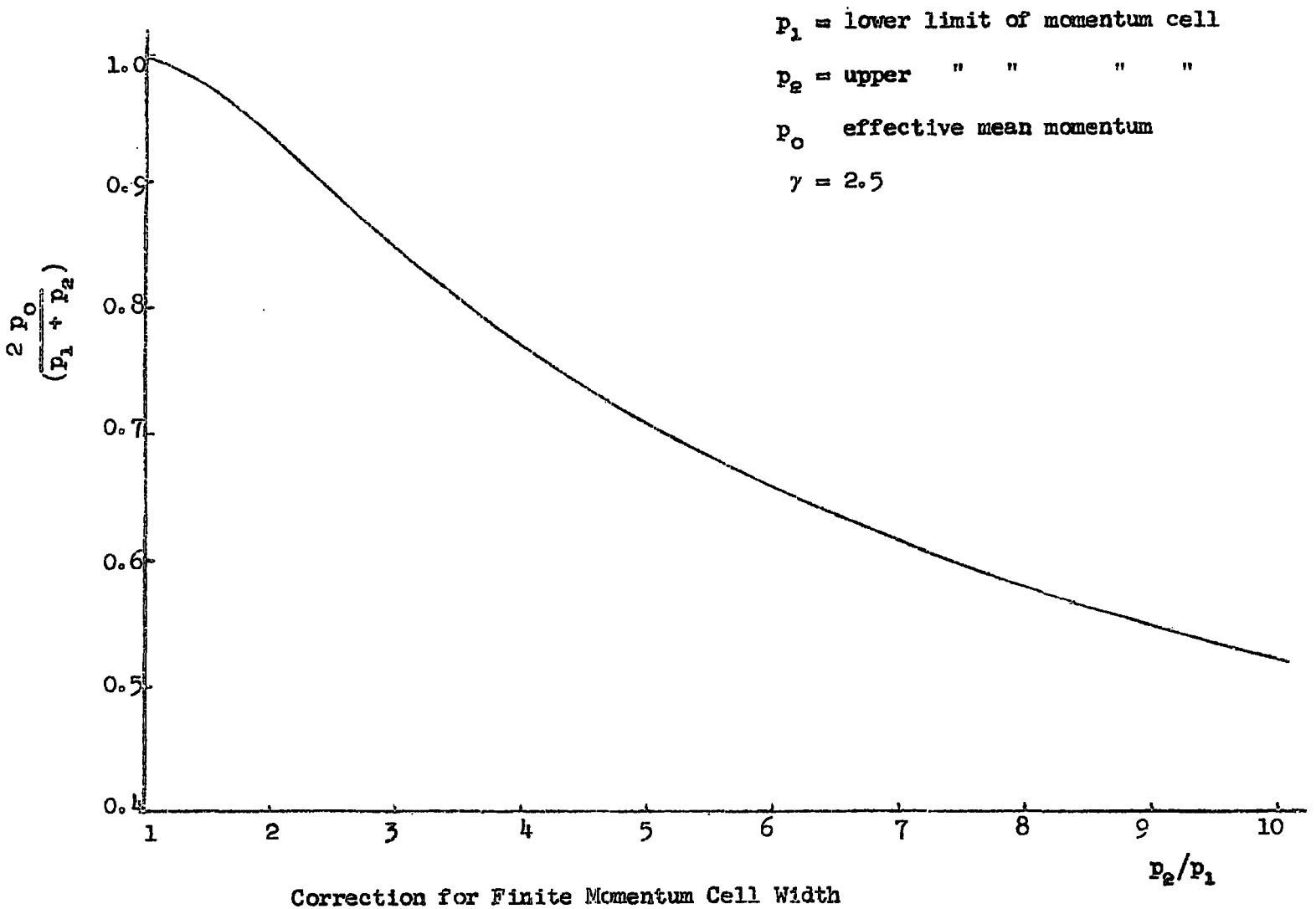

Correction for Finite Momentum Cell Width
Fig. A3.1

APPENDIX 4

THE PROBABILITY OF NO COLLISIONS IN A NUCLEUS

a) Statistical Model

Consider a nucleus, atomic number A and radius $R = R_o A^{\frac{1}{3}}$. If σ_N is the interaction cross-section of the type of particle considered with a single nucleon, then the interaction mean free path for such particles in nuclear matter $\lambda_n = \frac{4\pi R^3}{3.A\sigma_N}$

or
$$\lambda_n = \frac{4\pi R_o^3}{3.\sigma_N} \qquad A4.1$$

Assuming that the nucleons in a nuclues behave independently, the probability of a particle not interacting in a distance 2ℓ of nuclear matter is:-

$$P(0,2\ell) = \exp\left[-2\ell/\lambda_n\right] \qquad A4.2$$

If the perpendicular distance from a path length 2ℓ through the nucleus to the centre of the nucleus is x, the probability of a particle having a path length 2ℓ in the nucleus is:-

$$P(2\ell) = \frac{2\pi x dx}{\pi R^2} \qquad A4.3$$

The average probability of a particle not interacting in the nucleus is

$$P_o = \int_o^R P(2\ell).P(0,2\ell)$$

$$= \int_o^R \frac{2x}{R^2} \exp(-2\ell/\lambda_n)dx \qquad \text{A4.4}$$

Since $\ell^2 + x^2 = R^2$

equation A4.4 becomes:-

$$P_o = -\int_o^R \frac{2\ell}{R^2} \exp\left(\frac{-2\ell}{\lambda_n}\right) d\ell$$

$$= -\left[\left(\frac{2\ell}{\lambda_n} + 1\right) \exp -2\ell/\lambda_n \cdot \frac{\lambda_n^2}{2R^2}\right]_o^R$$

$$P_o = \left[1 - (2R/\lambda_n + 1) \exp(-2R/\lambda_n)\right] \frac{\lambda_n^2}{2R^2} \qquad \text{A4.5}$$

P_o is known as the transparency of a nucleus. The opacity of a nucleus, defined as (1-transparency), is shown in figure A4.1 as a function of R/λ_n.

b) Optical Model

In the optical model, the absorption coefficient, K, is given by $\frac{3.A\sigma_N}{4\pi R^3} = \frac{3.\sigma_N}{4\pi R_o^3}$. Then for a path length 2ℓ in nuclear matter, the incident wave is attenuated by a factor $\exp -2K\ell$. The amplitude of the emergent wave is interpreted as the probability of a particle not interacting in a distance 2ℓ. It is seen that the expression

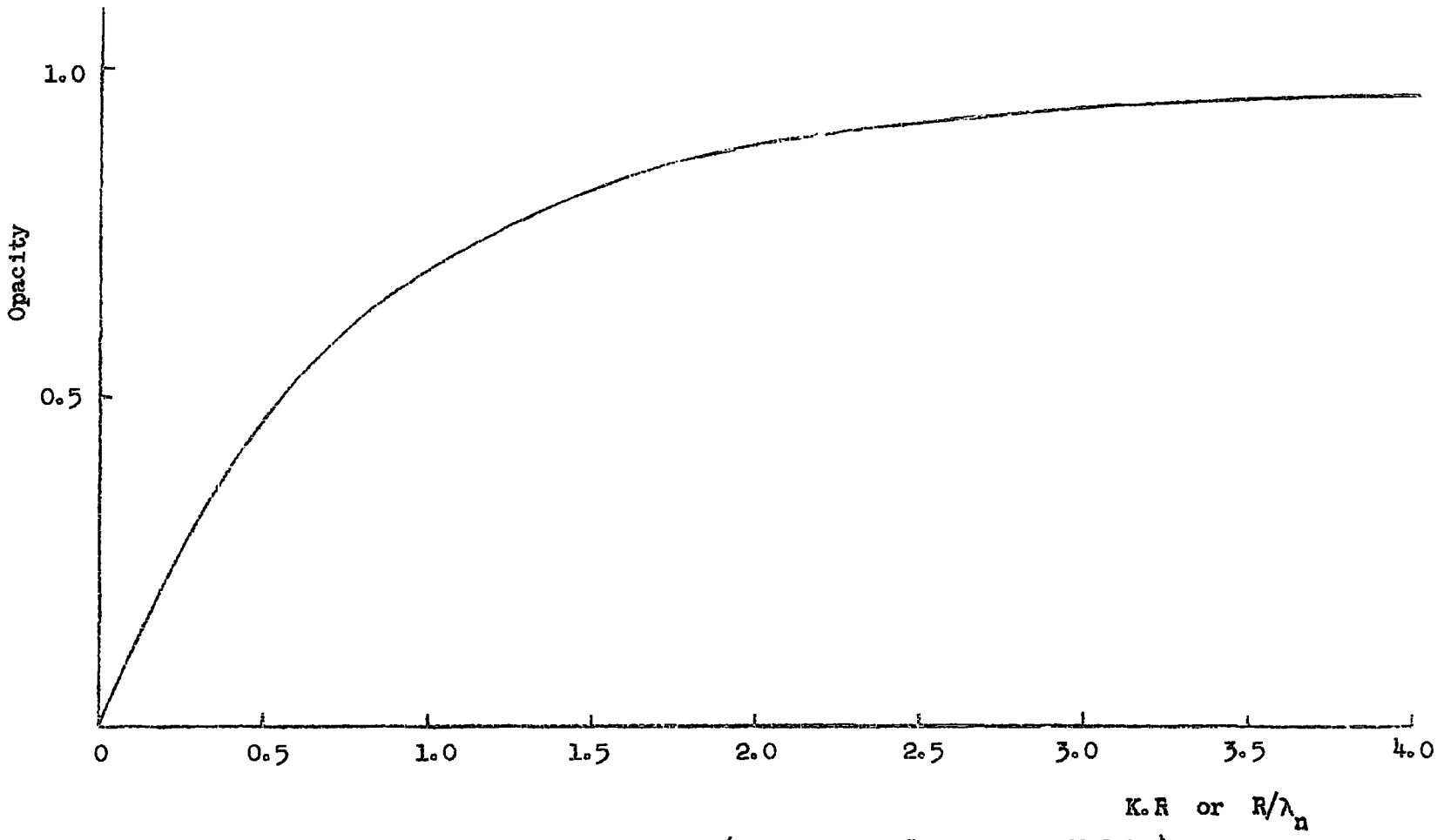

Calculated Opacity of Nuclei (Optical and Statistical Models)

Fig. A4.1

obtained from the optical model is the same as that from the statistical model (equation A4.2) since, from the definitions of λ_n and K, $K = \frac{1}{\lambda_n}$. Thus the variation of opacity with RK or R/λ_n is the same on both models.

APPENDIX 5

THE PROBABILITY OF n COLLISIONS IN A NUCLEUS

Using the same notation as in Appendix 4a, the probability of n collisions in a distance 2ℓ of nuclear matter is:-

$$P(n,2\ell) = \left(\frac{2\ell}{\lambda_n}\right)^n \frac{\exp(-2\ell/\lambda_n)}{n!} \qquad \text{A5.1}$$

The probability of n interactions in the nucleus is then:-

$$P_n = \int_0^R \frac{2\pi x}{\pi R^2} \left(\frac{2\ell}{\lambda_n}\right)^n \frac{\exp(-2\ell/\lambda_n)}{n!}\, dx$$

or

$$P_n = -\int_0^R \frac{2\ell}{R^2} \left(\frac{2\ell}{\lambda_n}\right)^n \frac{\exp(-2\ell/\lambda_n)}{n!}\, d\ell \qquad \text{A5.2}$$

$$= \frac{-\lambda_n^2 \exp(-2\ell/\lambda_n)}{2R^2\, n!} \left[\left(\frac{2\ell}{\lambda_n}\right)^{n+1} + \left(\frac{2\ell}{\lambda_n}\right)^n (n+1) + \left(\frac{2\ell}{\lambda_n}\right)^{n-1} n.(n+1) + \ldots\ldots \right.$$

$$\ldots\ldots + \frac{(n+1)!}{(n-m)!} \left(\frac{2\ell}{\lambda_n}\right)^{n-m} + \ldots\ldots$$

$$\left. \ldots\ldots + (n+1)! \left(\frac{2\ell}{\lambda_n}\right) + (n+1)! \right]_0^R$$

$$= \left(\frac{\lambda_n}{R}\right)^2 \frac{(n+1)}{2} - (n+1)\exp(-2R/\lambda_n) \left[\frac{2^n}{n!} \left(\frac{R}{\lambda_n}\right)^{n-1} + \frac{2^{(n-1)}}{n!} \left(\frac{R}{\lambda_n}\right)^{n-2} + \ldots\ldots \right.$$

$$\ldots\ldots + \frac{2^{(n-m-1)}}{(n-m)!} \left(\frac{R}{\lambda_n}\right)^{n-m-2} + \ldots\ldots$$

$$\left. \ldots\ldots + 1 + \frac{\lambda_n}{R} + \tfrac{1}{2}\left(\frac{\lambda_n^2}{R}\right) \right] \qquad \text{A5.3}$$

Equation A5.3 may be rewritten as:-

$$P_{(n+1)} = \left(\frac{\lambda_n}{R}\right)^2 \frac{(n+2)}{n} - (n+2)\exp(-2R/\lambda_n) \sum_{m=-1}^{m=n+1} \frac{2^{(n-m)}}{(n-m+1)!} \left(\frac{R}{\lambda_n}\right)^{(n-m-1)}$$

or

$$P_{(n+1)} = \left(\frac{n+2}{n+1}\right) P_n - \exp(-2R/\lambda_n) \frac{2^{(n+1)}}{(n+1)!} \left(\frac{R}{\lambda_n}\right)^n \qquad \text{A5.4}$$

Equation A5.4 is the most convenient form for numerical calculations of P_n.

In Table A5.1 are shown values of P_n for Carbon ($A = 12$) and nuclear emulsion ($\bar{A} = 32$) calculated for $\sigma_N = 43$ mb and $R_o = 1.35.10^{-13}$ cm. In each case, P_o was obtained from Figure A4.1. Also given in the table are the percentages of the total number of interactions in which n nucleons in the struck nucleus take part. From these, the mean number of nucleons in a Carbon nucleus struck by an incident nucleon is found to be 2.1 and for nuclear emulsion the mean number is 2.7.

n	Carbon		Emulsion	
	P_n	% of total no. of interactions	P_n	% of total no. of interactions
0	0.219	-	0.136	-
1	0.2864	36.7	0.2163	25.0
2	0.2345	30.1	0.2245	26.0
3	0.1445	18.5	0.1794	20.8
4	0.0723	9.25	0.1175	13.6
5	0.0208	2.66	0.0649	7.5
6	-	-	0.0301	3.5
7	-	-	0.0112	1.3

Table A5.1

APPENDIX 6

THE PRIMARY NUCLEON SPECTRUM

The composition of the primary cosmic radiation given by Waddington (1960) is expressed in two forms:- abundance by number of nuclei above constant rigidity and above constant energy/nucleon.

1. Composition above constant rigidity

Let the number of all types of nuclei with rigidity $>R = B.R^{-\gamma}$.

Let the fraction of these nuclei which have atomic no. Z and mass no. A be C_A.

i.e. The number of nuclei of type (A,Z) with rigidity $>R = C_A.B.R^{-\gamma}$.

$\therefore$ The number of nuclei of type (A,Z) with momentum >p/nucleus

$$= C_A\, B \left(\frac{p}{A}\right)^{-\gamma} = C_A\, Z^{\gamma}\, Bp^{-\gamma} \qquad \text{A6.1}$$

The number of nuclei of all types with momentum >p/nucleus

$$= B\, p^{-\gamma}. \sum_{\text{all } A} C_A\, Z^{\gamma} \qquad \text{A6.2}$$

The number of nucleons in the form of nuclei of type (A,Z) with momentum >p/nucleon

$$= A.C_A\, Z^{\gamma}(Ap)^{-\gamma} = C_A\, Z^{\gamma}\, A^{(1-\gamma)}\, Bp^{-\gamma} \qquad \text{A6.3}$$

∴ The number of nucleons occurring in any form and having momentum >p/nucleon

$$= B.p^{-\gamma} \sum_{\text{all } A} C_A \, Z^{\gamma} \, A^{(1-\gamma)} \qquad \text{A6.4}$$

From equations A6.2 and A6.4

The number of nucleons with momentum >p/nucleon

$$= \frac{\sum_{\text{all } A} C_A \, Z^{\gamma} \, A^{(1-\gamma)}}{\sum_{\text{all } A} C_A \, Z^{\gamma}} \text{ x the number of nuclei with momentum >p/nucleus} \qquad \text{A6.5}$$

2. Composition above constant energy/nucleon

Let the number of all types of nuclei with energy/nucleon >E = $D.E^{-\gamma}$.

Let the fraction of these nuclei which have mass no. A be P_A

i.e. the number of nuclei A with energy >E/nucleon = $P_A \, D.E^{-\gamma}$

the number of nuclei A with energy >E/nucleus = $P_A \, A^{\gamma}.D \, E^{-\gamma}$ A6.6

∴ The number of nuclei of all types with energy >E/nucleus

$$= D \, E^{-\gamma} \sum_{\text{all } A} P_A \, A^{\gamma}. \qquad \text{A6.7}$$

The number of nucleons in the form of nuclei A with energy >E/nucleon

$$= A.P_A \, D \, E^{-\gamma} \qquad \text{A6.8}$$

∴ the number of nucleons occurring in any form and having energy >E/nucleon

$$= D\, E^{-\gamma} \sum_{\text{all } A} P_A\, A \qquad \text{A6.9}$$

From equations A6.7 and A6.9,

The number of nucleons with energy >E/nucleon

$$= \frac{\sum_{\text{all } A} P_A\, A}{\sum_{\text{all } A} P_A\, A^{\gamma}} \text{ x the number of nuclei with energy >E/nucleus} \qquad \text{A6.10}$$

Waddington's data are given in Table A6.1. Equations A6.5 and A6.10 give the same factor for converting the primary nucleus spectrum to the primary nucleon spectrum only for $\gamma \approx 1.5$, i.e. the exponent of the primary spectrum at the energy at which the composition was measured.

In all of the present calculations it has been assumed that it is the rigidity spectrum which has constant composition.

The values obtained for the conversion factor, primary nucleus to primary nucleon spectrum, at primary energies $>10^{16}$ eV, for the three assumptions about the primary composition of section 9.1 are given in Table A6.2.

Group	Nuclear charge, Z	Above a Constant Rigidity (4.5 GV) Intensity, nuclei m^{-2} $sterad^{-1}$ sec^{-1}	Abundance by number of nuclei	Above a constant energy/ nucleon, (2.4 GeV/nucleon) Intensity, nuclei m^{-2} $sterad^{-1}$ sec^{-1}	Abundance by number of nuclei
Protons	1	600 ± 30	85.9%	1510 ± 150	94%
α-nuclei	2	89 ± 3	12.7%	89 ± 3	5.5%
L-nuclei	3-5	2.0 ± 0.2		2.0 ± 0.2	
M-nuclei	6-9	5.6 ± 0.2		5.6 ± 0.2	
			1.4%		0.5%
H-nuclei	10-19	1.88 ± 0.3		1.88 ± 0.3	
VH-nuclei	20-28	0.69 ± 0.16		0.69 ± 0.16	

Table A6.1

Primary Composition (above constant rigidity)	Intensity of nucleons with energy >E/nucleon / Intensity of nuclei with energy >E/nucleus
100% Protons	1
87.3% protons 12.7% α-particles	0.70
As Table A6.1	0.32

Table A6.2

APPENDIX 7

The integral $I = \int_0^1 f^{\alpha} (\ell n\, f)^{\beta}\, df$ may be evaluated by means of the substitution:-

$$f = e^{y} \text{ , for integral values of } \beta.$$

Then $I = \int_{-\infty}^{0} e^{(\alpha+1)y} . y^{\beta} dy$

Integrating by parts,

$$I = \left[\frac{e^{(\alpha+1)y} . y^{\beta}}{(\alpha+1)} \right]_{-\infty}^{0} - \int_{-\infty}^{0} \frac{e^{(\alpha+1)y}}{(\alpha+1)} \cdot \beta\, y^{(\beta-1)}\, dy$$

$$= \left[\frac{e^{(\alpha+1)y} . y^{\beta}}{(\alpha+1)} - \frac{\beta . e^{(\alpha+1)y} . y^{(\beta-1)}}{(\alpha+1)^2} + \frac{\beta(\beta-1)}{(\alpha+1)^3} e^{(\alpha+1)y} y^{(\beta-2)} \right.$$

$$\left. \cdots + \frac{(-1)^{\beta} . e^{(\alpha+1)y} . \beta!}{(\alpha+1)^{(\beta+1)}} \right]_{-\infty}^{0}$$

$$= \frac{(-1)^{\beta} . \beta!}{(\alpha+1)^{(\beta+1)}}$$

APPENDIX 8

The elasticity distribution for a single nucleon-air nucleus collision has been taken to be:-

$$P_1(f_1)df_1 = -(1+\alpha)^2 f_1^{\alpha} \ell n\, f_1\, df_1 \qquad A8.1$$

Suppose that the elasticity distribution after n collisions is:-

$$P_n(f_n)df_n = -\frac{(1+\alpha)^{2n}}{(2n-1)!} f_n^{\alpha} (\ell n\, f_n)^{(2n-1)}\, df_n \qquad A8.2$$

Then the elasticity distribution after (n+1) collisions is given by:-

$$P_{(n+1)}(f_{(n+1)})df_{(n+1)} = \int_{f=f_{(n+1)}}^{1} P_1\left(\frac{f_{(n+1)}}{f}\right) P_n(f)\,\frac{df}{f}\, df_{(n+1)}$$

$$= \int_{f=f_{(n+1)}}^{1} -(1+\alpha)^2 \left(\frac{f_{(n+1)}}{f}\right)^{\alpha} \ell n\, \frac{f_{(n+1)}}{f} \cdot \left[-\frac{(1+\alpha)^{2n}}{(2n-1)!} f^{\alpha} (\ell n\, f)^{(2n-1)}\right]\frac{df}{f}\, df_{(n+1)}$$

$$= \frac{(1+\alpha)^{(2n+2)}}{(2n-1)!} f_{(n+1)}^{\alpha} \int_{f=f_{(n+1)}}^{1} \left\{\ell n\, f_{(n+1)} - \ell n\, f\right\} (\ell n\, f)^{(2n-1)} df_{(n+1)}\, d(\ell n\, f)$$

$$= \frac{(1+\alpha)^{(2n+2)}}{(2n-1)!} f_{(n+1)}^{\alpha}\, df_{(n+1)} \left[\ell n\, f_{(n+1)} (\ell n\, f)^{2n} - (\ell n\, f)^{(2n+1)}\right]_{f_{(n+1)}}^{1}$$

$$= - \frac{(1+\alpha)^{(2n+2)}}{(2n+1)!} f_{(n+1)}^{\alpha} (\ell n\, f_{(n+1)})^{(2n+1)}\, df_{(n+1)} \qquad A8.3$$

A comparison of equations A8.2 and A8.3 shows that if equation A8.2 is true for $n = N$ collisions it is also true for $n = (N + 1)$ collisions. Equation A8.2 is true for $n = 1$, as in that case it reduces to equation A8.1, i.e. the assumed elasticity distribution for a single collision. The elasticity distribution after n collisions is then given by equation A8.2 for all $n \geq 1$.

APPENDIX 9

$$\text{If } I_\beta = \int_0^1 (1-K)^\alpha K^\beta \ell n(1-K)dK \qquad \text{A9.1}$$

Let $\ell n(1-K) = y$

$$\text{Then } I_\beta = -\int_0^{-\infty} e^{\alpha y}.(1-e^y)^\beta.y.e^y dy$$

$$= \int_{-\infty}^{0} (1-e^y)^\beta.y.e^{y(1+\alpha)}dy$$

By the binomial theorem,

$$I_\beta = \int_{y=-\infty}^{0} \sum_{m=0}^{\infty} \frac{(-e)^{my}\ \beta(\beta-1)\ \ldots\ (\beta-m+1).y.e^{y(1+\alpha)}dy}{m!} \qquad \text{A9.2}$$

$$\int_{-\infty}^{0} (-e)^{my}\ y\ e^{y(1+\alpha)}dy = (-1)^m \int_{-\infty}^{0} e^{(1+\alpha+m)y} y\ dy$$

$$= (-1)^m \left[\frac{e^{(1+\alpha+m)y}.y}{(1+\alpha+m)} - \frac{e^{(1+\alpha+m)y}}{(1+\alpha+m)^2} \right]_{-\infty}^{0}$$

$$= \frac{-(-1)^m}{(1+\alpha+m)^2} \qquad \text{A9.3}$$

Therefore equation A9.2 becomes:-

$$I_\beta = -\sum_{m=0}^{\infty} \frac{\beta(\beta-1)\ \ldots\ (\beta-m+1)\ (-1)^m}{m!\quad (1+\alpha+m)^2}$$

APPENDIX 10

Suppose the primary nucleon spectrum is of the form:-

$$N(E_P)dE_P = A\ E_P^{-\gamma}\ dE_P \qquad A10.1$$

Then, if γ = constant and the elasticity of nuclear interactions is not a function of energy, the nucleon intensities are attenuated exponentially in the atmosphere with attenuation length λ_a ($\lambda_a \neq$ function of energy).

The rate of production of pions with energy E_π at depth x to (x + dx) in the atmosphere is:-

$$\int_{E_{P_{min}}}^{\infty} A.E_P^{-\gamma}\ dE_P.\ \exp\left(\frac{-x}{\lambda_a}\right) \cdot \frac{dx}{\lambda_i} F'(E_\pi, E_P) \qquad A10.2$$

where λ_i = the interaction length for nucleons in air.

$F'(E_\pi, E_P)$ = the spectrum of pions produced in an interaction of a nucleon of energy E_P.

The pion production spectrum, $F(E_\pi)$

$$= \int_{x=o}^{t} \int_{E_{P_{min}}}^{\infty} A.E_P^{-\gamma}\ dE_P.F'(E_\pi, E_P)\ \exp\left(\frac{-x}{\lambda_a}\right).\ \frac{dx}{\lambda_i}$$

i.e. the spectrum of pions produced in all of the interactions in the atmosphere.

$$F(E_\pi) = \int_{E_{P_{min}}}^{\infty} A.E_P^{-\gamma}\, dE_P \cdot \frac{F'(E_\pi, E_P)}{\lambda_i} \left[-\lambda_a \exp \frac{-x}{\lambda_a} \right]_o^t$$

$$\approx \int_{E_{P_{min}}}^{\infty} A.E_P^{-\gamma}\, dE_P . F'(E_\pi, E_P) \frac{\lambda_a}{\lambda_i} \qquad \text{A10.3}$$

since exp - t/λ_a (t = total thickness of atmosphere) is negligible compared with unity.

Substituting from equation A10.3 in equation A10.2, the rate of production of pions with energy E_π at depth x to (x+dx)

$$= F(E_\pi) \exp\left(\frac{-x}{\lambda_a}\right) \cdot \frac{dx}{\lambda_a} \qquad \text{A10.4}$$

If γ and τ are the Lorentz factor and lifetime respectively of a relativistic pion of energy E_π, rest mass m_π,

the probability of the pion decaying in time $dt = \frac{dt}{\tau}$

" " " " " " " a distance $d\ell = \frac{d\ell}{c\tau}$

" " " " " " " thickness $dx = \frac{dx}{\rho c\tau}$

$$\tau = \gamma\, \tau_o \qquad (\tau_o = \text{rest lifetime})$$
$$= \frac{E_\pi}{m_\pi c^2}\, \tau_o$$

For an isothermal atmosphere, $\rho = \frac{x}{z_o} \cdot \cos\theta$ (Rossi, 1952) (θ = zenith angle)

$\therefore$ the probability of a pion decaying in thickness dx

$$= \frac{dx . m_\pi c z_o}{x E_\pi \tau_o \cos\theta}$$

and the rate of loss of pions by decay in thickness dx

$$= \frac{dx\, m_\pi c z_o N(E_\pi,x)}{x . E_\pi \tau_o \cos\theta} \qquad \text{A10.5}$$

The rate of loss of pions by absorption in thickness dx

$$= \frac{dx}{\lambda_\pi} N(E_\pi,x) \qquad \text{A10.6}$$

λ_π = attenuation length for pions in air.

Combining equations A10.4, 5 and 6, the rate of change of pion intensity with depth is given by:-

$$\frac{d\, N(E_\pi,x)}{dx} = F(E_\pi) \exp\left(\frac{-x}{\lambda_a}\right) \cdot \frac{dx}{\lambda_a} - N(E_\pi,x) \left[\frac{m_\pi c z_o}{x E_\pi \tau_o \cos\theta} + \frac{1}{\lambda_\pi}\right]$$

A10.7

Putting $\frac{m_\pi c z_o}{\tau_o}$ = B and multiplying equation A10.7 by the integrating factor:-

$$\exp\left[\int \left\{\frac{1}{\lambda_\pi} + \frac{B}{E\cos\theta} \cdot \frac{1}{x}\right\} dx\right] = x^{B/E\cos\theta} \exp x/\lambda_\pi,$$

$$\frac{d\, N(E_\pi,x)}{dx} x^{B/E\cos\theta} \exp x/\lambda_\pi + N(E_\pi,x) \left\{\frac{1}{\lambda_\pi} + B/E\cos\theta . \frac{1}{x}\right\} \exp x/\lambda_\pi . x^{B/E\cos\theta}$$

$$= F(E_\pi) \exp\left\{-\frac{x}{\lambda_a}\right\} \frac{x^{B/E\cos\theta}}{\lambda_a} \exp \frac{x}{\lambda_\pi}$$

or

$$\frac{d}{dx}\left\{N(E_\pi,x)\ \exp\frac{x}{\lambda_\pi}\ x^{B/E\cos\theta}\right\} = F(E_\pi)\ \exp\left\{-x\left(\frac{1}{\lambda_a}-\frac{1}{\lambda_\pi}\right)\right\}\cdot x^{B/E\cos\theta}\cdot\frac{1}{\lambda_a}$$

$$N(E_\pi,x)\exp\frac{x}{\lambda_\pi}\cdot x^{B/E\cos\theta} = F(E_\pi)\frac{1}{\lambda_a}\int_0^x \exp\left[-x\left(\frac{1}{\lambda_a}-\frac{1}{\lambda_\pi}\right)\right] x^{B/E\cos\theta}dx$$

$$= F(E_\pi)\frac{1}{\lambda_a}\left[\frac{x^{(B/E\cos\theta+1)}}{(B/E\cos\theta+1)} - \frac{x^{(B/E\cos\theta+2)}}{(B/E\cos\theta+2)\lambda'} + \frac{x^{(B/E\cos\theta+3)}}{(B/E\cos\theta+3)2!\lambda'^2} - \cdots\cdot\right]$$

where $$\frac{1}{\lambda'} = \frac{1}{\lambda_a} - \frac{1}{\lambda_\pi}\ .$$

$\therefore$ The intensity of pions with energy E_π to $(E_\pi+dE_\pi)$ at depth x,

$$N(E_\pi,x)dE_\pi = F(E_\pi)\frac{x}{\lambda_a}\exp-\frac{x}{\lambda_\pi}\left[\frac{1}{(B/E\cos\theta+1)} - \frac{x/\lambda'}{(B/E\cos\theta+2)} + \frac{(x/\lambda')^2}{(B/E\cos\theta+3)2!} - \cdots\cdot\right]$$